UNIVERSITY OF SOUTHERN CALIFORNIA.

CONSOLIDATED SEMIANNUAL PROGRESS REPORT

NO. 8

Covering Research Activity During The Period

1 April 1968 through 30 September 1968

FEB 2 0 1969

ELECTRONIC SCIENCES LABORATORY

CONSOLIDATED SEMIANNUAL PROGRESS REPORT

NO. 8
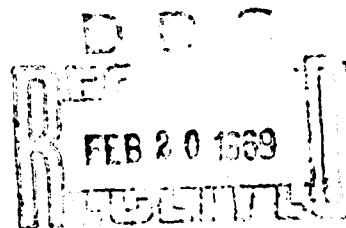
Covering Research Activity During the Period

1 April 1968 through 30 September 1968

Prepared by

The

Electronic Sciences Laboratory

of the

School of Engineering

University of Southern California

Los Angeles, California 90007

TABLE OF CONTENTS

iii

ACKNOWLEDGEMENT

Contract or Grant	Agency
GK-2716	National Science Foundation
GK-2908	National Science Foundation
GK-3303	National Science Foundation
GP-5902	National Science Foundation
GP-7804	National Science Foundation
GP-8636	National Science Foundation
GP-8960	National Science Foundation
GU-1559, EE	National Science Foundation
GU-1559, MS	National Science Foundation
DAHC-04-69-C-0003	Department of the Army
DA-ARO-D 31-124-450	Department of the Army, U.S. Army Research Office
DA-ARO 31-124-G764	Department of the Army, U.S. Army Research Office
DA-ARO-D 31-124-G929	Department of the Army, U.S. Army Research Office
DA-ARO-D 31-124-G930	Department of the Army, U.S. Army Research Office
DA-ARO-D 31-124-G990	Department of the Army, U.S. Army Research Office
DA-ARO-D 31-124-G1054	Department of the Army, U.S. Army Research Office

Contract or Grant	Agency
150-22-13-05-33	National Aeronautics and Space Administration
NGR-05-018-022	National Aeronautics and Space Administration
NGR-05-018-044	National Aeronautics and Space Administration
NGR-05-018-083	National Aeronautics and Space Administration
NGL-05-018-044	National Aeronautics and Space Administration
GM01724-02	Department of Health, Education and Welfare
HE 11915-01	Department of Health, Education and Welfare
NB-06196-02	Department of Health, Education and Welfare
NB-08207-01	Department of Health, Education and Welfare
GM-16197-01	Department of Health, Education and Welfare
AT(11-1)-113	Atomic Energy Commission

PARTICIPATING PERSONNEL OF THE
UNIVERSITY OF SOUTHERN CALIFORNIA
ELECTRONIC SCIENCES LABORATORY

DIRECTOR

Z. A. Kaprielian

Andrews, H. C.	Kleinman, D. A.	Pratt, W. K.
Angel, E.	Kroger, F. A.	Reed, I. S.
Arguello, C. A.	Kuehl, H. H.	Reichert, J. D.
Aseltine, J.	Lempel, A.	Rousseau, D.
Bedrosian, E.	Lindsey, W. C.	Rusch, W. V. T.
Bekey, G. A.	Louisell, W. H.	Scholtz, R. A.
Bellman, R. E.	McGhee, R. B.	Silverman, L. M.
Beroza, P. P.	Macmillan, R. S.	Smit, J.
Breuer, M. A.	Mager, G. E.	Spitzer, W. G.
Brook, R. J.	Marburger, J. H.	Steier, W. H.
Buell, J.	Meisel, W. S.	Swerling, P.
Crowell, C. R.	Meritt, M. J.	Sworder, D. D.
Daybell, M. D.	van der Meulen, Y.	Tooper, R. F.
DeShazer, L. G.	Moore, G. P.	Venuri, R. V.
Faust, W. L.	Munushian, J.	Wagner, W. G.
Gagliardi, R. M.	Murr, L. E.	Wang, R.
Gershenzon, M.	Nahi, N. E.	Weber, C. L.
Ginsburg, S.	Neustadt, L. W.	Welch, L. R.
Golomb, F. S.	O'Brien, B. B.	Whelan, J. M.
Grodins, F. S.	Ogawa, S.	Wilcox, W. R.
Halloran, M. H.	Ohlson, J. E.	Wittry, D. B.
Hurrell, J. P.	Payne, H. J.	Wolf, M. B.
Kashef, R.	Payne, R. T.	Yanagida, H.
Kim, Y. B.	Porter, W.	Young, G. O.
Klein, M.	Porto, S. P. S.	

LECTURERS AND GRADUATE RESEARCH ASSISTANTS

Allred, W. P.	Bowman, C. K.	Cosand A. E.
Arguello, Z. P.	Bradford, W. G.	Cumming, G.
Asa, M. L.	Brewer, J. H.	Davidheiser, R.
Assefi, T.	Canter, L. H.	Dawson, L. R.
Axelband, E. I.	Card, R.	DiLoretto, A. G.
Baenziger, G. P.	Cascell, W. S.	Dokken, R. D.
Baker, J. E.	Chandler, W. J.	Eastment, J. G.
Beguwala, M E.	Chiarg, C. L.	Edelson, R. H.
Borrey, R. G.	Colline, D. C.	Elliott, D. F.
Bottlik, I. P.	Cooper, C. A.	von der Embse, U.

Fielding, R. M.	Leung, P.	Rice, D. K.
Flannery, M. R.	Levy, M. E.	Rideout, V. L.
Fraas, L. M.	Lew, A. Y.	Roberts, G. I.
Fredrickson, H.	Li, C. T.	Schaefer, B. M.
Fuzak, C.	Lin, W. N.	Sherman, D. N.
Gray, R. M.	MacAnally, R. B.	Slobin, S.
Germann, D. A.	McAllister, G. G.	Stein, J. J.
Giuliano, J. A.	McCoy, J. H.	Stokes, R. B.
Gunderson, M. A.	Maloney, J. C.	Storwick, R.
Haney, G. M.	Mann, M. M.	Sullivan, J. R.
Hartman, R. C.	Meier, G. D.	Sun, C.
Hartwick, T. S.	Michalopoulos, D. A.	Tauseworth, R.
Herron, W.	Miller, D. S.	Thoene, R. B.
Hershman, G. H.	Morrison, L. W.	Thompson, G. D.
Hon, D. T.	Mowery, J. W.	Turner, G. B.
Horylev, R.	Murata, P. T.	White, D. R.
Hsieh, J. J.	Neal, C. B.	Wielin, S. A.
Huang, H. H. C.	Ng, W. K.	Wu, S. Y.
Huff, L.	Norton, R. J.	Yee, J. F.
Kim, J. K.	Otaguro, W. S.	Yeh, L. S.
Kosai, K.	Parker, R. D.	Young, J. W.
Kumar, U.	Peratt, A. L.	Yuan, L. T.
Kung, J. K.	Phatak, A. V.	Yuan, L. T.
LaFrance, T. S.	Proffit, W. P.	Yuan, R. S.
LaFrieda, J. A.	Rao Sahib, T. S.	Yuan, W. W.
Lee, L. C.	Rauch, D. J.	

TECHNICIAN SUPPORT PERSONNEL

Belda, J. F.	Izad, H.	Mueller, G. H.
Bruckmann, K. S.	Ketchum, D. J.	Muller, U. J.
Csige, G.	Krebs, W. E.	Soberay, W. G.
Garlinger, E. D.	Lee, S. S. Y.	Vonusa, J. S.
Hamada, S. S.	Maunders, E. A.	Wong, R.
Howland, D. L.	Molnar, E.	Owen, H. R.

ADMINISTRATIVE

Baker, W. P.	Lambert, J. W.	Potts, L. D.
Blood, L. J.	Lopez, F.	Rice, G. L.
Caldwell, C. J.	Lum, G. T.	Sakmar, M. C.
Di-Bernardo, L.	Lyness, C. J.	Shioya, K. H.
Dillon, E. P.	Marshall, J. W.	Tierney, R.
Henderson, M. K.	Mihalka, M. F.	Ward, R. A.
Iskandar, R. Z.	Mitchell, S. R.	Winter, J.
Kostewicz, C. M.	Nihei, J. T.	

1. SOLID STATE

1.1 SEMICONDUCTORS

1.1.1 Electron Probe Analysis of Semiconductors

AF-AFOSR-68-1414, Air Force Office of Scientific Research

D. B. Wittry, D. F. Kyser, J. H. McCoy, H. C. Marciniak,

T. Rao-Sahib and A. Van Couvering

Investigations are being conducted in the following areas:
cathodoluminescence, electron beam modulated reflectance, surface
state densities, non-linear effects in cathodoluminescence electron
probe x-ray microanalysis and selected-area electron spectrometry. A
brief report of the present status and recent progress in these investi-
gations follows:

1.1.1.1   Cathodoluminescence of Semiconductors

D. F. Kyser, H. Marciniak and D. B. Wittry

Work on the ultrahigh vacuum chamber and beam column has
continued since the last semiannual report. With this system, we hope
to provide a clean "atmosphere" in which to study semiconductor speci-
mens with minimum effects due to contamination. The vacuum chamber,
manufactured by Ion Dynamics Corporation has been attached to an

-1-

Ultek TNB ultrahigh vacuum system. A pressure of 3×10^{-7} Torr was achieved after only a few hours of pumping and it appears possible to reach the goal of better than 10^{-9} Torr.

With this system, it will be possible to vary the specimen temperature from 20°K to 500°K using an Air Products and Systems Cryo Tip refrigerator and an electric heater. A single magnetic lens will be used to focus an electron beam on the specimen. A standard ARL microprobe light optics assembly will be used to focus the luminescence on a high resolution grating spectrometer. The first application of this system will be the study of the temperature dependence of cathodoluminescence of semiconductors. Additional experiments planned include electron beam modulated reflectance at low temperatures and studies of the changes in surface recombination velocities with surface conditions.

1.1.1.2 Electron Beam Modulated Reflectance of Semiconductors
J. McCoy and D. B. Wittry

As reported previously[1], a focused electron beam has been used to modulate the reflectivity of germanium. Further experiments have been made since the last semiannual report to determine the relative importance of excess carrier density and thermal effects. For example, the amplitude of the modulated response has been measured as a function of the beam current density. If the carrier lifetime is constant, the amplitude of the modulated reflectance should vary as the

-2-

one third power of the beam density for an effect caused by excess carriers. On the other hand, if thermal effects dominate, the modulated reflectance should vary as the one half power of the beam density. A one third power dependence was found over four orders of magnitude change in the beam density.[1]

The heat transport equation was solved for the case of a transient disk-shaped heat source on the surface of a semi-infinite medium.[2] This model approximates the case of heating by a defocussed electron beam which is pulsed as in the studies of electron beam modulated reflectance. The time response was obtained from a digital computation. These calculations have not ruled out the possibility of thermal effects as a cause of the modulated reflectance since the response time was found to be about the same as the expected carrier lifetime in germanium. Further experiments are in progress to measure the actual excess carrier densities obtained during electron bombardment. Hopefully these experiments will give more insight into the physical basis for the electron beam modulation of reflectance.

References

1. McCoy, J. H. and Wittry, D. B., Appl. Phys. Letters (to be published Oct. 15, 1968).

2. Carslaw, H. C., and J. C. Jaeger, "Conduction of Heat in Solids", (Clarendon Press, Oxford, 1947), p. 220.

1.1.1.3 Non-linear Cathodoluminescence of Semiconductors

T. Rao-Sahib and D. B. Wittry

The voltage dependence of cathodoluminescence has been previously used[1] to measure diffusion lengths and surface recombination velocities of n-type gallium arsenide. However, for p-type specimens, the experimental results do not agree with theory, or appear to indicate unreasonably low surface recombination velocities (e.g., $S = 0$) or unreasonably large space charge depletion layer widths (i.e., $d = .4\mu$ in heavily doped material).

Most p-type gallium arsenide has exhibited a non-linear relation between luminescence intensity and electron beam current at constant voltage. Modifications to the theory for a one dimensional case can be made to account for this non-linearity, but we have not been able to construct a satisfactory theory for the three dimensional case. For this reason, we have attempted to use experimental conditions that more closely approximate the one dimensional case.[2] This is done by irradiating a large area of the specimen and using a selected area aperture in the plane of the image formed by the objective lens; that is at the entrance slit of the monochromator. Two cases have been examined, namely, a) a beam diameter of 180 μ and a selected area corresponding to 27 μ by 27 μ, and b) a beam diameter of 72 u and a selected area corresponding to 5 μ by 5 μ. The experimental results obtained on a Zn doped GaAs specimen (carrier concentration $10^{18}/cm^3$) are summarized in Table I.

Table I

	power (mW)	Average exponent m	S	d/L	L(μ)
Case a	5	1.0	10	0.033	0.8
	50	1.2	10	0.033	0.75
Case b	15	1.2	50	0.033	0.96
	40	1.4	50	0.033	0.8

It can be seen from Table I that the values obtained with various power levels are consistent. This is due to the use of calculated curves that take account of the appropriate exponent m in the relation $I = i^m$ where I is the intensity and i is the current at constant voltage. In each case, the average value of the exponent m is determined for the power level actually used in the voltage dependence curves. The fit of the experimental curves to the calculated curves is within experimental error for the cases shown in Table I, indicating some progress in our understanding of the voltage dependence of cathodoluminescence of p-type GaAs. Further experiments are planned on p-type specimens of GaAs with various doping levels.

References

1. Wittry, D.B., and Kyser, D.F., J. Appl. Phys. **38**, 375-382 (1967).

2. Kyser, D.F., and Wittry, D.B., Proc. IEEE, **55**, 733-734 (1967).

1.1.1.4 Surface State Density Studies

H. Marciniak and D. B. Wittry

Experiments are being planned to measure the surface state density, width of the space charge depletion region, and surface recombination velocity for oxidized Si and for CdSe. Preliminary experiments are being conducted in the ARL microprobe, but because of the lack of a controlled environment, some of these experiments must be deferred until the new electron probe column is finished.

1.1.1.5 Quantitative Electron Probe Microanalysis

D. F. Kyser and T. Rao-Sahib

Measurement of x-ray intensity ratios from pairs of semiconductor compounds were repeated on the best available material and the results compared with the calculations of Brown et al.[1] The ratio of the AsK_α intensities from GaAs and InAs was measured to be 1.173 (30 kV beam potential, 52.5 degrees takeoff angle). Transport equation program calculations gave 1.209 without a fluorescence correction and 1.170 with the inclusion of a fluorescence correction. For the case of the GaK_α line the numbers were 1.828 (meas.), 1.791 (calc.), and 1.843 (calc. with fluor.). For the case of the InL_α line in InP and InAs the numbers were 1.326 (meas.) and 1.340 (calc.). There was no significant correction for fluorescence in this third case. In all three cases the agreement between theory and experiment was 1% or better.

Reference

1. Brown, D. B., Wittry, D. B., and Kyser, D. F. (to be published).

1.1.1.6 Selected Area Electron Spectrometry in the Transmission Electron Microscope

D. B. Wittry

An electron spectrometer system for use with the transmission electron microscope was constructed at the Cavendish Laboratory, University of Cambridge (during sabbatical leave). This system shown in Fig. 1 can be used for the study of the energy spectrum of electrons from a selected area of the image or diffraction pattern formed in normal operation of the electron microscope. A similar system is now being designed for use with the Hitachi HU 125 at the University of Southern California.

Preliminary results[1] obtained on a $1,000 \overset{o}{A}$ selected area of a polycrystalline BeO film are shown in Fig. 2. In this figure, the energy loss corresponding to oxygen K excitation can be seen as well as some fine structure similar to that observed in soft x-ray absorption spectra. The preliminary results indicate that the x-ray energy loss spectra can be used for microanalysis in the transmission electron microscope with sensitivity significantly higher than that of electron microprobe x-ray analysis of thin specimens and light elements.

In addition to practical applications to microanalysis, the x-ray energy loss spectra are of considerable fundamental interest.
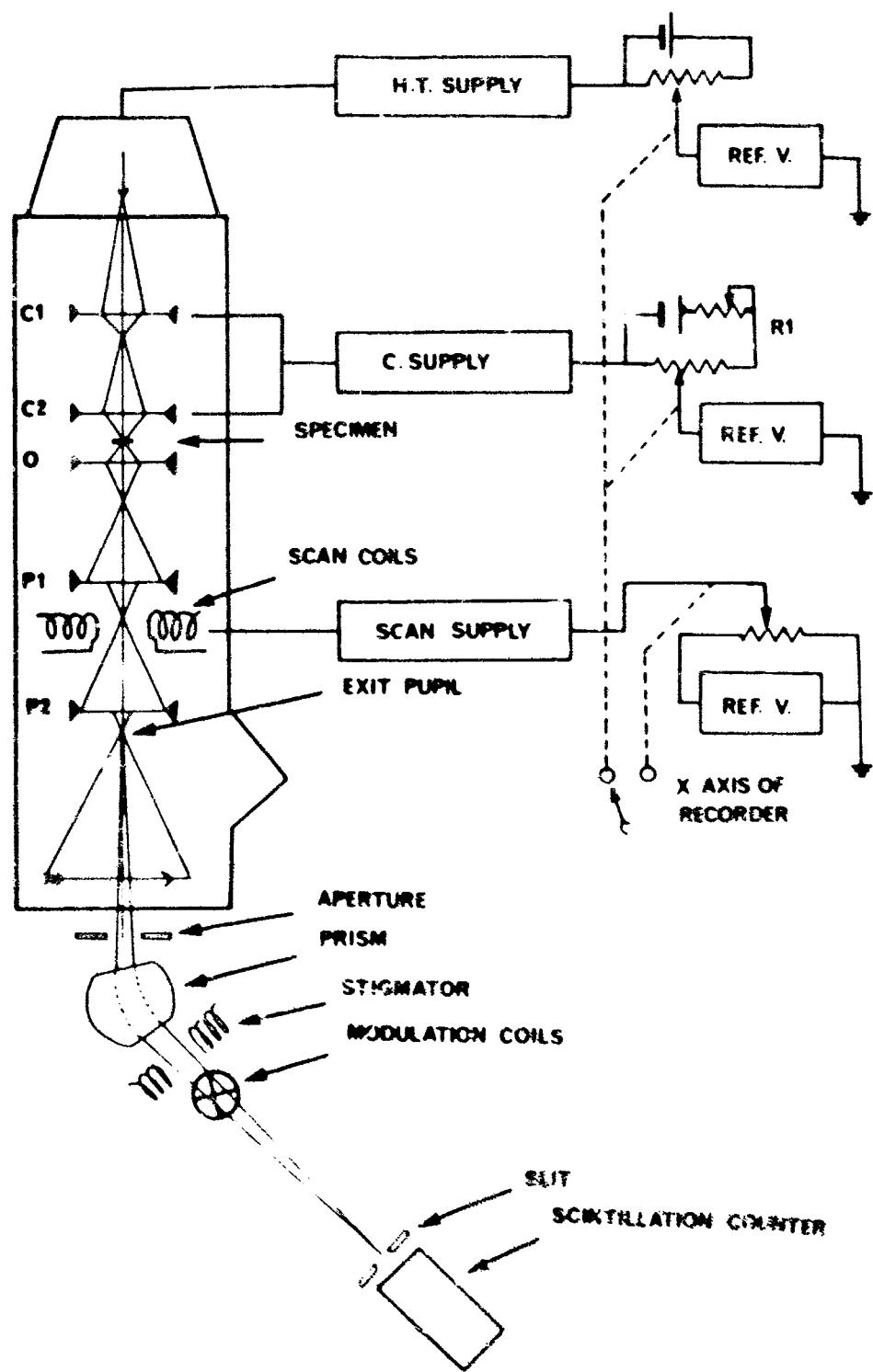
Fig. 1
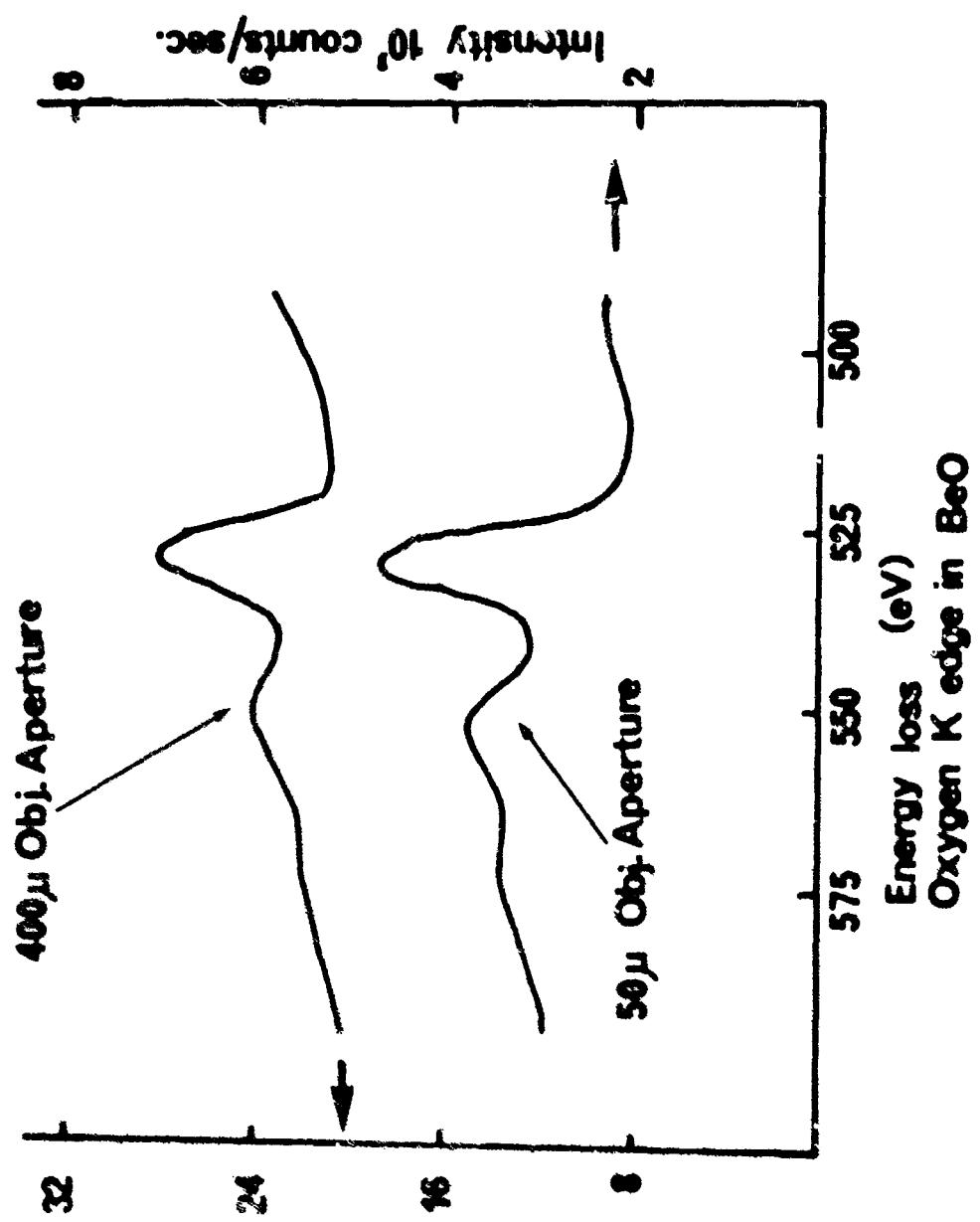
Fig. 2

Fundamental investigations of the fine structure in the energy loss

spectrum can be performed using the full capabilities of the transmission

electron microscope to determine the crystal structure and orientation of

the specimen.

Reference

1. Wittry, D. B., Ferrier, R. P., and Cosslett, V. E., V^{th} International Congress on X-Ray Optics and Microanalysis, Tubingen, Germany, 9-14, September 1968.

1.1.2 Site Distribution of Silicon in Silicon-Doped Gallium Arsenide

W. P. Allred, G. Cumming, J. Kung and W. G. Spitzer

Introduction

Gallium arsenide which is grown from a stochiometric melt and doped with silicon is always an n-type semiconductor. However, it is known[1,2] that at silicon concentrations of $[Si] > 10^{18} cm^{-3}$, the carrier concentration n, in the exhaustion range, may be much less than $[Si]$. The difference between the values of n and $[Si]$ is related to the amphoteric nature of silicon in GaAs. Silicon on a gallium site, Si_{Ga}, is a donor while Si_{As} is expected to be an acceptor. There is also some evidence[3] from photoluminescence studies for the existence of a substantial concentration of $\left(Si_{Ga} - Si_{As} \right)$ nearest neighbor pairs when the $[Si] \gtrsim 10^{19} cm^{-3}$.

There have been several recent studies of the infrared absorption associated with localized vibrational modes of impurities in semiconductors. In particular, three of these studies[4,5,6] have dealt with silicon impurities in GaAs. It was found that one could correlate

many of the observed absorption bands with the presence of different point defects involving silicon. The present work uses this identification to investigate the influence of the other impurities, specifically tellurium and zinc, on the site distribution of silicon.

Review

There has been considerable progress in the understanding of the localized vibrational mode absorption in silicon-doped GaAs. Because of the importance of previous studies for the interpretation of the present results, a brief review will be presented here. This review is particularly important since, at the time of this writing, one of the more important papers[6] is not yet published.

Silicon, as an isolated substitutional impurity on either the gallium or arsenic sublattice, has tetrahedral point group symmetry. To terms quadratic in the displacement of the silicon, the potential energy is that of a spherically symmetric, harmonic oscillator. Because the silicon is lighter than either the gallium or arsenic, one can expect spatially localized vibrational modes associated primarily with the motion of the silicon impurity at frequencies above the highest phonon frequency[7] of the unperturbed lattice. A single silicon defect will give three vibrational modes, and because of the symmetry of the potential, the modes will be degenerate. Thus a single infrared absorption band is expected for Si_{Ga} and another one for Si_{As}. The two sites can have different frequencies because of a slightly different mass defect and also because the different nearest neighbors in the two cases should

-12-

influence the effective force constants. In Table I it is seen that the observed local mode frequencies are $\omega = 384$ cm^{-1} for Si$_{Ga}$ and 399 cm^{-1} for Si$_{As}$.

In some cases the silicon impurity is no longer isolated from other defects but is paired with another silicon or another impurity on a neighboring site. There can be different reasons for the existence of these ion pairs. There is evidence already mentioned[3,6] that $\left(\text{Si}_{Ga} - \text{Si}_{As} \right)$ pairs tend to form at high [Si]. Moreover, the samples are strongly n-type and hence the resulting free carrier absorption must be reduced by the introduction of an electrically compensating impurity. Lithium or copper is diffused at elevated temperature to produce the compensation. Since the material is initially n-type, the compensating diffusant must produce acceptors which are generally assumed to be Li$_{Ga}$ or Cu$_{Ga}$. There is also a tendency for the Si$_{Ga}$ donors and the Li$_{Ga}$ or Cu$_{Ga}$ acceptors to interact resulting in $\left(\text{Si}_{Ga} - \text{Li}_{Ga} \right)$ or $\left(\text{Si}_{Ga} - \text{Cu}_{Ga} \right)$ pairs. Clearly, in these cases, the silicon is no longer in a site with tetrahedral symmetry.

For the $\left(\text{Si}_{Ga} - \text{Li}_{Ga} \right)$ pairs where the defect involves impurities on second neighbor sites, a weak coupling model can give reasonable agreement[6] with experiment. The effect of one atom is to alter the potential of the other atom. Since the nearest neighbor gallium sites are along a $< 110 >$ direction, which is not a symmetry rotation axis of the tetrahedral point group, the triply degenerate Si$_{Ca}$

-13-

band will be split into three bands with frequencies nearly independent of the lithium isotope. These bands will be located near the Si_{Ga} frequency of 384 cm^{-1}. A simple perturbation argument[8] gives

$$\omega^2 = \frac{1}{3} \sum_{i=1}^{3} \omega_i^2 \quad ,$$

where ω is the frequency of the triply degenerate mode and the ω_i values are the perturbed frequencies. In the $\left(Si_{Ga} - Li_{Ga} \right)$ defect case there will also be three bands involving primarily lithium motion. The frequencies of both the predominently silicon modes and those due to lithium are given in Table I.

The $\left(Si_{Ga} \quad Si_{As} \right)$ defect is more complicated[6, 9] in that the two impurities are strongly coupled, and both are light compared to the atoms they replace. The pair axis is in a $< 111 >$ direction which is a three-fold rotation axis, and the six vibrational modes are expected to contain two sets of doubly degenerate modes. Thus there can be four frequencies of which three are identified in Table I. The fourth mode is either too small in absorption to be observed or, as calculation indicates[6], falls in a region of large absorption from the GaAs host lattice. The location of all bands observed in lithium or copper diffused, silicon-doped GaAs is listed in Table I. For completeness, the location of some bands related to lithium paired with lattice defects[10] in undoped GaAs is also given. These latter bands are not related to the silicon impurity but can occur in all samples[4] which are lithium diffused at sufficiently high

-14-

Table I

Defect	Impurity	Mode Frequency (cm^{-1})		
		^{7}Li	^{6}Li	Cu
Li-lattice defects	Li		352	
		365	389	
		379	406	
Si$_{Ga}$ - Li$_{Ga}$	Li$_{Ga}$	438	470	
		447	480	
		454	487	
	Si$_{Ga}$	374	374	
		379	379	
		405	405	
Si$_{Ga}$ - Cu$_{Ga}$	Si$_{Ga}$			374
				376
				399
Si$_{Ga}$	Si$_{Ga}$	---	--- 384	---
Si$_{As}$	Si$_{As}$	---	--- 399	---
Si$_{Ga}$ - Si$_{As}$	Si$_{Ga}$ - Si$_{As}$	---	--- 367	---
		---	--- 393	---
		---	--- 464	---

The frequencies of infrared absorption bands in lithium- or copper-diffused, silicon doped GaAs.

temperature.

There have been a number of experiments which have
suggested that the distribution of silicon among the various defects
mentioned will be influenced by the presence of other impurities. Some
electrical and radio-tracer measurements of selenium plus silicon-doped
GaAs indicated[1] that the Se_{As} donors could change $\eta = [Si_{As}]/[Si_{Ga}]$
from < 1 to > 1. Local mode measurements of a sulfur plus silicon-
doped sample[4] showed the Si_{As} band at 399 cm^{-1} to be larger than the
Si_{Ga} band at 384 cm^{-1}. In similarly silicon-doped samples but without
sulfur[6], the 384 cm^{-1} band is ~ 4-5 times as strong as the 399 cm^{-1}
band. However, the bands in the sulfur-doped sample were small and
close to some very large Li-lattice defect bands, thus making the results
uncertain. Another study showed that silicon site transfer could take
place[5] as a result of lithium diffusion at temperatures $\gtrsim 800^{\circ}C$. The
sulfur plus silicon-doped sample[4] was diffused at $\sim 800^{\circ}C$ again making
this result uncertain.

Experimental Results and Discussion

Table II lists several ingots of GaAs with the doping levels
anticipated near the seed end on the basis of the impurities added and
published[11] distribution coefficients. Samples were taken from each
ingot and diffused with lithium. In some cases samples were taken from
both the seed end and near the back end of the ingot. The temperature of
diffusion was T_d 700°C in order to avoid the site redistribution[5]

-16-

Table II

Ingot #	Dopants	Doping Concentrations
1	Si	$\sim 1\text{-}2 \times 10^{18} \text{cm}^{-3}$
2	Si	$\sim 2\text{-}3 \times 10^{19} \text{cm}^{-3}$
3	Si, Te	$[\text{Si}] \sim 1 \times 10^{18} \text{cm}^{-3}$, $[\text{Te}] \sim 3\text{-}4 \times 10^{18} \text{cm}^{-3}$
4	Si, Te	$[\text{Si}] \sim 6\text{-}8 \times 10^{18} \text{cm}^{-3}$, $[\text{Te}] \sim 5\text{-}6 \times 10^{18} \text{cm}^{-3}$
5	Si, Zn	$[\text{Si}] \sim 6 \times 10^{18} \text{cm}^{-3}$, $[\text{Zn}] \sim 1 \times 10^{18} \text{cm}^{-3}$
6	Si, Zn	$[\text{Si}] \sim 6 \times 10^{18} \text{cm}^{-3}$, $[\text{Zn}] \sim 3\text{-}4 \times 10^{18} \text{cm}^{-3}$
7	Si, Zn	$[\text{Si}] \sim 6 \times 10^{19} \text{cm}^{-3}$, $[\text{Zn}] \sim 3 \times 10^{19} \text{cm}^{-3}$

GaAs ingots used in the present study with doping concentrations
near the seed end of the crystal

---

observed for $T_D \geq 800^\circ C$. The diffusion was done from a surface alloy

phase while in an argon atmosphere. The method of diffusion has been

described previously[8].

Samples from the silicon-doped ingots 1 and 2 were lithium

diffused and the infrared absorption measured at liquid nitrogen tempera-

ture is given in Fig. 1. Also shown for comparison is the measured

absorption curve for pure GaAs. The curves show the spectral region

containing most of the local mode bands which are labeled with the related

defect. Although, as indicated in Table I, some bands occur at $\omega > 430$

cm^{-1}, they have been shown in previous measurements[4,6] and will not

be of major importance for the present work.

The crosses of Fig. 2 show the peak absorption coefficient

α_p for the Si_{Ga} band at 384 cm^{-1} plotted against α_p for the Si_{As} band at
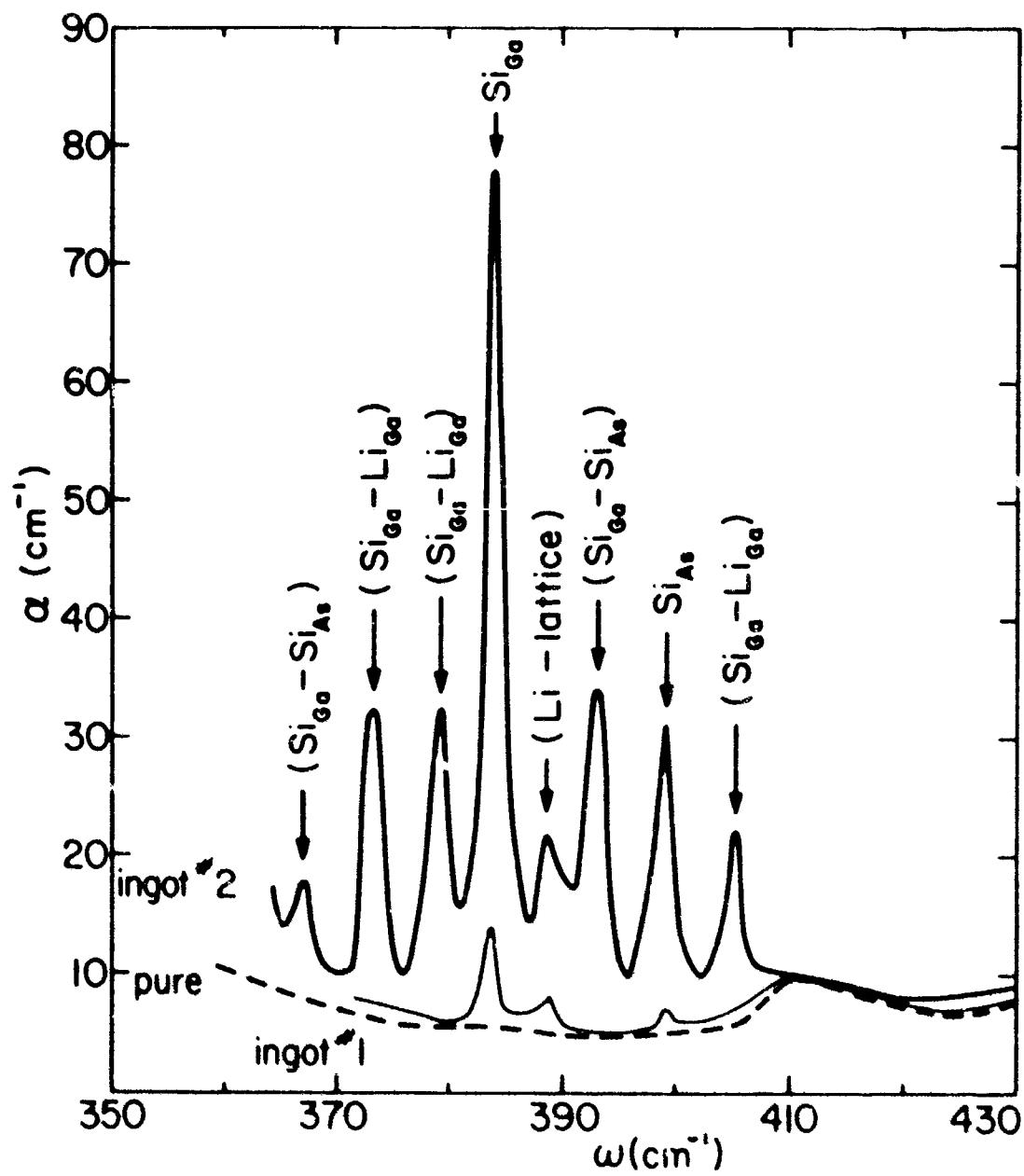
Fig. 1. Liquid nitrogen temperature absorption of samples from ingots 1 and 2 of Table II. The samples were ^{7}Li diffused at 700°C for 24 hours.
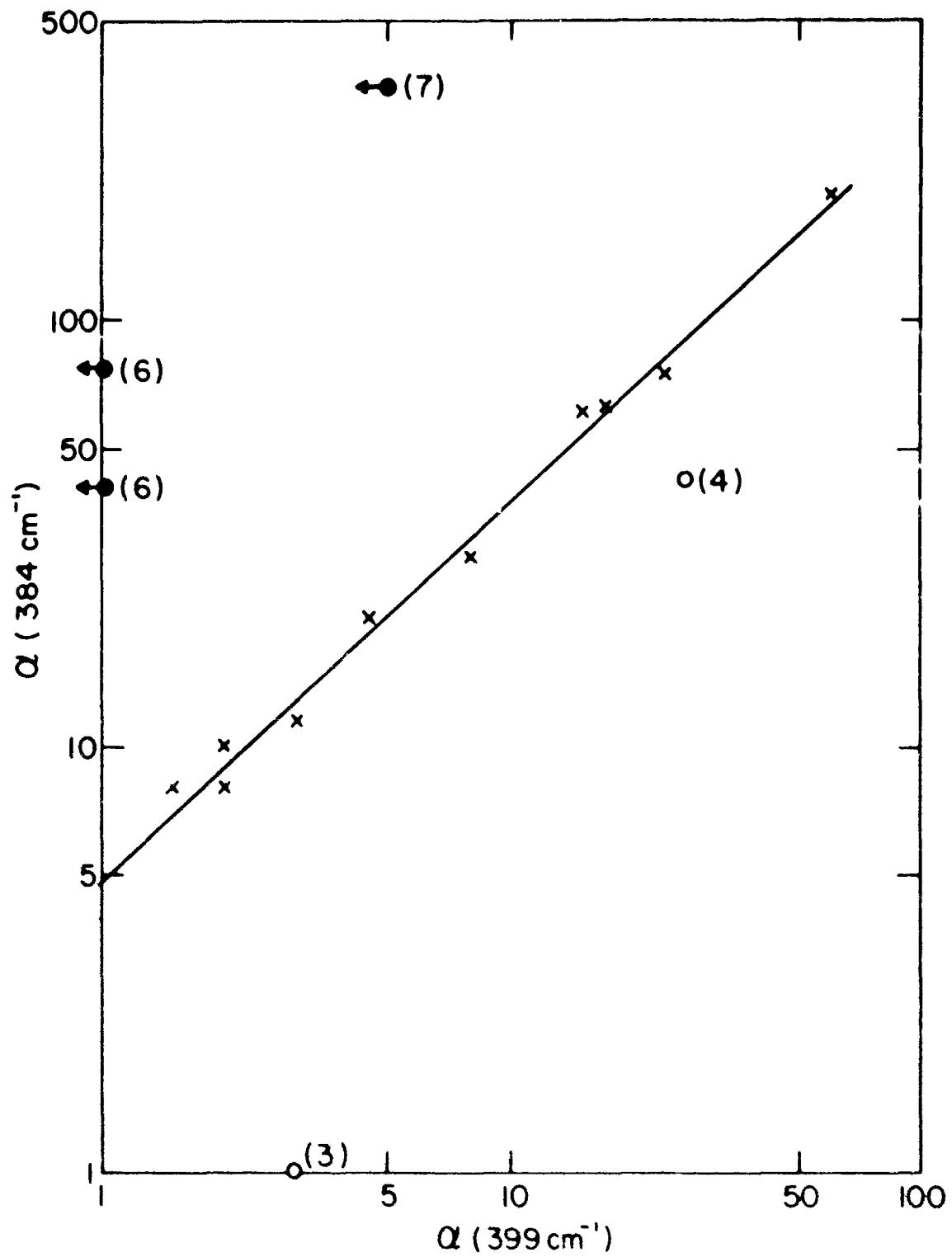
Fig. 2. A plot of the peak absorption coefficient of the Si_{Ga} band at $384\ cm^{-1}$ vs that for the Si_{As} band at $399\ cm^{-1}$. The x are for silicon doped samples, the o for silicon and tellurium doped samples, and a o are for silicon and zinc doped samples. The numbers indicate the ingot of Table II. All samples are lithium diffused.

399 cm^{-1}. The data are taken from a number of silicon-doped samples which are all diffused with lithium at $T_D \leq 800^{\circ}C$. Most of these samples were measured as part of an earlier study[6]. The points are close to a line of slope ~ 0.9 indicating that the Si_{As} band grows slightly more rapidly than the Si_{Ga} band with increasing [Si]. It is to be emphasized that silicon is the only major dopant in these samples.

The absorption of samples from ingots 3 and 4, which are doped with silicon plus tellurium and diffused with ^7Li is shown in Fig. 3. Comparison with Fig. 1 shows several new features. The bands near 475 cm^{-1} and 391 cm^{-1} are due to $\left(Li_{Ga} - Te_{As} \right)$ and have been previously studied[12]. The band at 379 cm^{-1} is largely a Li-lattice defect band and shows a large lithium isotope shift, i.e., 379 cm^{-1} → 406 cm^{-1} when $^7Li → ^6Li$. The bands at 464, 393, and 367 cm^{-1} in the sample from ingot 4 are the $\left(Si_{Ga} - Si_{As} \right)$ bands mentioned earlier and listed in Table I. A principal difference between the samples of Fig. 3 and Fig. 1 is the change in the relative strengths of the Si_{Ga} and Si_{As} bands at 384 and 399 cm^{-1}. The absorption peak values less background for these bands of the silicon plus tellurium samples of Fig. 3 are shown as circles on Fig. 2 and labeled with the ingot number. The effect of the tellurium has been to substantially enhance the fraction of the [Si] which resides on arsenic sites. More extensive measurements should give results which can be compared with thermodynamic predictions.

The most interesting results are obtained from samples
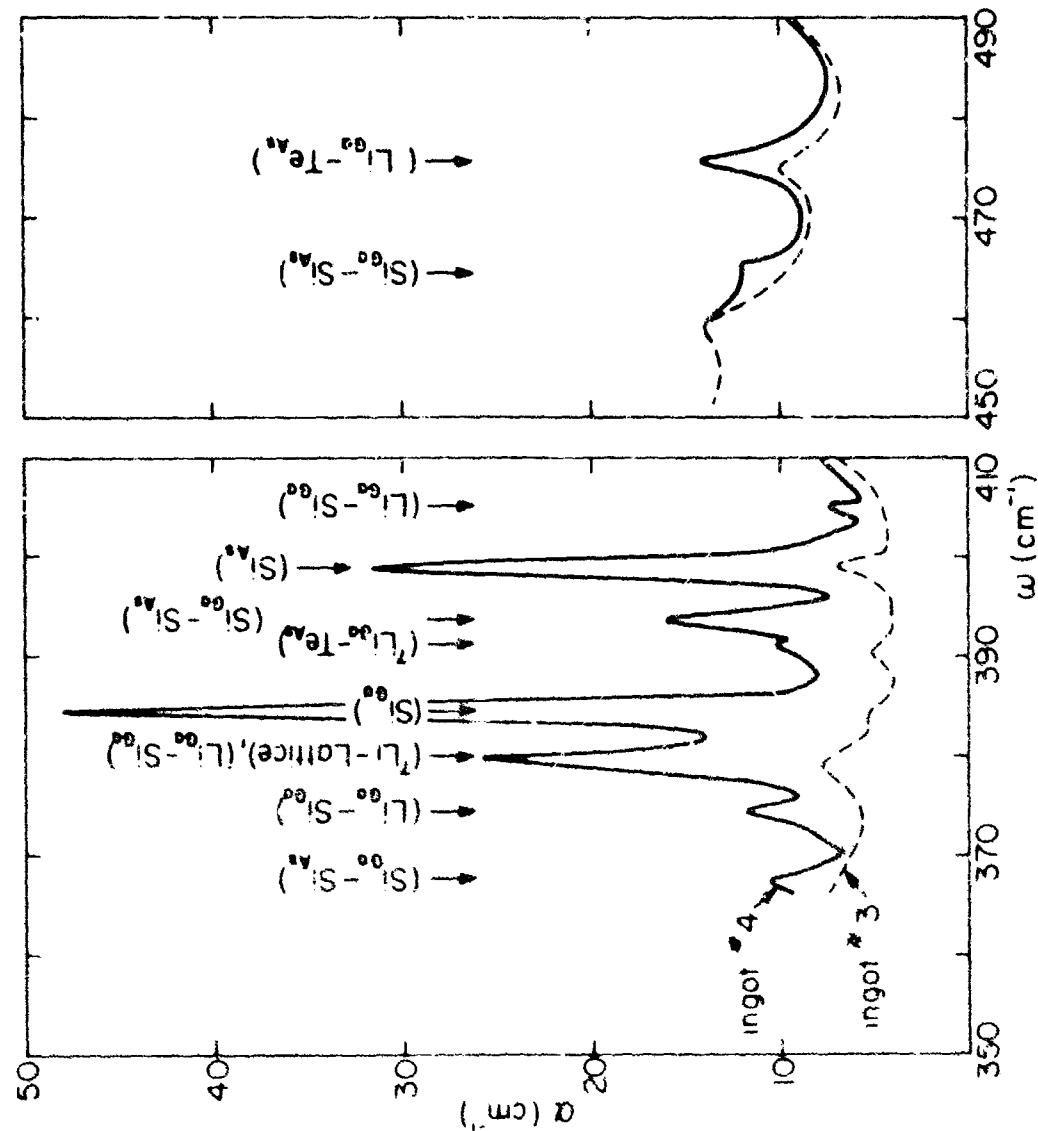
Fig. 3. Liquid nitrogen absorption of ingots 3 and 4 of Table II. The samples are doped with silicon and tellurium and diffused with lithium.

taken from ingots 5, 6, and 7 which were doped with silicon plus zinc.

Figure 4 shows the absorption for several samples diffused with ^{7}Li.

Figure 5 shows, for each of two ingots, a comparison of two samples

taken from adjacent wafers and diffused with ^{7}Li and ^{6}Li respectively.

From previous studies[8] of zinc-doped and lithium compensated samples

it is known that there are four lithium bands, presumably associated with

(Li-Zn) pairs. These bands are nearly equal for a given [Zn] and are

located at 405, 378, 361, and 340 cm^{-1} for ^{7}Li and at 433, 404, 385,

and 361 cm^{-1} for ^{6}Li. Many of these bands are observed in Figs. 4 and

5 and are taken into account in some of the quantitative discussion which

will follow.

The Si$_{As}$ acceptor band at 399 cm^{-1} is observed only in the

most lightly zinc-doped ingot (5). Within experimental accuracy this

band is totally absent in Fig. 4 from the samples of ingots 6 and 7. We

also note from Figs. 4 and 5 that the (Si$_{Ga}$ - Si$_{As}$) bands are totally absent

(at 464, 393, and 367 cm^{-1}) in the heavily zinc-doped ingots. Moreover,

several of the samples show the appearance of three new bands of

approximately equal strength. These bands are at 395, ~382, and 378

cm^{-1}.

The 378 cm^{-1} band requires some discussion. In Fig. 5,

the band at 378 cm^{-1} could involve contributions from 3 absorption bands

seen in previous work. In GaAs with (^{7}Li-Zn), there is a band at 378

cm^{-1}, but it should be equal in strength to the (^{7}Li-Zn) band at 405 cm^{-1}.

There is also a (^{7}Li-lattice) defect band at 379 cm^{-1} which could be

-22-
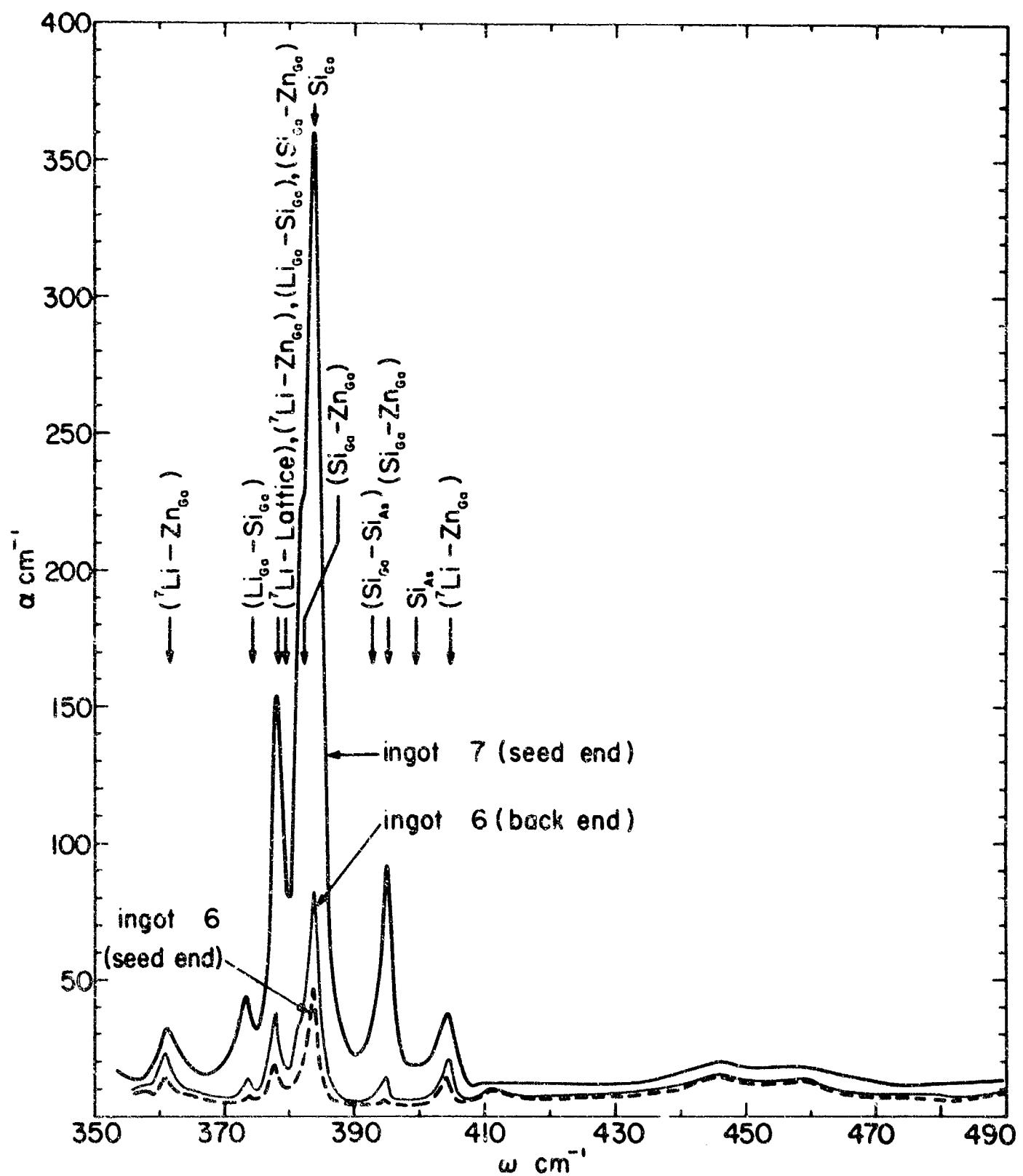
Fig. 4. Liquid nitrogen absorption of silicon and zinc doped samples from ingots 6 and 7 of Table II.
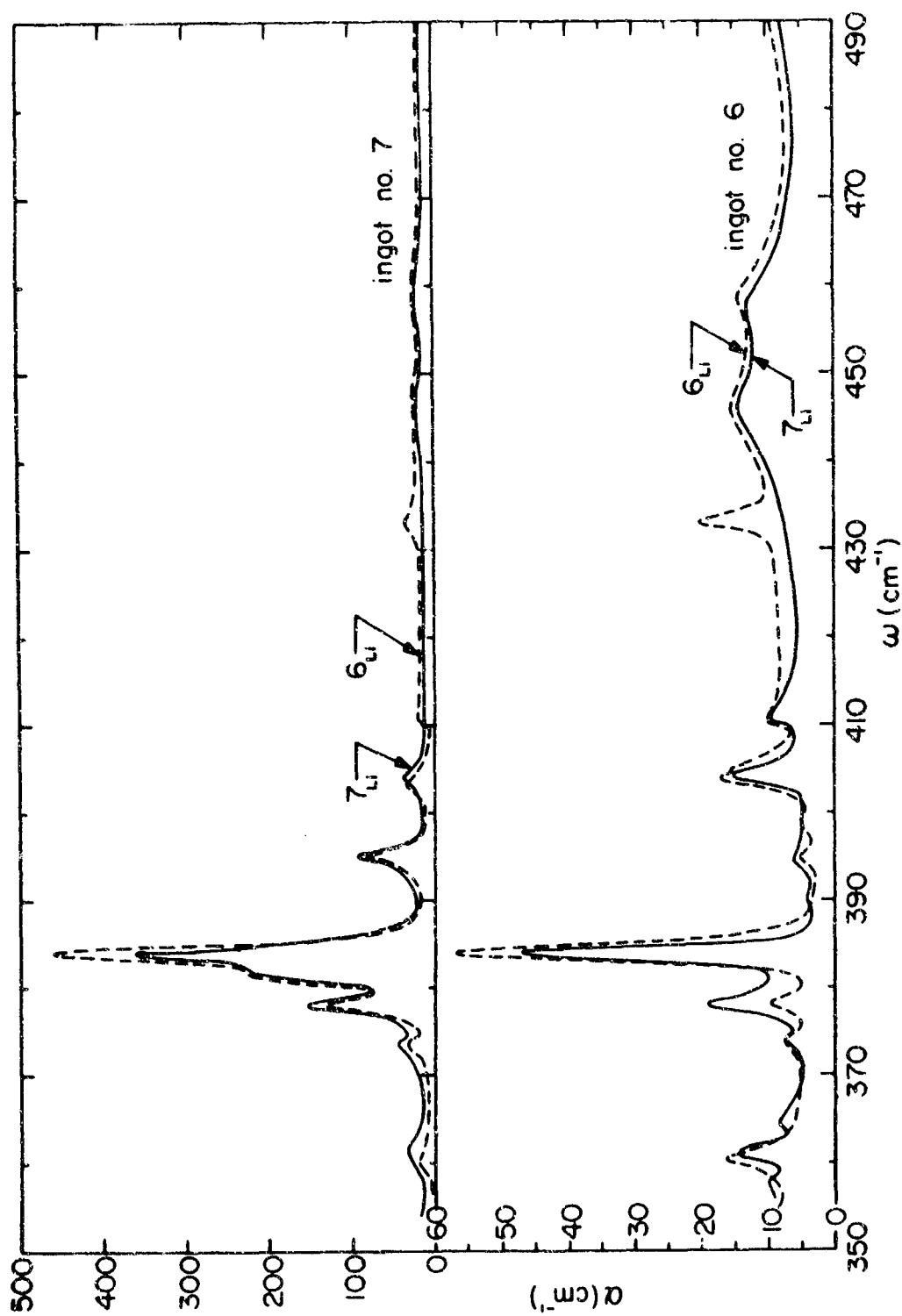
Fig. 5. Comparison of the liquid nitrogen absorption of ^{6}Li and ^{7}Li diffused samples from ingots 6 and 7 of Table II.

contributing. However, both the (^{7}Li-lattice) and the (^{7}Li-Zn) bands shift to near 405 cm^{-1} if ^{6}Li is used. Comparison of the ^{7}Li and ^{6}Li samples of ingot 7 in Fig. 5 shows little change in the 378 cm^{-1} band. The remaining previously known contribution to the absorption near 378 cm^{-1} comes from a 379 cm^{-1} silicon mode for (Si_{Ga} - Li_{Ga}) defect (see Table I). However, this contribution should only be as large[6] as the much weaker band at 374 cm^{-1} (see Fig. 5, ingot 7). Therefore, we have the result that most of the strength of the 378 cm^{-1} band of ingot 7, Fig. 5 cannot be accounted for in terms of any of the previously known defects.

The enhanced strength of the 378 cm^{-1} band occurs only in those cases where the 395 and 382 cm^{-1} bands are also observed. The three new bands do not show any lithium isotope shift, and they occur only in samples with large [Si_{Ga}] and [Zn_{Ga}]. It is reasonable to assume that these new bands arise from (Si_{Ga} - Zn_{Ga}) defects where the silicon and zinc are on nearest neighbor gallium sites (second neighbor positions). or such a pair, the axis is < 110 > and, as discussed for (Si_{Ga} - Li_{Ga}), the three fold degeneracy of the tetrahedral potential will be completely lifted. Since the mass, M(Zn) = 65, is close to the M(Ga) = 70 which it replaces, we expect to see only three silicon modes split in frequency about the Si_{Ga} band. Application of the frequency rule given previously yields

$$\omega = \left\{ \frac{1}{3} \left[(395)^2 + (382)^2 + (378)^2 \right] \right\}^{\frac{1}{2}} = 384.\frac{5}{-} \text{ cm}^{-1} \ .$$

-25-

This result is in good agreement with the 384 cm^{-1} value for the Si$_{Ga}$ band.

The concentration of (Si$_{Ga}$ - Zn$_{Ga}$) may be crudely estimated as follows: It is assumed that the total absorption cross section for the (Si$_{Ga}$ - Zn$_{Ga}$) bands is the same as that for the Si$_{Ga}$ band, i.e., the only effect of the zinc has been to lift the degeneracy of Si$_{Ga}$ but the total absorption per center is unchanged. Then, $\dfrac{[\text{Si}_{Ga} - \text{Zn}_{Ga}]}{[\text{Si}_{Ga}]} = \dfrac{\alpha_{395} + \alpha_{382} + \alpha'_{378}}{\alpha_{384}}$. The prime on α'_{378} is to specify that the other sources of absorption at that frequency have been already subtacted. From other studies[5,6] it is known that the absorption cross section for the 384 cm^{-1} band is given by $\alpha_{384}/[\text{Si}_{Ga}] \simeq 7.3 \times 10^{-18}$ cm^2. Thus [Si$_{Ga}$ - Zn$_{Ga}$] for the ingot 7 samples of Fig. 5 is $\sim 3 \times 10^{19}$ cm^{-3} and [Si$_{Ga}$] $\sim$ 4-5 $\times 10^{19}$ cm^{-3}. The total silicon concentration of 7-8 $\times 10^{19}$ cm^{-3} compares favorably with the doping estimate of $\sim 6 \times 10^{19}$ cm^{-3} given in Table II. The total zinc concentration of ingot 7 is $\sim$ 4-5 $\times 10^{19}$ cm^{-3}. This concentration includes both [Zn$_{Ga}$ - Si$_{Ga}$] $\sim 3 \times 10^{19}$ cm^{-3} and [Zn$_{Ga}$ - Li$_{Ga}$] $\sim 102 \times 10^{19}$ cm^{-3} as estimated from the 405 cm^{-1} and 361 cm^{-1} bands and previous published[8] α vs. [Zn$_{Ga}$ - Li$_{Ga}$] data. Again the total [Zn] is regarded as in reasonable agreement with the estimate of 3 $\times 10^{19}$ cm^{-1} given in Table II. It may also be noted that if the Zn$_{Ga}$ and Si$_{Ga}$ were randomly distributed on the gallium sublattice then the [Zn$_{Ga}$ - Si$_{Ga}$] is 10^{17} to 10^{18} cm^{-3} for these samples. This concentration is substantially smaller than the estimate given above.

The measurements of samples taken from ingot 6 and 7 have been used to obtain the points given by solid dots on Fig. 2. Recall that in these samples no detectable band was observed at 399 cm^{-1}, and thus the arrows indicate that the points have been placed at the maximum possible value for α (399 cm^{-1}). The true value is probably substantially smaller. The points indicate that for ingots 6 and 7, the $[Si_{As}]$ has been decreased by at least one order of magnitude, and a more realistic estimate gives $\sim$ two orders of magnitude for a given $[Si_{Ga}]$. Although not plotted in Fig. 2, a comparison of Fig. 1 with Figs. 4 and 5 gives a similar conclusion for $[Si_{Ga} - Si_{As}]$.

It is reasonably clear that studies of silicon site distribution as functions of $[Si]$, $[Te]$, and $[Zn]$ should lead to quantitative estimates of distribution coefficients and the dependence of specific defects on impurity concentrations. Moreover, correlations with electrical measurements should yield information on the electrical nature of each of the defects. This work is now being carried out.

References

1. J. M. Whelan, J. D. Struthers, and J. A. Ditzenberger, Proc. International Conference on Semiconductors (Czechoslovak Academy of Science, Prague, 1960), p. 943.

2. C. Kolm, S. A. Kulin, and B. L. Averbach, Phys. Rev. 108, 965 (1957).

3. H. J. Queisser, J. Appl. Phys. 37, 2909 (1966).

4. O. G. Lorimor and W. G. Spitzer, J. Appl. Phys. 37, 3687 (1966).

5. W. G. Spitzer and W. Allred, Appl. Phys. Letters 12, 5 (1968).

6. W. G. Spitzer and W. Allred, to be published, J. Appl. Phys.

7. The highest phonon frequency of the pure GaAs is ~ 295 cm^{-1} --see M. Hass, Semiconductors and Semimetals, Vol. 3, edited by R. K. Willardson and A. C. Beer, Academic Press, New York, 1967, p. 3.

8. O. G. Lorimor and W. G. Spitzer, J. Appl. Phys. 38, 3008 (1967).

9. R. J. Elliott and P. Pfeuty, J. Phys. Chem. Sol. 28, 1627 (1967).

10. M. Levy and W. G. Spitzer, J. Appl. Phys. 39, 1914 (1968).

11. R. K. Willardson and W. P. Allred, Proc. International Symposium on Gallium Arsenide (Institute of Physics and the Physical Society, Reading, 1966), p. 35.

12. O. G. Lorimor and W. G. Spitzer, J. Appl. Phys. 38, 2713 (1967).

1.1.3 Thin Film and Interface Phenomena

AF-AFOSR-496-67, Joint Services Electronics Program

C. R. Crowell

A program of device-oriented studies related to current transport and charge storage in metal-semiconductor (Schottky) contacts.

1.1.3.1 Surface State and Interface Effects on the Capacitance-Voltage Relationship in Schottky Barriers

C. R. Crowell and G. I. Roberts

The analysis given in the previous report has been completed and submitted for publication. A further modification gives the relationship between the surface state charge density, σ, in zero temperature approximation and for a finite temperature T. The precise result is shown to be

$$
\frac{d\sigma}{dE_f} = q \left[n_{ss}(E_f) + \frac{\pi^2}{12} (kT)^2 \left. \frac{d^2 n_{ss}}{dE^2} \right|_{E_f} + \theta T^4 + \ldots \right]
$$

where $n_{ss}(E_f)$ is the surface state density per unit area per unit energy at the Fermi energy E_f. Thus as long as the curvature of the n_{ss} versus E relationship at the Fermi energy is small compared with $n_{ss}(E_f) |kT|^2$, the zero temperature approximation will be satisfactory.

The results of this analysis will be used as a tool for further experimental studies of surface states in metal semiconductor systems.

1.1.3.2   Thermionic-Field Resistance Maxima in Metal-

Semiconductor (Schottky) Barriers

C. R. Crowell and V. L. Rideout

A maximum in the differential resistance versus applied bias relationship of metal-semiconductor contacts is predicted to occur when current flow is predominantly by thermionic-field (thermally excited tunnel) emission. The predicted resistance peaks are generally asymmetrical with respect to voltage and may occur on either side of zero bias. The peak location has only an indirect correlation with the Fermi kinetic energy in the semiconductor. The theoretical approach is generally applicable to any metal-semiconductor system when the dominant carrier flux is associated with the tail of a Fermi-Dirac distribution. The theory is in reasonable agreement with recent experimental resistance measurements on Cr-Si Schottky barrier diodes at 77°K.

Anomalies in the differential resistance versus applied bias relationship near zero bias have been observed in p-n junctions[1-5], metal-insulator-metal[6-8] or semiconductor[9-12] structures, and metal-semiconductor (Schottky) barriers[13-19]. In addition Gray[9], Esaki and Stiles[10], and Chang[20] have used the WKB tunneling approximation for the insulator barrier to calculate the incremental resistance of metal-insulator-semiconductor structures. Stratton and Padovani[21] have similarly applied the WKB expression to Schottky barriers. The present report is concerned with the differential resistance associated with

thermionic-field (thermally excited tunnel) emission currents in metal-semiconductor contacts.

Recently Crowell and Rideout[22] (C-R) have analyzed the thermionic-field current-voltage characteristics of Schottky barriers in a normalized formulation which uses the WKB tunneling approximation. From consideration of the principles of detailed balance and reciprocity of tunneling coefficients, C-R showed that the current density, J, versus applied bias, V_f, relationship for thermionic-field emission (i.e., current flow dominated by the Maxwell-Boltzmann tail of Fermi-Dirac distributions in both semiconductor and metal) is of the form

$$J = J_s \exp (qV_f/nkT)[1 - \exp (-qV_f/kT)] \qquad (1)$$

(cf., equation (23) of C-R). J_s is the saturation current density and $n \equiv (q/kT) \, dV_f/d\ln J_f$, where J_f is the forward component of the carrier flux ($J_f \approx J$ for $V_f \gg kT/q$). Equation (1) will not, however, be valid when pure field emission becomes dominant at high semiconductor carrier density and low temperatures. Band-tailing density of states effects[13-15], many body electron-polaron interactions[16] and phonon excitations[17,18] ha e been proposed as responsible for resistance anomalies observed in metal-degenerate semiconductor contacts. Although such effects are not considered per se in this report, equation (1) is generally applicable to any metal-semiconductor contact when the dominant carrier flux is associated with the tail of a Fermi-Dirac distribution.

-31-

From equation (1) the incremental resistance, $R \equiv dV_f/dJ$, normalized by the incremental resistance at zero bias, $R_o = kT/qJ_s$, is

$$R/R_o = n \exp(-qV_f/nkT)[1 + (n-1)\exp(-qV_f/kT)]^{-1} . \qquad (2)$$

The applied voltage, V_{fm}, at which a resistance maximum (conductance minimum) occurs (i.e., when $d^2J/dV_f^2 = 0$) is

$$V_{fm} = (2kT/q) \ln(n-1) . \qquad (3)$$

In equations (2) and (3) we have assumed that there is only a slow variation of the parameters J_s and n with V_f.

Figure 1 shows the normalized incremental resistance, R/R_o, as a function of the normalized applied voltage, qV_f/kT, for selected values of n (cf. equation (2)). The pip mark on each curve indicates the value of qV_{fm}/kT (cf. equation (3)). In general the resistance peaks do not occur exactly at zero bias nor are they symmetrical with respect to qV_f/kT. Equation (2) does, however, have the following symmetry characteristics: a curve with a maximum at some negative value of V_f and defined by $n = n_-$ has a mirror image reflected in the zero bias line at $n = n_+$ where $1/n_- = 1-1/n_+$ (cf. Figure 1). For values of $n > 2$ the metal-semiconductor contact behaves like a backward diode. When $n = 2$ the resistance peak is symmetrical about zero bias:

$$R/R_o \big|_{n=2} = [\cosh(qV_f/2kT)]^{-1} . \qquad (4)$$

-32-
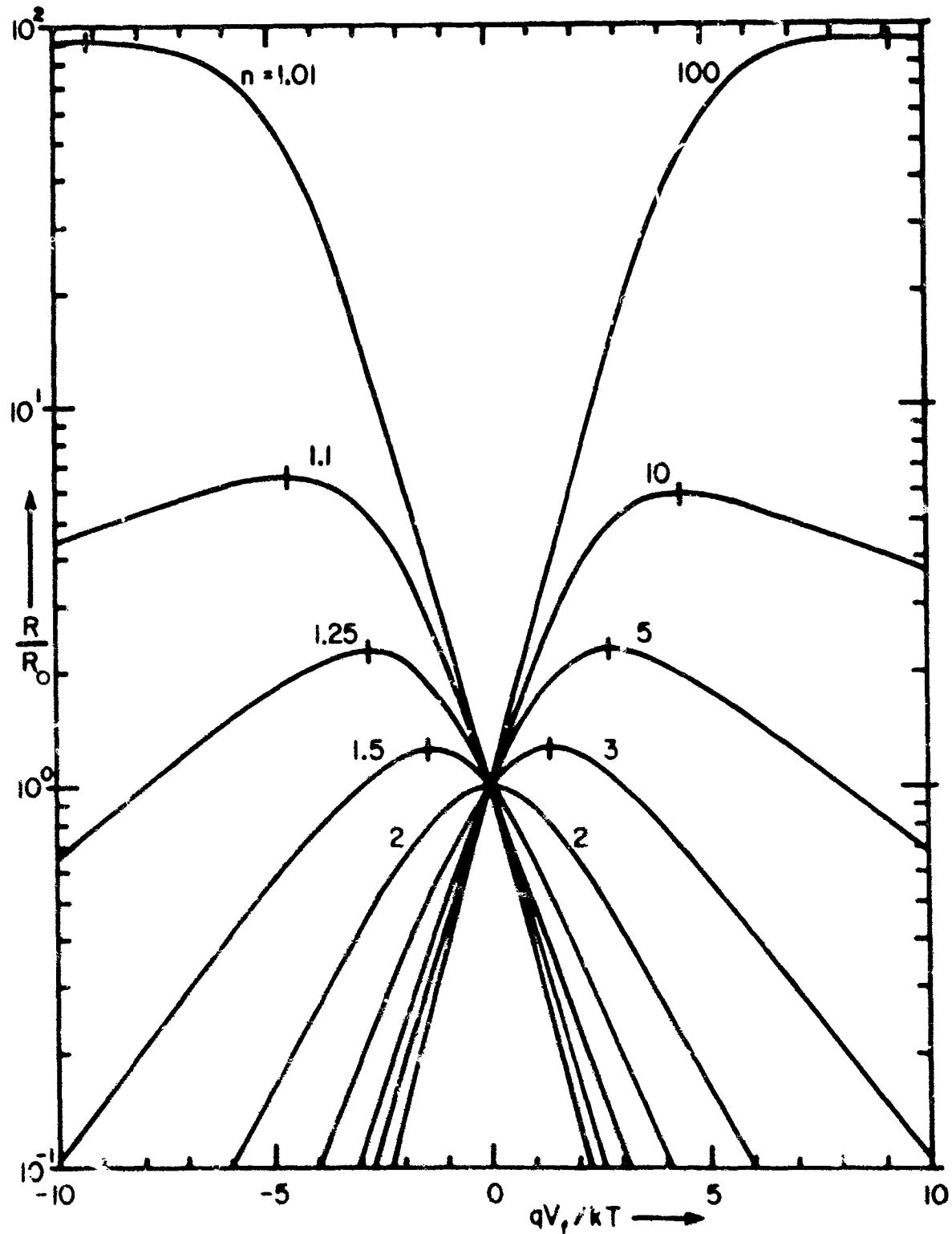
Fig. 1. Normalized incremental resistance R/R_o versus normalized applied bias qV_f/kT for selected diode n values. The pip mark on each curve indicates the position of the resistance maximum as defined by equation (3). Note that each curve has an image reflected across the zero bias line.

Once any experimental R-V_f characteristic has been fitted to equation (2), the subsequent degree of agreement with any detailed theory of thermionic-field emission depends upon the accuracy with which the parameters n and R_o (or J_s) can be correlated with other measurements. C-R have calculated n and J_s as a function of kT/E_{oo} with normalized bandbending E_b/kT as parameter (cf. Figures 6 and 7 of C-R). The term E_{oo}, a constant of the material[16,23], is associated with the one-dimensional single-particle WKB expression for the transmission of the barrier for carriers at the bottom of the conduction band (cf. equation (8) of C-R):

$$E_{oo} = (qh/4\pi)(N/m^*\epsilon)^{\frac{1}{2}} = 18.5 \times 10^{-12}(N/m_r\epsilon_r)^{\frac{1}{2}} \text{ eV} , \tag{5}$$

where N is the semiconductor doping concentration in units of cm^{-3}, m_r the tunneling effective mass measured in units of the free electron mass, and ϵ_r the semiconductor static dielectric constant. The bandbending in the semiconductor depletion region in units of kT is

$$E_b/kT = (q/kT)(\varphi_b - \varphi_s - V_f) , \tag{6}$$

where φ_b is the metal-semiconductor barrier height, and φ_s is the difference between the semiconductor Fermi level and the bottom of the conduction band (φ_s is negative for degenerate semiconductors). The quantity kT/E_{oo} determines the magnitude of the kinetic energy relative to the bandbending E_b at which the maximum injection of carriers through

the barrier occurs (cf. equation (14) and Figures 3 and 4 of C-R). Thus kT/E_{oo} indicates whether the predominant character of the current flow is thermionic, thermionic-field, or field emission.

Figure 2, deduced from Figures 7 and 11 of C-R, shows the close correlation of the diode n value with kT/E_{oo}. Larger values of n and J_s would be predicted from theories which added effects of image force lowering[24], a two band model for the complex k portion of the E-k relationship[15,25], an interfacial layer between the metal and the semiconductor[26,27], or an increased semiconductor surface doping. For resonant tunneling phenomena[12], n and R_o are sufficiently strong functions of V_f that equation (1) should not be expected to be an appropriate form for analysis of the experimental data. It would also not be desirable to apply the C-R analysis to cases where $(n-1) \leq 0.02$ for which image force lowering is important[24], or where n >> 1 for which field emission is dominant. C-R have derived criteria for the bias range for the transition from thermionic-field emission to field emission. For reverse bias voltages less than V_{r-max}, the maximum of the energy distribution of emitted carrier flux occurs above the Fermi level in the metal:

$$V_{r-max} \approx \varphi_s + \varphi_b \sinh^{-2}(E_{oo}/kT) \ . \tag{7}$$

For degenerate semiconductors a corresponding maximum forward bias voltage is given by

$$V_{f-max} = V_{r-max} \sinh^2(E_{oo}/kT) \ . \tag{8}$$

-35-
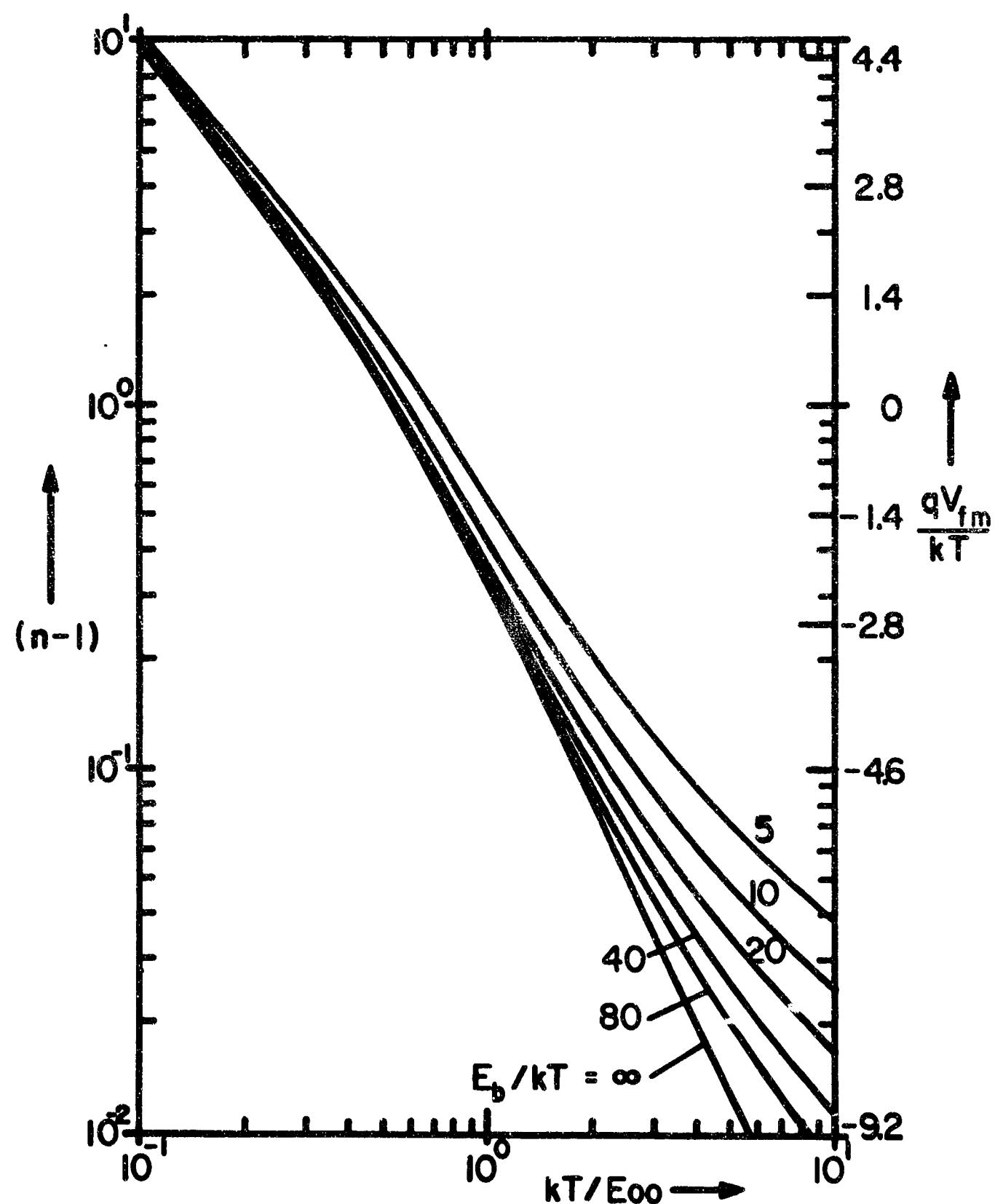
Fig. 2. Barrier constant (n-1) versus normalized materials parameter kT/E_{oo} for selected values of the normalized bandbending E_b/kT. The right hand ordinate indicates the bias in units of kT/q for occurance of the resistance maximum.

-36-

Saxena has recently measured the incremental resistance in the neighborhood of zero bias for Cr n-type Si Schottky diodes under conditions where appreciable contributions from T-F emission could be anticipated. His experimental data at 77°K are shown in Figure 3. From equation (2) $n \approx (-q/kT)dV_f/d \ln R$ for $qV_f/kT \gg 1$. From Saxena's data we obtain a value for n of 5.7. For $E_b/kT \approx 90$ and $n = 5.7$, Figure 2 gives $kT/E_{oo} = 0.18$ which corresponds to $N = 1.2 \times 10^{19} cm^{-3}$ at 77°K (cf. equation (5)). The bulk doping concentration of the Si used by Saxena as determined from Hall coefficient measurements was $N_{Hall} = 7 \times 10^{18} cm^{-3}$. The doping concentration throughout the wafer may of course differ from the average measured by the Hall effect. In addition, the local surface doping concentration may be different from N_{Hall}. Also it is possible that the Cr-Si diodes contain an interfacial layer which has resulted in an increased diode n value.

When R_o and n of equation (2) are chosen to match Saxena's data for $V_f \gg kT$ as shown by the dashed line in Figure 3, the experimental data are matched at the peak of the T F curve. This occurs at $qV_{fm}/kT = 3.1$. The barrier height associated with the value of R_o is 0.61 eV, in agreement with that typically observed by Saxena for diodes of low doping concentration. The value of the barrier height used by Padovani and Stratton is not known. The disagreement at low bias between Saxena's experimental data and the prediction of the T-F model of C-R is expected since the criteria for T-F emission implied by equations (7) and (8) can only be satisfied by non-zero V_{r-max} and V_{f-max}
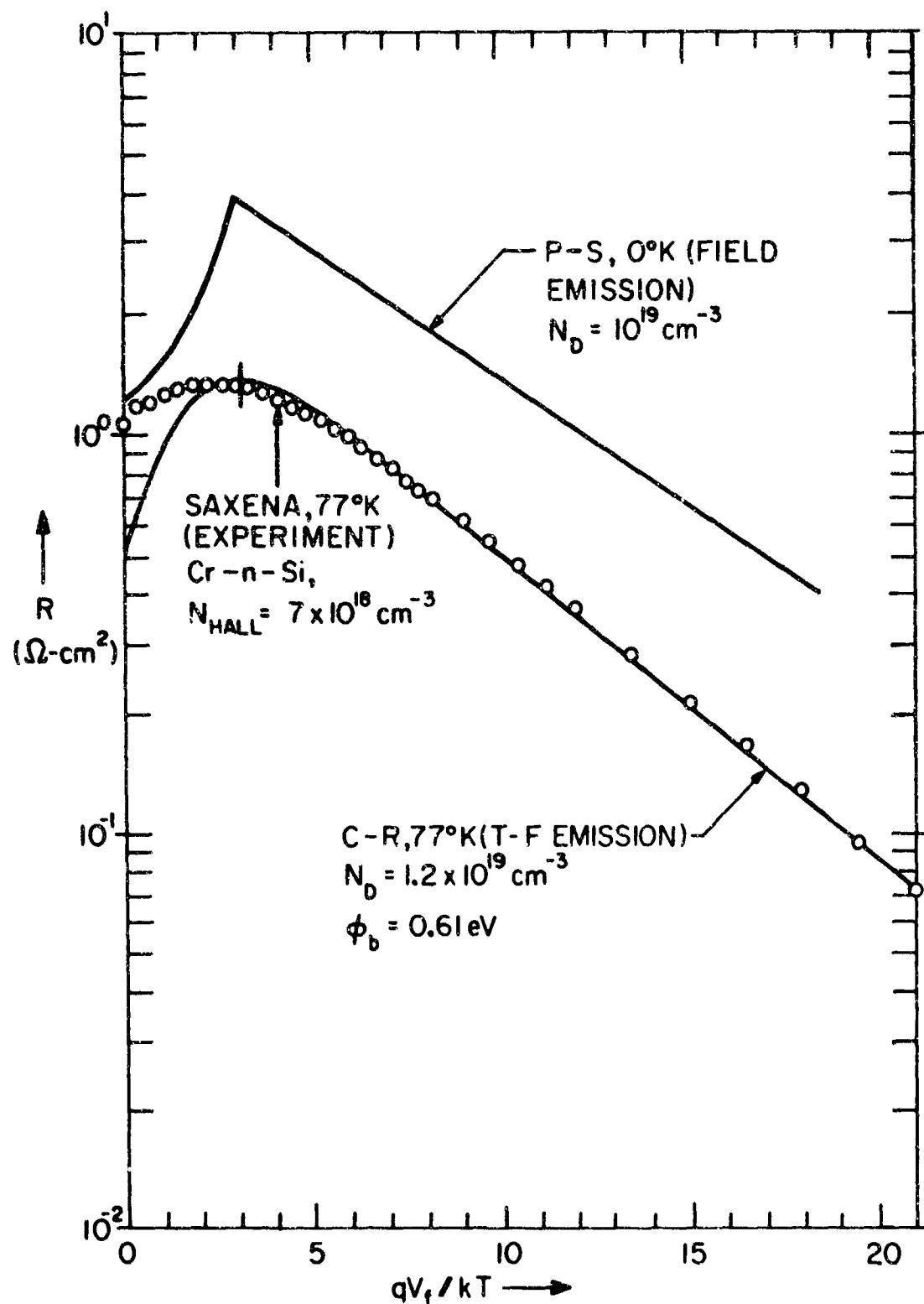
Fig. 3. Differential resistance versus forward bias in units of kT/q. The experimental data of Saxena are compared with the T-F emission theory of Crowell and Rideout (C-R) and the field emission theory of Padovani and St·atton (P-S).

above 120°K (assuming that $N_{Hall} = 7 \times 10^{18} cm^{-3}$ is the appropriate doping). A sufficiently large percentage of the tunnel current flux arises from carriers above the Fermi energy that the form of equation (3) is a good approximation for moderate forward bias. The experimental curve near zero bias is unquestionably characteristic of Fermi-Dirac distributions. Note that the T-F emission theory fits as well at 77°K as the zero temperature calculation of Padovani and Stratton[23]. The shapes of the $R-V_f$ characteristics for the two models are even remarkably similar considering that the Maxwell-Boltzmann approximation in the model of C-R does not contain the inflection point in the occupation probability at the Fermi level. It is apparent that measurements similar to those of Saxena over a wide range of temperature and semiconductor doping would be of interest.

We wish to thank Dr. A. N. Saxena for permission to quote his experimental results prior to publication.

References

1. R. N. Hall, J. H. Racette, and H. Ehrenreich, Phys. Rev. Lett. 4, 457 (1960), R. N. Hall and J. H. Racette, J. Appl. Phys. 32, 2078 (1961).

2. R. A. Logan and J. M. Rowell, Phys. Rev. Lett. 13, 404 (1964).

3. R. M. Williams and J. Shewchun, Phys. Rev. Lett. 14, 824 (1965). ibid. Phys. Rev. Lett. 15, 160 (1965).

4. R. T. Payne, Phys. Rev. 139, A570 (1965), ibid. Phys. Rev. Lett. 21, 284 (1968).

5. B. M. Vul, E. I. Zavaritskaya, and N. V. Zavaritsky, J. Phys. Soc. Japan, Kyoto Conference Supplement, 21, 598 (1966).

6. A. F. G. Wyatt, Phys. Rev. Lett. 13, 401 (1964).

7. A. F. G. Wyatt and D. J. Lythall, Phys. Lett. 25A, 541 (1967), ibid. Phys. Rev. Lett. 20, 1361 (1968).

8. J. M. Rowell and L. i. L. Shen, Phys. Rev. Lett. 17, 15 (1966), ibid. Phys. Rev. 165, 566 (1968).

9. P. V. Gray, Phys. Rev. Lett. 9, 302 (1962), ibid. Phys. Rev. 140, A179 (1965).

10. L. Esaki, J. Phys. Soc. Japan, Kyoto Conference Supplement, 21, 589 (1966), L. Esaki and P. J. Stiles, Phys. Rev. Lett. 16, 1108 (1966).

11. J. Shewchun, A. Waxman and G. Warfield, Solid-St. Electron. 10, 1187 (1967), ibid. 10, 1165 (1967).

12. E. L. Wolf, Phys. Rev. Lett. 20, 204 (1968).

13. J. W. Conley, C. B. Duke, G. D. Mahan, and J. J. Tiemann, Phys. Rev. 150, 466 (1966).

14. J. W. Conley and J. J. Tiemann, J. Appl. Phys. 38, 2880 (1967).

15. G. D. Mahan and J. W. Conley, Appl. Phys. Lett. 11, 29 (1967).

16. J. W. Conley and G. D. Mahan, Phys. Rev. 161, 681 (1967).

17. C. B. Duke, S. D. Silverman, and A. J. Bennett, Phys. Rev. Lett. 19, 315 (1967).

18. W. Salaneck, Y. Sawada, E. Burstein, and R. Payne, Solid-St. Comm. 5, xi (1967).

19. A. N. Saxena, to be published.

20. L. L. Chang, J. Appl. Phys. 39, 1455 (1968).

21. R. Stratton and F. A. Padovani, Solid-St. Electron. 10, 813 (1967).

22. C. R. Crowell and V. L. Rideout, Solid-St. Electron. , to be published.

23. F. A. Padovani and R. Stratton, Solid-St. Electron. 9, 965 (1966).

24. S. M. Sze, C. R. Crowell and D. Kahng, J. Appl. Phys. 35, 2534 (1964).

25. F. A. Padovani and R. Stratton, Phys. Rev. Lett. 16, 1202 (1966).

26. C. R. Crowell, H. B. Shore and E. E. LaBate, J. Appl. Phys. 36, 3842 (1965).

27. C. R. Crowell and S. M. Sze, Solid-St. Electron. 9, 1035 (1966).

1.1.4 Radiative Recombination in Semiconductors

NGR-05-018-044, National Aeronautics and Space

Administration

GKF 1764, National Science Foundation

AF-AFOSR-496, Joint Services Electronics Program

DA-ARO-D-31-124-G1054, U.S. Army Research Office,

Durham

M. Gershenzon

General Objectives

1. To determine the mechanisms of radiative and of non-radiative

   recombination, particularly in wide band-gap semiconductors.

2. To correlate extrinsic recombination processes with the defects

   responsible for them.

3. To survey a number of relatively unexplored wide band-gap

   materials, seeking efficient luminescence mainly in the visible

   spectrum.

4. To study competing recombination processes as a function of

   temperature.

5. To investigate luminescent devices where the minority carriers are

   created by electrical injection.

Progress and Plans

1. GaN

   In the last report we described various vapor transport

methods which produced small crystallites of GaN and indicated the feasibility of epitaxial deposition. In order to grow larger platelets required for the optical work we attempted to reduce the growth variables by using the material grown previously as the source in a closed-tube halide (chloride)disproportionation vapor transport technique. After optimizing temperatures, temperature gradients and halide concentration to yield relatively large crystals, it was discovered that these were in reali β Ga_2O_3 rather than GaN which was introduced as a contaminant in the source material. Thus we have recently prepared uncontaminated source material by a direct open tube liquid $Ga-NH_3$ reaction and are repeating the optimization process for single crystal preparation via the closed tube halde transport process.

Our future plans remain the same as before, namely the study of the optical, electrical and luminescent properties of the "pure" material as well as the effects of doping with elements which should act as shallow donors or acceptors or as luminescent centers.

2. AlP

In the last report we described a closed tube iodide transport method which transported AlP source material obtained by several methods very rapidly. Now this process has been optimized to some extent $(T = 1100^\circ, \Delta T - 40^\circ)$ to produce flat ribbons and whiskers up to 1 cm in length These are large enough for luminescence measurements but too narrow for absorption work. The student working on this project

-43-

has left the laboratory. Hence this project will be delayed until a
replacement is found for him.

3. Si

Our plans to look for isolated donor-acceptor pair recombi-
nation emission lines are proceeding. Double doped (B, P) Si ingots
were grown as described in the last report. A high resolution grating
spectrometer (Perkin-Elmer E1) is being calibrated and equipped for
photoluminescence measurements aimed at measuring and optimizing
the broad, distant donor-acceptor pair band at 4.2^{o}K prior to exciting
a high power CW GaAs laser in the attempt to saturate the distant pairs
and allow the closer, isolated pair lines to be obse. ed.

4. ZnS: Cu

We hope to elucidate the mechanism of the very efficient
green emission of Cu activated ZnS at room temperature by exciting this
emission at 4.2^{o}K with very high intensity radiation in its characteristic
excitation absorption band and looking for any changes in the emission
spectrum, notably the possible appearance of lines. A pulsed molecular
N_2 laser (average cw power 100 mw) whose output wavelength matches the
excitation band very well has been set up. ZnS crystals obtained from
various sources are being doped with Cu and as co-activator Al or a halide.
A quartz prism monochromator (Perkin-Elmer Model 99) was calibrated
and is being used for photoluminescence measurements to establish the
presence and efficiency of the Cu-green emission. It is planned to
excite the efficient samples with the focussed laser beam looking for

-44-

sharp lines in the time resolved spectra using a high resolution grating instrument (Bausch and Lomb, 2 Meter) and integrating the signal either via photographic recording or via a photomultiplier and a boxcar integrator.

5. Cubic ZnS

We have obtained some platelets of ZnS having large areas of the zincblende structure which are relatively free of stacking faults. We hope to study the absorption edge and luminescence due to free exciton, bound exciton and "edge emission" in such cubic crystals utilizing the high resolution capabilities of the Bausch and Lomb spectrograph and invoking uniaxial stress and Zeeman splittings where possible. For this work a quartz dewar is being constructed with capabilities for absorption, photoluminescence and photoexcitation work in conjunction with the high resolution spectrometer.

1.1.5 Electron Tunneling in Solids

R. T. Payne

Our technology has produced a large number of electronic solid state devices which rely on the quantum mechanical phenomena of tunneling (the ability of a particle to go through a barrier rather than over it). Typical examples of these devices are p-n diodes, Esaki or Tunnel diodes, Schottky diodes, Gunn Effect oscillators, MOS or Cold Cathode structures, superconducting junctions, and Josephson junctions.

Previous work by the author indicated that by using low temperatures, high magnetic fields, and high pressures, these electron tunneling devices could be used as probes to study the properties of the solid lattice and properties of the electron gas in the solid. Other investigators have shown potential uses for these devices in a variety of fields, such as microwave spectroscopy, ultrasonics, infrared spectroscopy, and low energy electron spectroscopy.

In October 1966, the Electron Tunneling Laboratory was established to use these electron tunneling devices in the study of the fundamental properties of solids, solid surfaces, and general physics. The laboratory will eventually have facilities for high magnetic fields (100 kilo=oersted), high pressure (60,000 psi), and low temperatures (1.0°Kelvin). It will require a variety of measuring devices, a multiple-derivative plotter, a susceptibility bridge, microwave sources, receivers and frequency standards, a nano-volt potentiometer and

-46-

voltage references.

To date, the multi-derivative plotter, high pressure system (45,000 psi), low temperature system to ' $3^{O}K$, medium duty evaporator, and cold cathode sputtering module have been put into operation. These systems are being used in the research to be discussed in the following sections.

1.1.5.1   Study for a Measurement of Galactic and Stellar

Emission Spectra in the 500 Micron Region. Part II

NGL-05-018-044 Suppl. #2, National Aeronautics

and Space Adminstration

R. T. Payne and F. Schrey

This is a contract to study wide band detectors for use in the 500 micron region. One such detector is a Josephson Junction. Since transition metal alloys provide the highest transition temperature for the Josephson effect these materials are under study. Before the contract period (1 July 1968-) it was decided to terminate study on Nb_3Sn because the preparation of the alloy sputtering source was unsuitable. Apparently, the composition of the alloy was not close enough to the Nb_3Sn crystal phase to produce superconducting films. Further, the shape of the source made it difficult to use. Examination of the material is in progress.

At the beginning of the contract period a tantalum metal source was obtained for sputtering experiments at R. D. Mathis Co.

-47-

Mr. Schrey commuted (and still does) to the company to sputter tantalum films on glass substrates for study. The resulting films look satisfactory and have resistivities close to that of the bulk material. Cryogenic tests of these films are in progress. A V_3Ga metal source which has been on order since April should be arriving soon. This source will be used to study the sputtering of alloy films in place of the Nb_3Sn.

1.1.5.2 Excitonic Insulators in Semiconductor Junctions
AF-AFOSR-496-67, Joint Services Electronics
Program
R. T. Payne

The excitonic insulator is a many body state similar to that of a superconductor. The author discovered the state while investigating the properties of semiconductor junctions. Experiments are still in progress to discover the transition temperature dependence on pressure, carrier concentration, and impurity atoms.

Another possible material for study is chromium. During the summer preliminary tests on chromium junctions were made. No results have been obtained to date. Further experiments are being encouraged at the Naval Ordinance Laboratory at China Lake, California.

1.1.5.3 A 100 Kilo-oersted Superconducting Magnet Facility

AF-AFOSR-496-67, Joint Services Electronics

Program

M. H. Halloran and R. T. Payne

The superconducting magnet facility has been started jointly with M. H. Halloran. A magnet has been ordered which is capable of producing a 100 Kilo-oersteds with a homogeneity of 4 parts in 10^4 in a 1 cm. sphere, a stability of 1 part in 10^5 and a total working volume of 3.810 cm. in diameter. Using this facility, experimental research will be pursued in the general area of electronic properties of metals and degenerate semiconductors at low tempe ture.

The specific scientific goals of this research are five-fold: to obtain complete Fermi surface information for the transition metal elements and certain intermetallic compounds (Halloran), to determine whether the theoretical explanation of the large B-H effects observed in the noble metals holds true (Halloran), to determine whether the effective mass of electrons in a metal is magnetic field dependent as suggested recently on the basis of field theory consideration (Halloran), to measure pressure effects of the Fermi surface of transition metals and compare these effects with theories of critical spin fluctuations (Payne), and to study the properties of electrons tunneling through semiconductor interfaces in the presence of intense magnetic fields and high pressures (Payne).

After repeated attempts to negotiate with the suppliers of the

magnet to obtain a properly working magnet the prospective users

decided to change vendors. Negotiations are now being made with

different suppliers for the same type of magnet. All research requiring

the high magnetic field has been suspended until a new supplier is found.

1.1.5.4   Magneto-Tunneling in Semiconductors under High

Pressure

AF-AFOSR-196-67, Joint Services Electronics

Program

R. T. Payne and J. Downs

It is planned to measure magneto-tunneling, the magnetic

field dependence of the tunneling current of semiconductor p-n junctions,

in the presence of hydrostatic pressure and at low temperatures. The

change in effective mass with pressure, the change in quasi-particle

"g" factor with pressure and other properties of the semiconductor may

be derived from this experiment and compared with theory. Preliminary

measurements of Ge back diodes have been made to 32,000 psi at room

temperature. Good comparison has been made with the work of M. E.

Sikorski and P. Andreath.

The summer was spent revising the high pressure equipment.

Present operation is now extended to 45,000 psi.

1.1.5.5   Pressure Dependence of the Magnetic Susceptibility,

the Fermi Surface, and the Effective Mass of

Palladium

AF-AFSR-496-67, Joint Services Electronics

Program

R. T. Payne

It is planned to measure the magnetic susceptibility, the
effective mass, and several extremal cross sections of the Fermi surface
of palladium as a function of pressure. These measurements will be
compared with similar magnetic measurements on alloys of palladium
and with the theory of Berk and Schrieffer on critical spin fluctuations.
A better understanding of the properties of palladium and of ferro-
magnetic exchange may be obtained.

At present a palladium single crystal has been bought.
Preliminary residual resistance measurements indicate the sample is
not pure enough for the primary objective. An electron beam zone
refiner now on order will be used to further refine the palladium. In
the meantime the possibility of using pieces of the sample for tunneling
experiments are being investigated.

1.1.6 Growth of GaAs and $Ga_x In_{1-x} As$ Thin Films

L. R. Dawson, C. T. Li and J. M. Whelan

The technique has been extended for growing thin films $(1-10\mu)$ of GaAs from Ga solutions saturated with arsenic. Previous difficulties with variable surface textures have been substantially reduced by protecting the substrate during the reduction of the residual oxide film on the liquid Ga surface. Surface defects are presently limited by dislocation densities in the substrates. These are particularly pronounced for the substrate orientations, (211) and (311). Except for dislocations, these orientations are favorable for thin film growth. The relative advantages of low dislocation substrates (less than 500 cm^{-2}) oriented in the [111], [$\overline{TTT}$], [110], [311], [$\overline{311}$] and [211] directions are being presently evaluated.

Film structures containing two films have been grown. Suitable structures for bipolar transistors and Gunn oscillators have been grown. Bipolar transistors were made using a $|\mu$ n film on a semi-insulating substrate which exhibited pinch off at 0.6 V bias. An n_j^+ 10μn film structure on an n^+ substrate was operated as a Gunn oscillator.

Techniques have been developed for doping the above GaAs films with Te, Sn and Ge. Germanium presently seems to be a superior

acceptor dopant than either An or Cd. Attempts to make npn or pnp transistor structures using Zn were unsuccessful because of the Zn diffusion.

Additional facilities for growing III-V alloys are completed and are being tested with GaAs.

Evaluation of electrical contacts are in progress. Electroplated Au-Sn followed by alloying looks promising as a reliable n type contact. The alloy depth is approximately $1\,\mu$.

1.2 QUANTUM ELECTRONICS AND LASERS

1.2.1 Quantum Theory of Noise

W. H. Louisell, J. H. Marburger, D. White

1. Lax has recently given a "classical" correspondence for a quantum stochastic process. We have been able to give a reformulation in such a way that we can show its connection with a classical correspondence introduced by Gordon[2]. In addition we have shown why Gordon's P_2 distribution function obeys a "classical" Fokker-Planck equation in which the diffusion matrix is non-singular and why his P_1 function has a diffusion matrix with negative eigenvalues.

In addition we have obtained a very simple derivation of the quantum regression theorem for general quantum systems in which multi-time averages can be computed from single time averages for Markoffian systems. This work is about to be written up for publication with J. H. Marburger.

2. Further work on the quantum theory of the laser has been done with Lax and is about ready to be submitted for publication as QXI in the series of quantum stochastic processes. In this report, after we eliminate the dipole moment operator adiabatically from the Langevin equations, we use the classical correspondence to convert to a classical problem in the population and field associated variables. The populations are eliminated classically which gives a further check on prior quantum

eliminations where there were ordering ambiguities. We express the results in the photon number, intensity and phase, and phase-number representations. We also obtain the linewidth due to phase diffusion and steady state solutions in the various representations

3. We a e also studying the optical parametric oscillator in which the atoms are treated explicitly rather than phenomenologically using the model of Graham and Haken[3]. In particular we are studying critically the various possible methods of eliminating the atoms. This work is being done with D. White and results are imminent.

References

1. M. Lax, Phys. Rev., 172, pp. 350-361 (1968).

2. J. P. Gordon, Phys. Rev., 161, pp. 367-386, (1967).

3. R. Graham and H. Haken, Zeits, für Physik, 210, pp. 276-302 (1968).

1.2.2 Interaction of High Intensity Light Beams with Matter

  AF-AFOSR-496-67, Joint Services Electronics Program

  W. G. Wagner

Our investigations center on the interactions of very intense

laser beams with materials, which are governed by nonlinearities pro-

ducing a number of qualitatively striking phenomena. Our immediate

objective is to study the propagation properties of intense light beams,

since only when these are known in some detail can reliable extraction

of material nonlinear coefficients be made from various experiments.

During the past period we have completed our study of the initial growth

of the instabilities in the propagation of electromagnetic waves of very

broad extent through low density fluids, and we have begun an attempt to

calculate the distortions in beam profiles resulting from density and

thermal variations induced in the medium by the passage of the optical

beam.

Our previous work had resulted in a very complicated disper-

sion relation which enabled one to calculate the temporal or spatial growth

rate for small amplitude disturbances to either the electromagnetic beam,

density, or temperature of the fluid. The theory was sufficiently general

to include the couplings of thermal deposition by absorption of radiation,

electrostriction, and a nonlinear dependence of the dielectric response

upon the electric field (Kerr effect). This dispersion relation was studied

numerically for cases of interest, and it was found that the correct

-56-

answers for the maximum instability growth rate and for the velocity of propagation of the disturbance was in very close agreement with our previously derived analytical estimates. The accuracy of the agreement (about 1%) is somewhat accidental as the analytical estimates were not expected to be that good.

We have also clarified the relation of our work to that of Brueckner and Jorna, and that of Livingston. Our results are in substantial agreement with Brueckner and Jorna, and in substantial disagreement with Livingston.

Further work on this problem is required in order to understand the nature of the beam distortion and possibly the saturated state of the instability development. Our only hope for the answers to such questions lies in an advanced digital computer study of the problem. Toward this end, a program for the solution of the system of seven partial differential equations in three independent variables is presently under development. Substantial effort has been made to invent a relatively sophisticated iteration technique so that the mesh size can be increased, but we will have to prove that this new technique is a stable one.

During this past period we have also completed work on a few projects that have been under less intensive investigation over a period of eighteen months. The first of these is the investigation of the effect of saturation on self-trapped optical beams in liquids. The conditions under which an electromagnetic beam can produce its own dielectric

-57-

waveguide and propagate without spreading have been discussed for a model of the nonlinear dielectric response which includes the effects of saturation. The model assumes that the principal contribution to the nonlinear response arises from the reorientation of anisotropic molecules. For the lowest order 'modes', the variation of the field amplitude over the cross section of the beam has been derived and presented graphically in a paper published in the IEEE Journal of Quantum Electronics. It has also been shown that, for 'cigar'-type axially symmetric molecules, there are two trapped beams possible which have no nodes, but which have the same total power.

In another paper published during this period in the IEEE Journal of Quantum Electronics, we have examined the equations of laser Q switching for a homogeneously broadened two-level material. It was shown that inertial effects in the material polarizability may play an important role in Q switching of lasers of narrow material linewidth. It was further shown that it is possible to amplify pulses of durations shorter than the inverse linewidth of the active material, provided the pulses are energetic enough to produce appreciable nonlinear behavior of the material. In this way it should be possible to produce, from a relatively long pulse, pulses of short duration as compared to the inverse linewidth of the amplifying material. Numerical examples were given based on parameters appropriate to the CO_2 laser. Even though the model of a homogeneously broadened two-level system is an oversimplification of CO_2 laser operation, it is believed that guidelines for future work on CO_2 systems can be gleaned from these results.

1.2.3 Optical Experiments with Laser Sources

AF-AFOSR-496-67, Joint Services Electronics Program

DAHC-04-69-C-0003, U.S. Army

W. L. Faust

During the past period we have successfully operated the large CO_2 laser contemplated in the previous report. The unit delivers Q switched pulses at a rate of 400 sec^{-1}, on various vibrational-rotational lines of CO_2 selected by a grating. We have performed a simple (but very direct, and inexpensive) calorimetric measurement of the time-average power, making use of the known heat of vaporization of liquid nitrogen. This average power is about one watt. We estimate the peak power during a pulse to be of the order of 25 KW, but we have not yet equipped ourselves with an adequately fast detector to make a reliable measurement. Unfortunately, the laser tends to run on two rotational lines (or more) at once; the grating and cavity configuration at present do not afford sufficient discrimination, even with the use of an iris. We are presently contriving to double the effective optical length of the cavity, which should solve this problem. We are also under way in the construction of a second such laser, since the physical experiments we anticipate (two of them, quite distinct) involve interaction between beams at two different frequencies. These experiments are i) high intensity (for double-quantum effects) two-beam studies of the local mode of $Ca F_2$: H and ii) rotational relaxation studies on CO_2 itself. On another front, we have inherited a Korad ruby laser capable of about 25 KW pulses at a 1

sec^{-1} rate. We hope to be able to perform Stokes Raman scattering

experiments with this unit as a source. The principal problem is expected

to be discrimination against intense scattered light from the primary

laser beam, which (apart from likely destruction of a photo mutliplier

tube!) could easily overwhelm Raman scattering having an absolute

intensity which would otherwise be readily detectable. We are consi-

dering as filters $GaAs_{1-x}P_x$ alloy films, which should be able to be

fabricated if sufficient interest can be aroused. If upon a pure GaP

substrate slab, there were built up an alloy layer $\geq 20\,\mu$ thick on each

side, with $0.30 \leq x \, 0.32$, the result should be ideal. The filter should

be essentially transparent for $\lambda \geq 7000\,\overset{o}{A}$ Stokes Raman scattering, but

should exhibit (very strong) direct interband electronic absorption at the

ruby laser wavelength. Consultation with an autority (J. Whelan, of the

Materials Science Dept. of this university) leads us to believe that fabri-

cation should be possible, giving collaboration with workers having the

necessary facilities. Our particular scattering problem of interest is in

local modes of impurities in GaP (we are in collaboration with W. G.

Spitzer at this point), but it is clear that such a filter would be a boon for

any sort of Stokes Raman scattering study with a ruby laser source.

We continue expansion of other general facilities, such as a

vacuum evaporation deposition system for making our own metal/dielectric

t..irrors, special gratings, etc.

1.2.4 First Order Raman Effect in Wurtzite Crystals

C. A. Arguello, D. L. Rousseau, and S. P. S. Porto

First order Raman scattering from four crystals (BeO, ZnO, ZnS, and CdS) with the Wurtzite (C_{6V}) structure has been investigated to better understand the effects of the competition between the long range electrostatic and the short range interatomic forces, and to determine the contribution of the electro-optic coefficient to the polar phonon scattering intensity.

The Raman scattering data from ZnO and CdS are in substantial agreement with prior investigations on these crystals.[1,2] In the analysis of BeO, both the transverse and longitudinal components of the A_1 and the E_1 species were observed and both E_2 modes were found. The BeO frequencies are: A_1 LO-1081 cm^{-1}; A_1 TO-678 cm^{-1}; E_1 LO-1097 cm^{-1}; E_1 TO-722 cm^{-1}; E_2-684 cm^{-1} and 338 cm^{-1}. For all of these crystals the angular dependence of the transverse and longitudinal modes is in agreement with theory.[3] The analysis of the Raman data from ZnS is in disagreement with the previous Raman investigations.[4,5] In the present study it is shown that the crystal anisotropy does not split the transverse or longitudinal phonons. They were located at 274 and 352 cm^{-1} respectively. The E_2 phonons were demonstrated to occur at 274 cm^{-1} (accidentally degenerate with the transverse phonon) and at 55 cm^{-1}. A line previously assigned as an E_2 phonon[4] at 68 cm^{-1} was shown to have the wrong depolarization characteristics to be of E_2

symmetry.

Loudon[3,6] has shown that the scattering cross section of a longitudinal phonon depends on a deformation potential term and an electro-optic term while the intensity of a transverse phonon depends only on a deformation potential term. The electro-optic coefficient Z_{ij} may be written in the form

$$Z_{ij} = \pm (AS_\ell^{\frac{1}{2}} \pm BS_t^{\frac{1}{2}}),$$

where S_ℓ and S_t are the scattering efficiencies for the longitudinal and transverse phonons respectively, and A and B are known constants. By measuring intensities of the transverse and longitudinal phonons the three independent electro-optic coefficients were determined for each of the crystals BeO, ZnO, and CdS. Comparison of these values with those measured by other methods at constant strain[7] demonstrates that very accurate measurements of electro-optic coefficients may be made by the Raman effect.

References

1. T. C. Daman, S. P. S. Porto, and B. Tell, Phys. Rev. 142, 570 (19 6).

2. B. Tell, T. C. Daman, and S. P. S. Porto, Phys. Rev. 144, 771 (1966).

3. R. Loudon, Advan. Phys. 13, 423 (1964).

4. H. Poulet, W. E. Klee, and J. P. Mathieu, in Proceedings of the International Conference on Lattice Dynamics, Copenhagen, 1963, (Pergamon Press, Inc., New York, 1965), pp. 337-341.

5. O. Brafman and S. S. Mitra, Phys. Rev. 171, 931 (1968).

6. R. Loudon, Proc. Roy. Soc. $\underline{A276}$, 218 (1963).

7. I. P. Kaminow and E. H. Turner, Appl. Optics $\underline{5}$, 1612 (1966).

1.2.5 Quantum Electronic Investigation of Cross-Relaxation

in Rare-Earth Crystals

NGR-05-018-044, National Aeronautics and Space

Administration

L. G. DeShazer, M. M. Mann, E. A. Maunders and

D. K. Rice

Determination of relaxation processes in laser media is currently of great importance in understanding interaction of radiation with optically pumped media. We are exploring correlations between relaxation effects in gain saturation of laser amplifiers, time-resolved emission spectra of laser oscillators, and mode-locked operation of laser oscillators. In particular, we are examining neodymium crystals and neodymium glass as the laser media. This work is directed towards development of a model for the relaxation mechanism, and determination of rate equations for the spectral flux and spectral inversion density. The model will be used to derive the relaxation term for the rate equation.

Details of this investigation are described in six publications from this laboratory and are briefly summarized below:

1. Employing relaxation effects for controlling the frequency of a laser oscillator.[1,2]

Frequency and polarization selection of neodymium glass laser oscillators was achieved by utilizing light from a controlled secondary source. When light from the secondary source was injected into the laser medium, the laser emission duplicated the spectral properties of this light. Thus, a narrowband emission was obtained from the normally broadband laser by injecting narrowband light at a matching wavelength. Similarly, a polarized emission was obtained from the normally unpolarized laser by using polarized light from the secondary source. The rapid energy transfer between the neodymium ions allowed the laser emission to duplicate the spectral properties of this secondary radiation.

2. Spectral broadening of rare-earth ions in laser media. [3,4,5]

This program is studying classical experimental procedures of determining line broadening parameters of rare-earth ions in solid hosts. Systematic spectroscopic studies were made on trivalent neodymium ions in various laser glasses. Analysis of the absorption and fluorescence spectra and their temperature dependence (from 4°K to 300°K) determined the energy levels of neodymium. The complete Stark splitting of the low-lying multiplets showed that the rare-earth ions occupied sites of low symmetry in the glass. The magnitude of the splittings correlate closely with those determined from oxide crystals. The inhomogeneity of the glass structure is manifested in the large broadening of the spectral lines. The profile of the component lines is Gaussian with halfwidths from 40 to 85 cm^{-1}. There is no thermal

-64-

variation of linewidths, indicative of inhomogeneous broadening. Previously reported fluorescence linewidth variation with temperature is explained by the thermal variation in the population distribution over the Stark components.

A study of europium glass was made to supplement and support these results on neodymium glass. The spectrum of europium contained many simple features greatly assisting this analysis. Absorption and fluorescence from singlet levels of europium made it possible to study the linewidths without the complication of Stark structure. Observation of $J = 0 -- J = 0$ transitions in europium glass limits the ion site symmetry to a low symmetry point group, regardless of the mechanism invoked for allowing the transition.

3.   Measurements on cross-relaxation processes between ions having an inhomogeneously broadened fluorescence line.[6]

The laser injection oscillator experiments demonstrated their feasibility in studying ionic relaxation. By this technique, laser oscillations were forced to develop from the narrowband radiation injected into the laser cavity, instead of broadband optical noise. The interionic transfer allowed the feeding of this narrowband radiation by ions having frequencies outside this interval. The efficiency of energy extraction within the narrow bandwidth measured the cross-relaxation rate. A new experiment is being constructed utilizing amplification of saturating giant-pulse laser radiation. If successful, this experiment will give,

-65-

for the first time, all the line broadening parameters of a rare-earth ion

in a solid host.

References

1. L. G. DeShazer, paper FB12. Meeting of the Optical Society of
    America San Francisco, California, October 18-21, 1966. L. G.
    DeShazer, J. Opt. Soc. Am. 56, 1443 (1966).

2. L. G. DeShazer and E. A. Maunders, "Spectral Control of Laser
    Oscillators by Secondary Light Sources", paper 16P3, International
    Quantum Electronics Conference, Miami, Florida, May 13-17, 1968.
    Paper to be published in October number of IEEE J. of Quan. Elect.

3. D. K. Rice, M. M. Mann and L. G. DeShazer, "Energy Levels and
    Spectral Broadening of Rare Earth Ions in Laser Glass", paper
    FC 11, Meeting of the Optical Society of America, Pittsburgh, Pa.,
    October 9-11, 1968.

4. M. M. Mann, "Energy Levels and Spectral Broadening of Neodymium
    Ions in Laser Glass", dissertation, University of Southern California,
    1968.

5. D. K. Rice and L. G. DeShazer, "Spectral Broadening of Europium
    Ions in Glass", to be published.

6. L. G. DeShazer, "An Investigation of Ionic Cross Relaxation by a
    Quantum Electronics Technique", in Optical Properties of Ions in
    Crystals, edited by H. M. Crosswhite and H. W. Moos, Interscience
    Publishers (1967).

1.2.6 Intensities of Crystal Spectra of Rare-Earth Ions

M. M. Mann, T. S. LaFrance, and L. G. DeShazer

In this program the mechanisms which give rise to parity-forbidden transitions in the spectra of rare-earth ions in crystals are being investigated. The parity-forbidden transitions are the most commonly occuring transitions in rare-earth ions, and all presently observed laser action in rare-earth crystals is due to these transitions. The present theories of laser action in rare-earth crystals treat transition probabilities in a phenomenological manner. In order to develop a more fundamental description, it is necessary to have a suitable model for the transition probabilities. Thus, it is hoped that this study will lead to a more fundamental understanding of laser processes in rare-earth crystals. Also, this understanding will hopefully help choose the "best" laser host for rare-earth ions, a very illusive host at present.

1. Enforced Electric Dipole Transitions of Rare-Earth Ions.

Both the initial and final states associated with the emission transitions of interest belong to the same electronic configuration. Then, two types of radiation in crystal spectra must be considered: a) magnetic dipole and electric quadrupole which also occur in the free ion spectra, and b) electric dipole which does not occur in the free ion spectra but does in the crystal spectral. This parity-forbidden electric dipole radiation is called enforced electric dipole radiation, and occurs due to

...c interaction of the rare-earth ion with the electric field of the crystal. Judd[1] and Ofelt[2] have presented theoretical analyses of the intensities associated with the enforced electric dipole transitions. They have shown that a substantial admixture of 4f and 5d wavefunctions occurs when the rare-earth ion is not located at an inversion center. This removes the parity restriction and allows electric dipole transitions.

We have studied the fluorescence and absorption oscillator strengths of the transitions of europium in $LaCl_3$. A preliminary fit of the Judd-Ofelt model to this data was made. It was observed that in addition to the intensity measurements, the anisotropy of $LaCl_3$ must be known to permit comparison of the experimental results with theoretical predictions. Therefore, a theoretical analysis of atomic radiation in anisotropic media was made for non-resonant, linear and lossless media.[3] The derived expressions provide an analytical means of relating oscillator strengths to measured intensity data. It has also been shown that the multiple intensity distribution sensitively reflects both the macroscopic and microscopic dielectric properties of the host.

No general expression can be given for the local field parameters. A suitable analytical model must be chosen for each case. The local field parameters may be more profitably viewed as experimentally determined constants. Thus measurements of spatial intensity distribution can be used to obtain information on the local environment of the radiating ion.

2. Pseudo-Quadrupole Transitions of Rare-Earth Ions.

It was observed that certain fluorescence lines of Eu: $LaCl_3$ were unduly intense and caused a peculiar parameter fit to the Judd-Ofelt model. When these intense transitions were neglected, the Judd-Ofelt model predicted the remaining intensity data in a reasonable way. These intense transitions were named "seudo-quadrupole" because they mimic electric quadrupole selection rules. After recognition of these transitions, it was observed that almost all of the strong laser transitions from rare-earths appear to be pseudo-quadrupole.

For rare-earths in various solutions, Jorgensen and Judd[4] noted that the intensities of a few transitions were hypersensitive to the solvent, while the intensities of the other transitions were insensitive. The hypersensitive transitions mimicked electric quadrupole selection rules. Following this hint, we are preparing an experiment on the europium ion in europium ethylsulfate and europium magnesium nitrate crystals under conditions of varying pressure. Large single crystals of europium ethylsulfate have been grown and are being prepared for this study.

References

1. B. R. Judd, Phys. Rev. <u>127</u>, 750 (1962).

2. G. S. Ofelt, J. Chem. Phys. <u>37</u>, 511 (1962).

3. M. M. Mann and L. G. DeShazer, "Atomic Multipole Radiation in Anisotropic Media", to be submitted.

4. C. K. Jorgensen and B. R. Judd, Mol. Phys. <u>8</u>, 281 (1964).

1.2.7 Experimental Studies in Nonlinear Optics

G. L. McAllister, L. Huff, L. G. DeShazer

This experimental program is investigating the nonlinear effects in the propagation of light in organic liquids. The main emphasis in this program is on self-focussing effects and saturated absorption effects. Considerable attention was given to the development of a high-power narrow-pulse laser. Recent studies on mode classification of a giant-pulse laser are being submitted for publication. The investigation of pulse shaping due to the time-dependent behavior of the electric field in self-focussing situations has been started. For intensities below the threshold of self-focusing, such as occurs at the beginning and end of the laser pulse, the on-axis intensity of a beam decreases due to the diffractive spreading. If this beam passes through a nonlinear medium, such as nitrobenzene, the spreading effect can be counteracted by self-focusing. For intensities above the self-focusing threshold, the beam is squeezed and the net result is suppression of the leading and lagging edges and enhancement of the pulse center. This appears as a time compression of the pulse. By this experiment, much information can be obtained on threshold power and self-focusing length.

Experiments on saturated transmission of ruby laser radiation by organic dye solutions were continued. Saturated transmission is a reversal of the well-known observation that the absorption of high

power laser radiation by many organic materials reduces with increased laser power. The sulfonated forms of the indanthrone dye become opaque to intense radiation. At present, four sulfonated forms have been carefully studied for powers from 0.1 to 100 megawatts per cm^2.

1.2.8 Computer Studies of Self-Focusing Optical Beams

DA-ARO-D-31-124-6920, U.S. Army Research Office

J. Marburger, E. Dawes, R. Reynolds, L. Huff,

J. Wagner, J. Reichert

The numerical work reported in the previous semiannual progress report has been completed and either published or submitted for publication[1,2,3]. During this period we began a theoretical investigation of the effects of relaxation of the nonlinear refractive index on the dynamical self-focusing of an intense laser beam. We have found on the basis of simple arguments that relaxation effects (which cause a delay between the nonlinear response and the applied field) should have the same qualitative effect on the focusing beam as the saturation effects studied during the previous reporting period. Work is now underway to establish this connection more rigorously and use it to estimate the properties of small scale trapped filaments of light.

Additional numerical solutions of the "steady state" self trapping equations have been obtained. This work, which augments that of Reichert and Wagner[4] and Gustafson et al[5], was motivated by the

discovery of a technique for treating the nonlinear local field theory of

Lorentz correctly to all orders in the applied field. In references 4 and

5 the local fields were treated only in a rough way. We have found that

the saturation properties of the nonlinear refractive index, which accord-

ing to some theories determine the size of small scale trapped light fila-

ments, depend sensitively upon the local field corrections. The results

of this investigation are reported in reference 6.

References

1. W. G. Wagner, H. A. Haus, J. H. Marburger, Phys. Rev. 175 (1968).

2. J. H. Marburger, E. L. Dawes, Phys. Rev. Letters 21, 556 (1968).

3. E. L. Dawes, J. H. Marburger, to be published.

4. J. Reichert, W. G. Wagner, IEEE J. Quant. Electr. 4, 221 (1968).

5. T. K. Gustafson, P. L. Kelley, R Y. Chiao, R. G. Brewer, Appl.
    Phys. Letters 12, 165 (1968).

6. J. H. Marburger, L. Huff, J. Reichert, ʷ G. Wagner, to be
    published.

1.3 MAGNETISM

1.3.1 Nuclear Magnetic Resonance in Ni Rich Ni-Cu Alloys

AF-AFOSR-496-67, Joint Services Electronics Program

S. Ogawa

The magnetic moment of the Ni atoms originates from 0.6 holes per atom in the 3d band. Since the magnetization of Ni decreases by 1 Bohr magneton when one Ni atom is replaced by one Cu atom, it becomes zero at about 60 atomic percent of Cu. However, the screening effect of the Cu nuclear charge attacts the excess electrons to fill Ni holes near the Cu atom.

The NMR method was used to investigate this localization of charge by observing hyperfine field spectra of both Ni and Cu nuclei in alloys up to 10% Cu in Ni metal. The hyperfine field is proportional to the spin density of electrons. By means of a computer calculation the spectra were analyzed assuming a statistical distribution of the Cu atom. One Cu atom replacing one Ni atom as a first or second neighbor to a Ni atom reduces the field by 4.3 and 2.5% of that of pure Ni metal, respectively. The effect of the same replacement as a first, second or third neighbor of a Cu atom causes the reductions of 8.2, 5.4 and 1.8% of the Cu hyperfine field, respectively. From these data the following conclusions can be drawn:

1. Ni hyperfine field is mainly produced by the core polarization and the contribution of neighboring Ni atoms for it

is about 1/3. The Cu hyperfine field is produced by the

conduction electron polarization of the neighboring Ni atoms.

2. The effect of Cu atoms in Ni metal is screened out by the

    several neighbor shells.

3. The average Cu hyperfine field, calculated with the effective

    factors and probability numbers of Cu atoms of the successive

    shells, decreases with Cu concentrations as does the change

    of the saturation magnetization.

1.3.2 Ion Configuration in Spinels

AF-AFOSR-496-67, Joint Services Electronics Program

J. Smit

The saturation magnetic moment and other technical

properties of ferrites are largely determined by the distribution of the

various metal ions over the available crystallographic sites. In spinels

and garnets, which are the crystal structures of the most important

ferrites, the iron group metal ions occupy either octahedrally or tetra-

hedrally coordinated sites, the nearest neighbors being anions like

oxygen or sulfur. The magnetic moments of the metal ions on these

sites are anti-parallel.

The anions are asymmetrically surrounded by the metal ions,

so that an electrical field at the anions results, which gives rise to a

polarization which lowers the energy. It is shown that in spinels this

-74-

energy should always favor the so-called normal configuration in which divalent ions occupy tetrahedral sites. Exceptions occur, but then the ions on tetrahedral sites always have a d^5 or d^{10} electronic configuration. This condition is favorable for a partly covalent bonding, which is particularly stable in these configurations.

Recently ferromagnetic spinels of the type $CuCr_2S_4$ have been reported in literature. There seems to be strong evidence that the Cu ion in these compounds is monovalent, and one of the Cr ions quadruvalent. It is shown that these configurations are quantitatively consistent with the above mechanisms, as they are stabilized by the strong polarization of the sulfur ions.

A report of these considerations is published in "Solid State Communications".

1.3.3 Mossbauer Effect Study of Mixed Lithium-Zinc Ferrites

AF-AFOSR-496-67, Joint Services Electronics Program

J. Young and J. Smit

Abstract

Mossbauer spectra were measured at room temperature for six samples of the lithium-zinc ferrite system, $(Zn_x^{2+}Fe_{1-x}^{3+} | Li_{0.5-x/2}^{1+} Fe_{1.5+x/2}^{3+})0_4$. Hyperfine magnetic fields decrease and eventually vanish as the zinc content is increased. For pure lithium ferrite, the fields are 515 Koe for the tetrahedral sites and 520 Koe for the octahedral sites.

Pure zinc ferrite is paramagnetic with a quadrapole splitting of 0.40 mm/sec. Intermediate samples show a gradual transition from ferrimagnetic to paramagnetic behavior.

The main features of the observed spectra can be accounted for by a model assuming only nearest neighbor inter-sublattice exchange interactions are important.

Experimental Procedure

The mixed lithium-zinc ferrites have the molecular formula $(Z_{n_x}^{2+} Fe_{1-x}^{3+} | Li_{0.5-x/2}^{1+})O_4$. Samples having x = 0, 0.2, 0.4, 0.6, 0.8, and 1.0 were made by wet mixing ZnO, Li_2O, and Fe_2O_3 powders in the appropriate stoichiometric ratios, drying, pressing into pellets, and firing overnight at $1050^{o}C$. The resulting reddish-brown pellets were ground to a fine powder and set in sample holders with paraffin. Sample thickness was adjusted to provided about 30 mg of iron per cm^2.

Mössbauer spectra were measured using a system manufactured by the Technical Measurement Corp., operating in its analog sample mode and later, with a special modification, in a synchronized multiscaling mode. The measured linewidths of a thin natural iron foil are about 0.35 mm/sec. Measurement times varied from sample to sample in order to achieve suitable signal-to-noise ratios with spectra of different complexities. The Mössbauer source was 5 mc Co^{57} in Pd.

Discussion of Results

The Mössbauer spectra of all the samples are shown in

Fig. 1. Six-line spectra characteristic of magnetic ordering are observed for the samples having $x = 0$ through 0.6. In pure lithium ferrite ($x = 0$), the lines corresponding to tetrahedral (A) and octahedral (B) sites are not clearly resolved. However, line widths and line shapes vary, and the spectrum can be decomposed into two sets of lines having slightly different magnetic fields and isomer shifts. Neither set shows any appreciable quadrupole splitting.

The $x = 0.2$ and 0.4 samples show a set of small narrow lines clearly separated from a set of large broad lines. The large lines have asymmetrical line shapes with steeper slopes on their high velocity sides. Approximate measurements of the ratios of the areas under the large and small lines give results close to the ratios of iron atoms on octahedral and tetrahedral sites. This suggests assigning the small lines to the tetrahedral sites. However, these small lines also show a considerable quadrupole splitting and in general are similar, though not identical, to the spectrum of $\alpha\text{-}Fe_2O_3$. Hence, they may be the result of a separate phase of Fe_2O_3 present in these samples. It is expected that x-ray diffraction studies will resolve this question.

In the $x = 0.8$ sample, the small lines have disappeared and the large lines have become very broad and shallow. Also, a quadrupole split central doublet has appeared indicating that some iron on octahedral sites has become paramagnetic. The x 0.8 and 1.0 samples show only the central doublet. Apparently all the iron in these materials has become paramagnetic.

$\left(Zn_x^{2+} \; Fe_{1-x}^{3+} \; | \; Li_{0.5 \cdot \frac{z}{2}}^{+} \; Fe_{1.5 \cdot \frac{z}{2}}^{3+} \right) O_4$
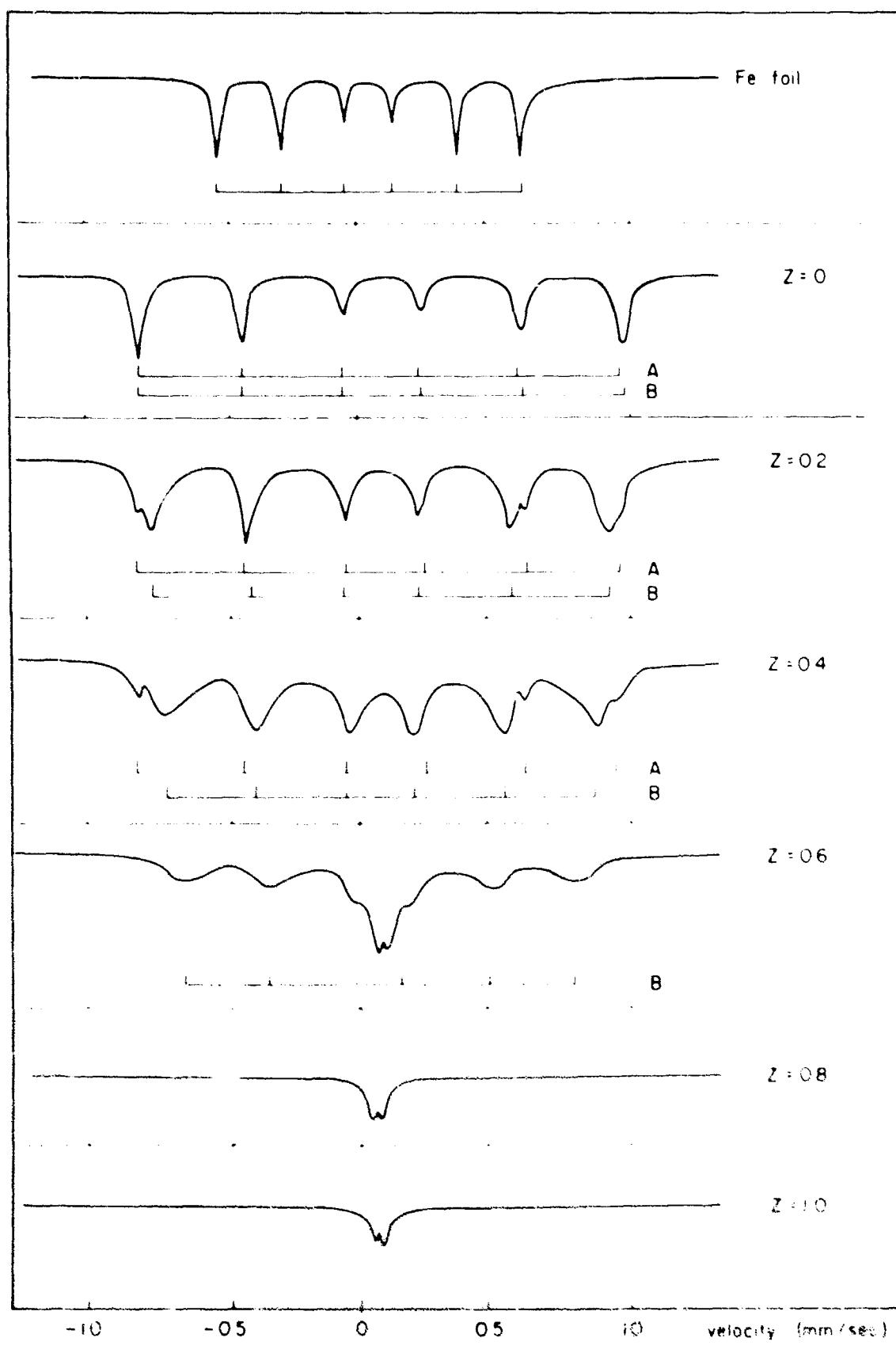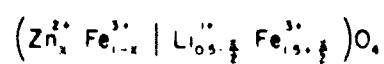
Figure 1

A summary of the hyperfine magnetic fields, quadrupole splittings and isomer shifts of all samples is given in Table I. Isomer shifts are measured relative to the center of symmetry of natural iron.

Table I

Sample	x = 0		0.2		0.4			0.6	0.8	1.0
Site	A	B	A	B	A	B	B	B(para)	B	B
Hhf (Koe)	515	520	527	486	524	462	404	0	0	0
ΔE_Q (mm/sec)	+.02	0.0	+.24	+.05	+.30	0.0	.05	.39	.40	.39
ΔI mm/sec.	27	0.0	.37	.37	.40	.40	.25	.20	.20	.20

Theoretical Calculations of the Spectra

We have attempted to explain two main features of the observed spectra, the decrease in the hyperfine field experienced by B sites and the broadening and increasingly asymmetrical shape of these lines as zinc content is increased. The model used assumes that the hyperfine field at the nucleus of an Fe^{57} atom is proportional to its time average spin, and that the spin is determined by inter-sublattice exchange interactions between an iron atom and its nearest neighbor iron atoms on the opposite sublattice. In this approximation, the value of the inter-sublattice exchange integral, J^{AB}, is $-kT_c/42.8$ for pure lithium ferrite which has $T_c = 970^{\circ}K$. We assume that the value of J^{AB} is unchanged by the addition of zinc. Thus, the effect of the zinc is assumed to be due only to a change

-79-

in the number of nearest neighbor Fe's seen by atoms on the two sublattices.

In the spinel lattice, each A site "sees" 12 nn B sites, and each B site "sees" 6 nn A sites. On the average an A site "sees" $n_B(x) = 9 + 3x$ nn Fe's on B sites, and a B site "sees" $n_A(x) = 6 - 6x$ nn Fe's on A sites.

The time average spins of Fe atoms on A and B sites are then given by:

$$S_z^A = \frac{5}{2} B_{5/2} \left(5n_B \frac{J^{AB}}{kT} S_z^B \right)$$

and

$$S_z^B = \frac{5}{2} B_{5/2} \left(5n_A \frac{J^{AB}}{kT} S_z^A \right) .$$

At $T = 300^\circ K$, $\frac{J^{AB}}{kT} = -0.0755$. If, as a first approximation, we take $S_z^A = \frac{5}{2}$ and $S_z^B = -\frac{5}{2}$ within the arguments of the Brillouin functions, we find $S_z^A = \frac{5}{2} B_{5/2}(0.944\, n_B)$ and $S_z^B = -\frac{5}{2} B_{5/2}(0.944\, n_A)$. It appears that the proportionality constant relating the spin may be different for the two sites. Thus, $H_{hf}^A = \alpha_A |S_z^A|$ and $H_{hf}^B = \alpha_B |S_z^B|$. These constants can be determined from the measured fields of pure lithium ferrite. We find $\alpha_A = \frac{2}{5} \cdot 525$ Koe and $\alpha_B = \frac{2}{5} \cdot 542$ Koe. Taking n_A and n_B characteristic of each sample, we can calculate the expected hyperfine fields for the A and B sites. Table II gives the calculated and measured field.

Table II

Sample	Calculated Field		Measured Field	
	A	B	A	B
x = 0	515 Koe	520 Koe	515 Koe	520 Koe
0.2	520	498	527	486
0.4	520	466	524	462
0.6	520	396		404

1.4 DEFECTS IN CRYSTALS

1.4.1 <u>Defect Chemistry of CdS</u>

AF-AFOSR-496-67, Joint Services Electronics Program

1.4.1.1 High Temperature Hall Effect Measurements

F. A. Kroger and G. Herschman

Apparatus for high temperature Hall effect measurements of CdS in Cd vapor has been modified to make possible the use of graphite yarn as current lines. Measurements on three different crystals with foreign donors (Al) in the concentration range $5 \times 10^{16} - 10^{17}$ cm^{-3} all show the following features:

1) in the range 500 - 700°C, the concentration of electrons $\propto p_{Cd}^{1/4}$, indicating precipitation - dissolution equilibrium for the donor (Al_2S_3).

2) between 700 - 900°C, the concentration of electrons is constant at low p_{Cd}, but increases with p_{Cd} at higher cadmium pressures. This indicates that Cd excess gives rise to donors (Cd or V_S). It has so far not been possible to decide between single and double ionization of the native donors.

1.4.1.2 Cd Self Diffusion

F. A. Kroger and V. Kumar

Measurements of the self diffusion of cadmium in CdS under well-defined conditions (P_{Cd}, T) using radio active Cd have been started.

The goal of this project is the determination of the species responsible for the transport of cadmium and its thermodynamic formation parameters. Diffusion constants found so far in the purest CdS available (containing $\approx 10^{17} cm^{-3}$ Al) are of the order $10^{-10} - 10^{-11} cm^2 sec^{-1}$, 2-3 orders of magnitude smaller than those reported by Woodbury in a similar study.

1.4.2 Electrochemistry of Solids

1.4.2.1 Zirconia as an Oxygen Pump

F. A. Kroger and D. Yuan

With a cell consisting of a zirconia tube with inside and outside platinum electrodes, oxygen can be transferred from inside to outside by passing a current (outside positve). Start with nitrogen containing $\approx 2 \times 10^{-5}$ atm. of O_2 flowing at a rate of $\approx 300 cm^3$ per minute through the tube, oxygen pressures as low as 10^{-36} atm may be reached. This low pressure limit is determined by the onset of electronic conduction in the zirconia.

1.4.2.2   The Conduction Properties of ZrO_2 and ThO_2

F. A. Kroger and H. Yanagida

The point where electronic conduction sets in differs from
material to material. We are investigating which factors are responsi-
ble for these differences. The point where the electronic transference
is 1/2 can be found by studying the cell

$$Al, Al_2O_3 \mid ZrO_2 \mid O_2 \; ,$$
$$ThO_2$$
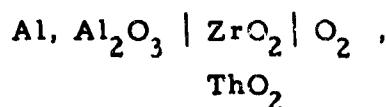
and comparing the emf with that corresponding to the free enthalpy of the
reaction $2Al + \frac{3}{2} O_2 \rightarrow Al_2O_3$. In order to be able to make dense materials,
it was necessary to study the sintering behavior of ZrO_2 and ThO_2. Gas
tight disks can now be made.

1.4.2.3   Sulfur Electrodes

F. A. Kroger and D. Yuan

Three types of electrochemical cells sensitive to S vapor
are being investigated

$$1) \quad Pt\, O_2 \mid Zr O_2 \mid C, S(g)$$

This cell responds to the sulfur pressure, the empf increasing with p_S.
This suggests that the zirconia acts as an oxygen electrode in the usual
way, a low oxygen activity being caused by the reaction

$$S(g) + O_2 \rightarrow SO_2$$

2) Na | Na glass | C,S

3) Na | $Na_2O \cdot 11Al_2O_3$ | C,S
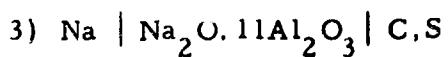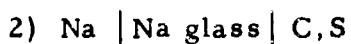
1.4.2.4 Polarization Studies of AgCl

F. A. Kroger and Y. van der Meulen

Measurements have been carried out of current as f(E) for cells

$$Ag | AgCl | C \quad and \quad C, \quad Cl_2 | AgCl | C \quad or \quad Pt$$
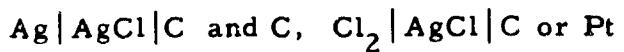
The former show abnormally large noise effects. In addition, they have currents $\propto \exp(Ee/\alpha kT)$ with $\alpha > 1$. Probe measurements are now being made to see where the noise is generated and to find out whether surface barriers play a part.

The Cl_2 cells show more normal behavior; however, α cannot be determined because of the presence of an emf at zero current. A new type of cell is being made in which the Pt electrode is inside the crystal; this should eliminate the emf.

1.4.2.5 The Conduction Mechanism of NH_4Cl

F. A. Kroger

In order to complement the emf measurements carried out previously, the conductivity of NH_4Cl as f (temperature) was measured in various gas atmospheres $N_2 + x\,NH_3 + y\,H_2$. No significant variation of the conduction with the gas composition was observed. This indicates

that the emf's are established by equilibration of a relatively thin surface
layer.

Papers Submitted for Publication

1. P. B. P. Phipps and F. A. Kroger, J. Phys. Chem. Solids. Long-
    Wave Length Absorption in Brominated AgBr.

2. F. A. Kroger, J. Phys. Chem. Solids, Defects and Phase Stability
    of Transition Metal Compounds.

3. H. Yanagida and F. A. Kroger, J. Am. Ceram. Soc., The System
    Al - O.

4. D. Yuan and F. A. Kroger, J. Electrochem. Soc., Stabilized
    Zirconia as an Oxygen Pump.

1.4.3 Defect Chemistry of Al_2O_3

AF-AFOSR-68-1405, Air Force Office of Scientific

Research

F. A. Kroger, R. J. Brook, J. Yee

1. In a program investigating the electrical properties and
defect structure of Al_2O_3, the emf of the cell

$$Pt(O_2) | Al_2O_3 | Pt(O_2')$$
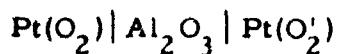
is being measured on crystals grown from a PbF_2 flux and doped with

MgO and SiO_2. Ionic conduction is indicated for undoped Al_2O_3 up to the

highest temperature used ($1400^{\circ}C$).

2. The conductivity of the crystals is being measured using

a volume guard ring to eliminte leakage currents. A constant activation

energy of 2.5 eV is observed over the range 900° to $1400^{\circ}C$.

3. An attempt is being made to observe the mass transfer expected during conduction by Al^{+++} migration with metallographic techniques; the usual weight change method is susceptible to errors introduced by surface conduction paths.

4. Measurements of the conduction parameters at very low oxygen pressures are now being prepared using the zirconia oxygen pump described above (section 1.4.2.1).

The combination of these approaches should afford a description of the defect structure of the oxide.

1.4.4 Grain Growth in Ceramics

GK 1487, National Science Foundation

R. J. Brook

Grain growth phenomena are of importance both in the processing and the properties of ceramic materials, and the present program is an attempt to define the parameters that determine the type and the kinetics of grain growth for a given system.

Emphasis has been placed on the effect of two variables, namely, impurity concentration and microstructure.

Theoretical aspects of impurity-influenced normal grain growth were described in the previous report[1]; present work is concerned with defining the role of porosity in the growth process under

conditions of different grain size, pore size, and pore distribution.

Experimental verification for the impurity effects is being sought in a study of impurity distribution at different grain sizes in MgO by means of electron microscopy and electron microprobe analysis.

Verification for the microstructural effects is being studied by comparing observed growth kinetics in very small grain size (thin film) ZnO with those predicted by the analysis.

Reference

1. R. J. Brook, "The Impurity Drag Effect and Grain Growth Kinetics", Scripta Met. (2) 375 (1968).

1.5 METALS

1.5.1 Experimental Studies of Fermi Surface Topology in Metals
AF-AFOSR-496-67, Joint Services Electronics Program
M. H. Halloran, J. Brewer and R. Parker

The experimental determination of Fermi surface topologies
in metals has been an active field of research in solid state physics for
several years. The importance of this research derives from the very
precise information which can be learned about the electronic band
structure at the Fermi energy. Comparison of this information with
theoretical energy band calculations provides the most accurate check
for these calculations at the present time. In addition, these studies
yield accurate determinations of electron effective masses, which serve
to provide information concerning the interaction of the electrons with
phonons and/or magnons via the resulting mass enhancement as well as
additional further information for checking the band calculations. Some
indirect measurement of electron mean collision time is also obtainable,
as well as carrier concentrations, magnetic breakdown probabilities and
open orbit directions. Our research is specifically directed to three
areas: Fermi surface studies in intermetallic compounds, B-H effects
in noble metals, and Fermi surface studies in transition metals and
rare-earth metals.

Fermi Surface Studies in Intermetallic Compounds

Data are being obtained presently on the intermetallic

-89-

compound $AuGa_2$ using the deHaas-van Alphen Effect as measured with
a sensitive torsion balance in fields up to 28 kOe. Magnetothermal
oscillations will also be used and a direct comparison of the relative
sensitivities of the two techniques should also be possible. A crystal
of $AuIn_2$ has been zone refined and will be checked soon to determine if
it is sufficiently pure to permit deHaas-van Alphen measurements. $AuGa_2$,
$AuIn_2$ and $AuAl_2$ form a family of compounds which possess many simi-
larities, but $AuGa_2$ has exhibited an anomalously large Knight shift and
it has been suggested that its Fermi surface may be substantially different
from the other two compounds. Early results[1,2] have not been conclu-
sive, but only a small portion of the Fermi surface is known thus far.
Studies on all three compounds are planned, and if low field results remain
inconclusive, additional studies in a 100kOe solenoid will be made.

B-H Effects in the Noble Metals

The measurement of non-linear effects in the deHaas-van
A'phen effect due to differences between B and H inside the sample have
been extensively investigated only in beryllium[3]. They have also been
observed in the noble metals[4,5] (Au. Ag and Cu) and perhaps other
materials. The effect is manifested in the line shape of the oscillations,
the appearance of large amplitude difference frequencies, and anomalous
oscillation amplitude dependence on temperature. A theoretical explana-
tion was successful in Be, but certain qualitative differences associated
with the Fermi surface topology complicate the interpretation in the
noble metals, and the detailed Fermi surface measurements with properly

shaped samples required for a complete explanation have not been made as yet. Recent nmr measurements[6] in silver have indicated the existence of domains due to the B-H effects, consistent with the earlier interpretations in beryllium. A good sample of silver is on hand and when higher fields are available in the near future we will undertake the required deHaas-van Alphen measurements.

Fermi Surface Studies in Transitio. Metals and Rare Earth Metals

These materials are racterized by d-bands or f-bands at the Fermi energy, resulting in large electronic masses, frequently with large mass enhancement due to phonon and/or magnon interactions with the electrons. Therefore very high fields and/or low temperatures are required to study the Fermi surfaces. To provide the former, a 100 kOe superconducting solenoid was delivered last January but failed to meet specifications and was returned. Subsequent testing by the manufacturer resulted in further performance degradation, and a second coil was also unsuccessful. A new coil from a different manufacturer should be delivered before January 1, enabling research in this area to commence. In the meantime, in a joint venture with Bell Telephone Laboratories and the use of their facilities, Fermi surface measurements have been made[7] on Nb and Ta which indicate that the Fermi surface model determined from APW band calculations and the mass enhancement is in agreement with estimates based on superconducting transition temperatures.

References

1. M. H. Halloran and J. H. Wernick, Bull. Am. Phys. Soc. 10, 450 (1965).

2. J. P. Jan, et al., Phil. Mag. 12, 1271 (1965).

3. M. H. Halloran and F. S. L. Hsu, Bull. Am. Phys. Soc. 10;
    J. H. Condon, Phys. Rev. 145, 526 (1966).

4. A. S. Joseph and A. C. Thorsen, Phys. Rev. 138, A1159 (1965);
    Phys. Rev. 140, A2046 (1965).

5. M. H. Halloran, F. S. I. Hsu and J. E. Kunzler, in Proceedings
    of the Tenth International Conference on Low Temperature Physics,
    Moscow (1966) - Vimiti Publishing House, Moscow.

6. J. H. Condon and R. E. Wolstadt, Phys. Rev. Letters 21, 612 (1968).

7. M. H. Halloran, J. E. Grebner and J. H. Condon (to be published).

1.5.2 Basic Structure - Property Correlations in Shock-Loaded

Metals and Alloys by Transmission Electron Microscopy

AF-AFOSR-496-67, Joint Services Electronics Program

L. E. Murr and J. V. Foltz[*]

This research has as its general purpose the study of the

relationship of residual mechanical properties to explosive-shock induced

defect structures in metals and alloys of engineering interest. The

general plan of attack follows the approach used in previous research,

portions of which were supported in part by this grant[1-3].

During the period covered in this report, assemblies of

shock-loaded Inconel 600 alloy (76% Ni, 16% Cr, 7% Fe, balance impuri-

ties) foil 0.001 in. thick sandwiched between pure nickel foils 0.004 in.

---

[*]Research Physicist, Ballistics Division, U.S. Naval Weapons Labora-
tory, Dahlgren, Virginia; on temporary duty assignment as a research
associate in the Department of Materials Science, U.S.C.

thick, as shown in Fig. 1, were disassembled; and the foils electropolished

for direct observation of the residual microstructures by transmission

electron microscopy. The unique feature of Inconel alloy in the initial-

annealed state is the presence of coherent $Ni_3(Ti, Al)$ precipitates in the

matrix. It was thus of fundamental interest to observe the influence of

such inclusions on the propagation of dislocations during the shock-front

passage, and their possible influence on the residual mechanical properties.

As an obvious approach to elucidating the residual mechanical

properties of shock-loaded Inconel, Vickers microhardness measurements

were made on the recovered sheet specimen using a 50 gm load. The

results, when compared with pure nickel as shown in Fig. 2, illustrate

quite strikingly the fact that in the pressure range 0 - 400 Kb, the

strengthening of the Inconel matrix continues while for nickel, hardening

is effectively complete after 200 Kilobars pressure.

The reason for the behavior shown in Fig. 2 is vested in the

residual defect structure; amenable to direct observation. Figure 3

illustrates the initial Inconel substrcture (before shock deformation),

and the typical appearance of the residual microstructure after shock

loading to 100 Kb pressure. The hardening at 100 Kb as observed in

Fig. 2 can now be observed to be due to dense dislocation structures; and

possibly the interaction of dislocations with the precipitates as shown in

Fig. 3(b). It is also of interest to point out in Fig. 3(b) that the dense

arrays of dislocations surrounding the precipitates were presumably

generated at the particle-matrix interface. This could only occur if the

-93-

ELECTRIC DETONATOR

LINE WAVE GENERATOR

MAIN EXPLOSIVE CHARGE

DRIVER PLATE

MOMENTUM TRAPS

1/2"

1"

SPALL PLATE

NICKEL THIN SHEET

INCONEL THIN SHEET

SPECIMAN SANDWICH

4"

TO WATER BATH
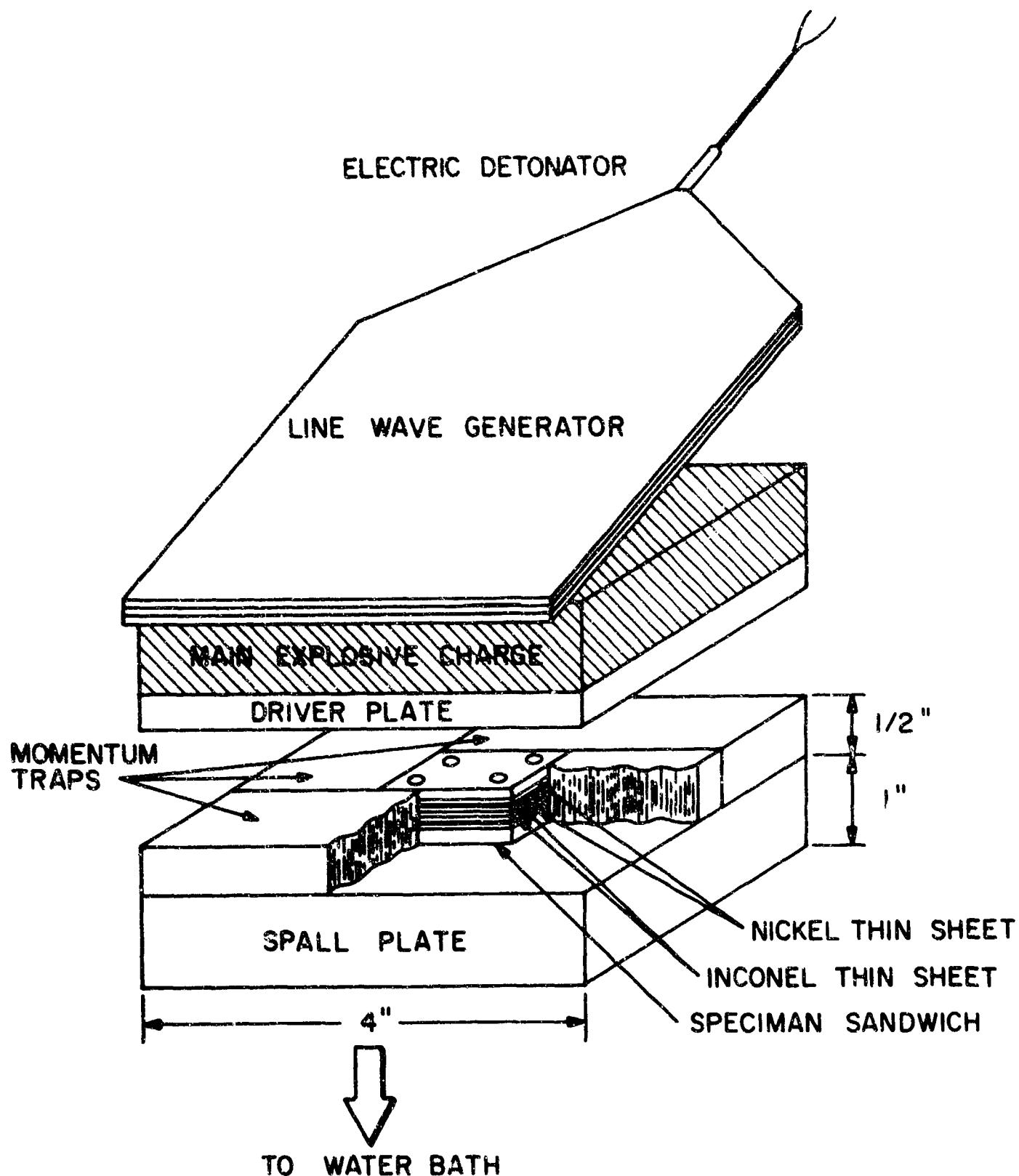
Fig. 1. Experimental Shock-loading assembly (After Murr and Grace)
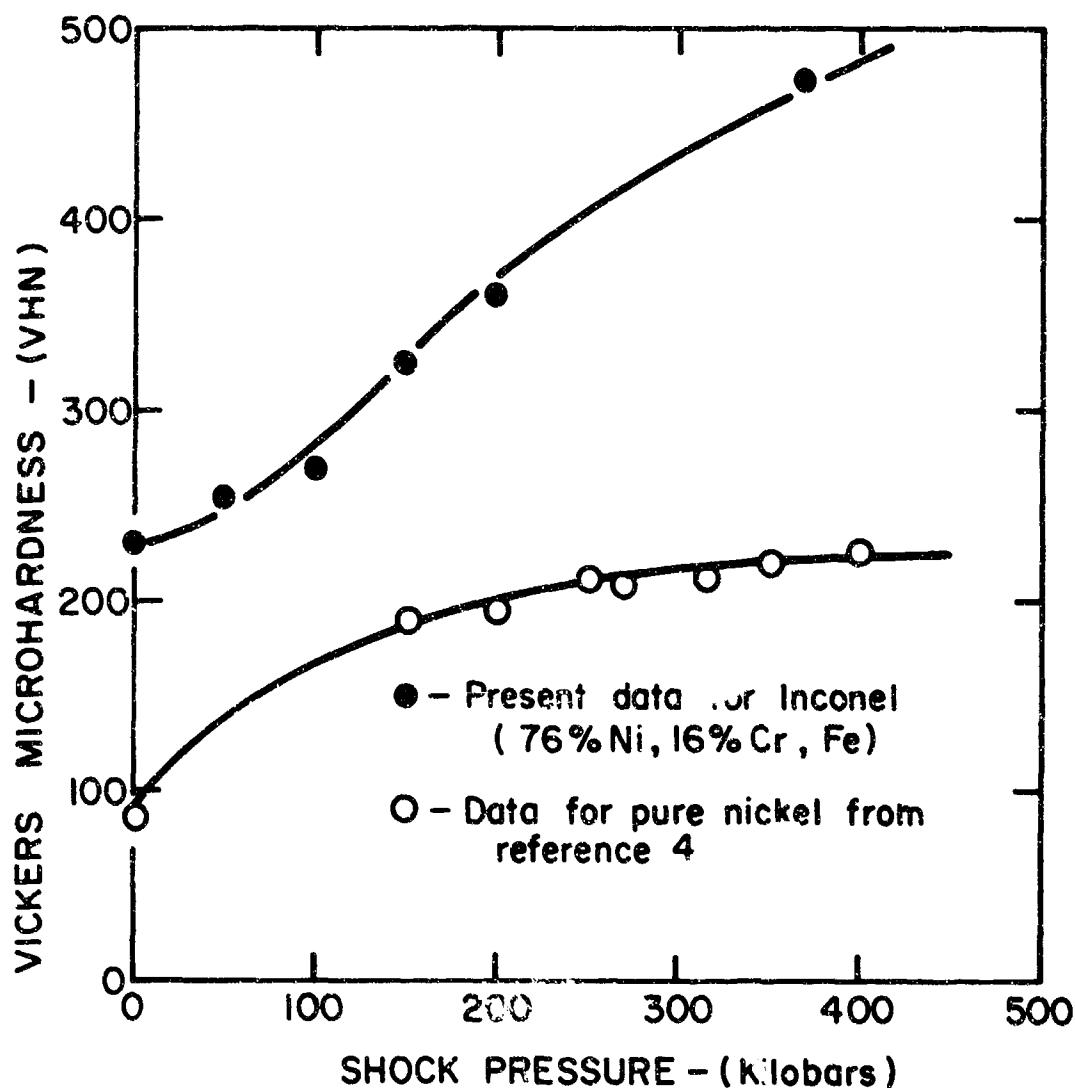
Fig. 2. Residual microhardness of thin nickel and Inconel alloy sheets
following explosive shock deformation.
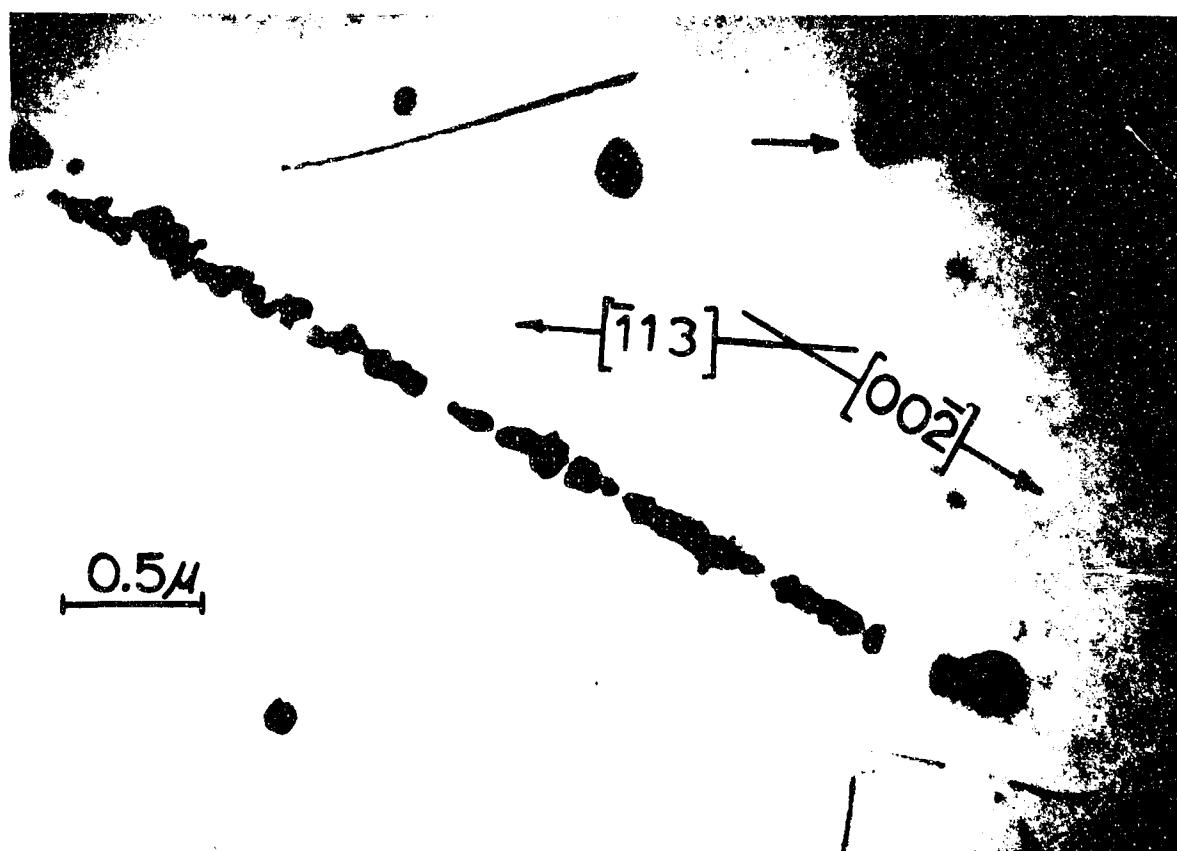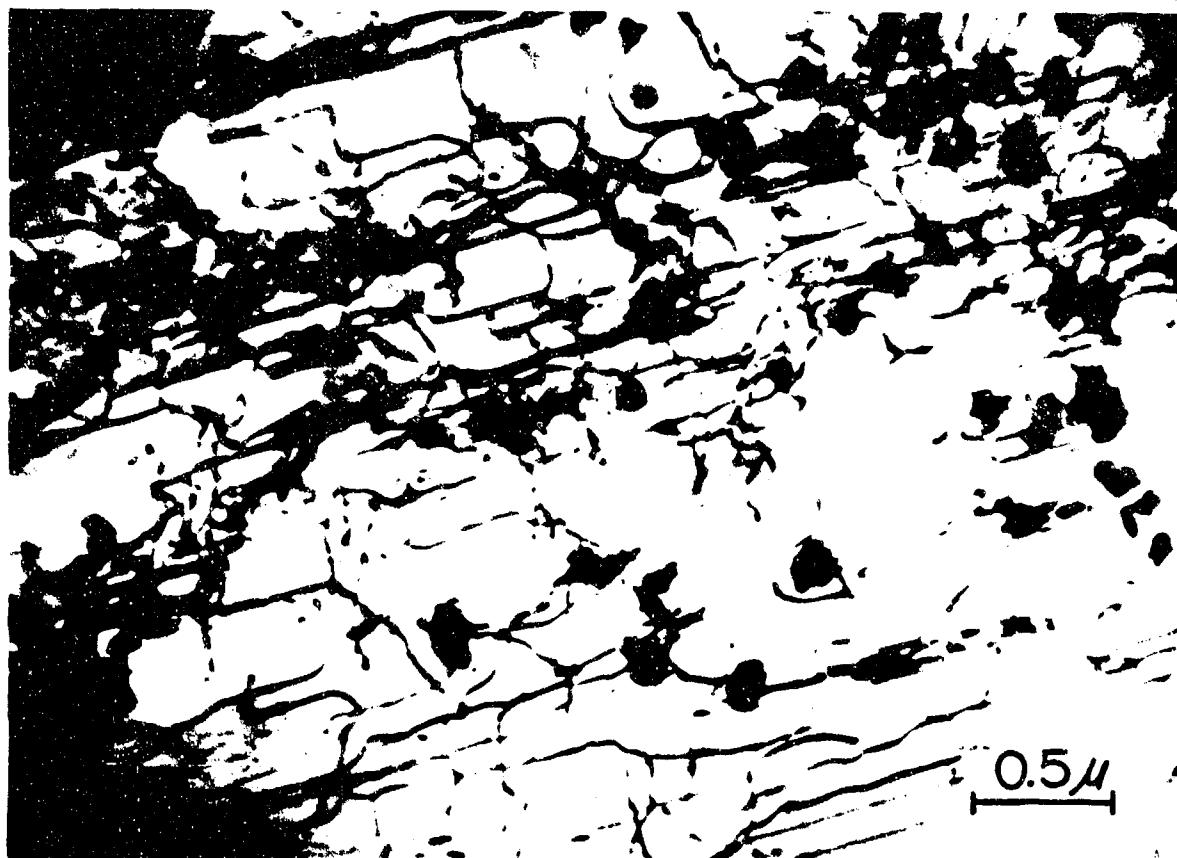
Fig. 3. (a) Undeformed (annealed) Inconel. Arrow indicates especially prominent
coherent strain contours at a precipitate. Other precipitates also display the line
of no contrast, normal to the diffraction vectors indicated. (b) Dislocation substruc-
ture in Inconel shock-loaded at 100 Kb. Note lack of coherency strains at the preci-
pitates and the interfacial dislocations. The surface orientation in (a) and (b) is
(110). (125 KV)

precipitates became strained from the matrix, i.e., they became incoherent. Evidence for this phenomenon is readily apparent from the fact that coherency strain contrast evident in Fig. 3(a) (especially prominent at the arrow) is not observed at the precipitates in Fig. 3(b) following shock deformation. In addition, the general lack of prismatic dislocation loops, and the high density of elongated and bowed dislocations suggests that the precipitates in many cases were sheared by the passage of dislocations, or acted as barriers to their motion.

Figure 4(a) shows the occurrance of twin-faults in the Inconel matrix as the mode of deformation at 370 Kb pressure. Figure 4(b) shows for comparison the corresponding defect substructure in pure nickel at the same pressure. We now observe that, with reference to Fig. 2, the marked contrast in shock hardening between pure nickel and Inconel alloy at higher pressures is due to the difference in the residual defect structure.

In the case of pure nickel, increasing shock pressures simply decrease the dislocation cell sizes, and this character of defect persists. On the other hand, the planar dislocation arrays in Inconel (Fig. 3(b)) increase in density, and transform to twin-faults in the pressure range above about 200 Kb.

Future work will concentrate on elucidating the mechanism of precipitate strengthening in the shock-loaded Inconel, and the effects of the lower stacking-fault energy of the Inconel as compared with pure nickel. In addition, work is continuing on the fabrication of very high
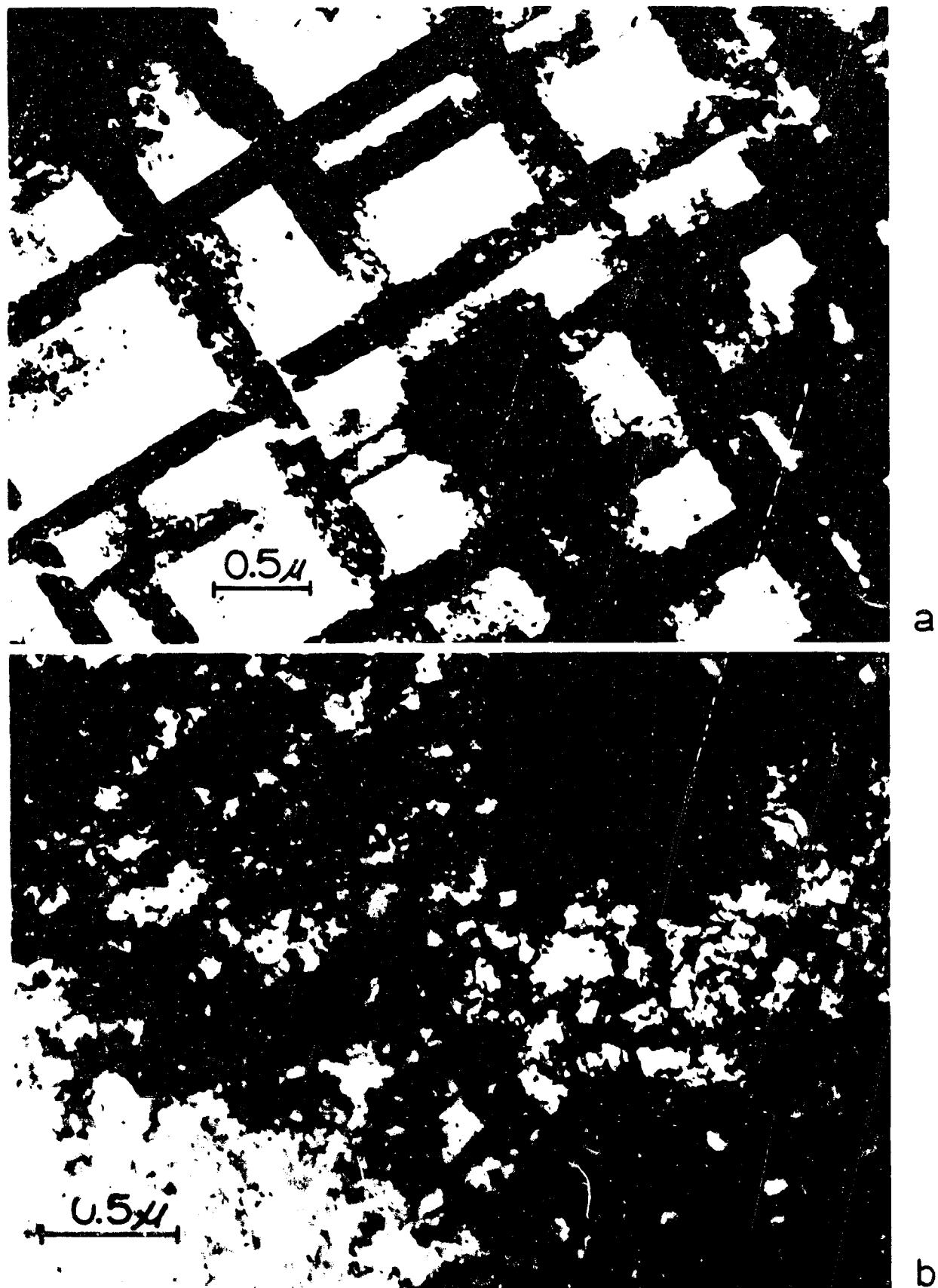
Fig. 4. (a) Deformation microtwin structure in Inconel foils following explosive shock-loading at 370 Kb. Note the region of no contrast where the twins intersect. The twin width can be measured directly from the width of this region. The surface orientation is close to (100). (b) Dislocation cell structure in pure nickel foils following shock deformation at 370 Kb pressure. The grain surface orientation is close to (110). (125KV)

-98-

pressure shock assemblies of 304 stainless steel. Three assemblies are
intended for explosive loading at pressures above 1 megabar and at low
temperatures in order to investigate the shock-recovery phenomenon
previously observed[2].

References

1. M. C. Inman, L. E. Murr, and M. F. Rose, ASTM STP 396, p. 39,
    (1966).

2. L. E. Murr and M. F. Rose, Phil. Mag. 18, 281 (1968).

3. L. E. Murr and M. F. Rose, Proc. Electron Microscopy Soc.
    America, 26th Annual Meeting Volume, p. 254 (1968).

4. M. F. Rose, Ph.D. Dissertation, Pennsylvania State University
    (1966).

5. L. E. Murr and F. I. Grace, Exp. Mechs. in the press.

1.5.3 Analysis of Grain Boundary Equilibrium and Relative

Interfacial Free Energy Phenomena in Thin Solid Films

AF-AFOSR-496-67, Joint Services Electronics Program

L. E. Murr and R. J. Horylev

This research has as its objective the investigation of inter-
facial free energy phenomena and equilibration processes in solids. The
mode of attack is the direct observation of interfacial structure and
geometry in representative thin sections by transmission electron
microscopy[1].

During the current research period, preliminary studies
concerning the characterization of low angle (energy) and high angle

(energy) grain boundaries in polycrystalline metals and alloys were conducted on 304 stainless steel. The method of analysis involves the observation of grain boundaries in the electron microscope and the recording of the selected area electron diffraction pattern in the adjoining grains. After the assurance of the accuracy of the grain orientations on opposing sides of the interface, the diffraction patterns are superposed, and the smallest angular difference between the [110] directions of grain orientation measured. The image contrast features are then employed in deciding the approximate nature of the interface (low or high energy); and the angles of misorientation are then plotted in corresponding histograms.

The preliminary results of this investigation have been very encouraging, since there is a marked difference in the angles of misorientation for the two boundary types. Figure 1 illustrates the preliminary data. The real significance of these results is that for the first time, grain boundary misorientations have been measured in a real solid as opposed to some fabrication of oriented single crystals.

Encouraged by the preliminary work, we are now pursuing the detailed analysis of crystal misorientation as it relates to grain boundary structure and energy. It now appears possible to determine the average values of low-angle grain boundary free energy. In order to pursue this point further, we are re-investigating the relative twin boundary grain boundary free energy ratio in stainless steel as previously measured by Murr[2]. However, in the present extension of this work,
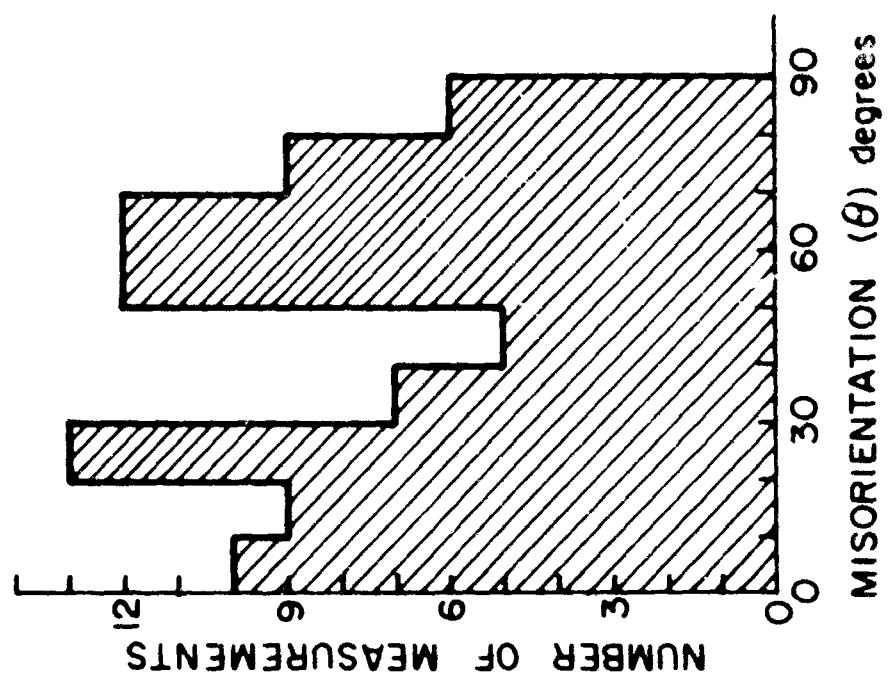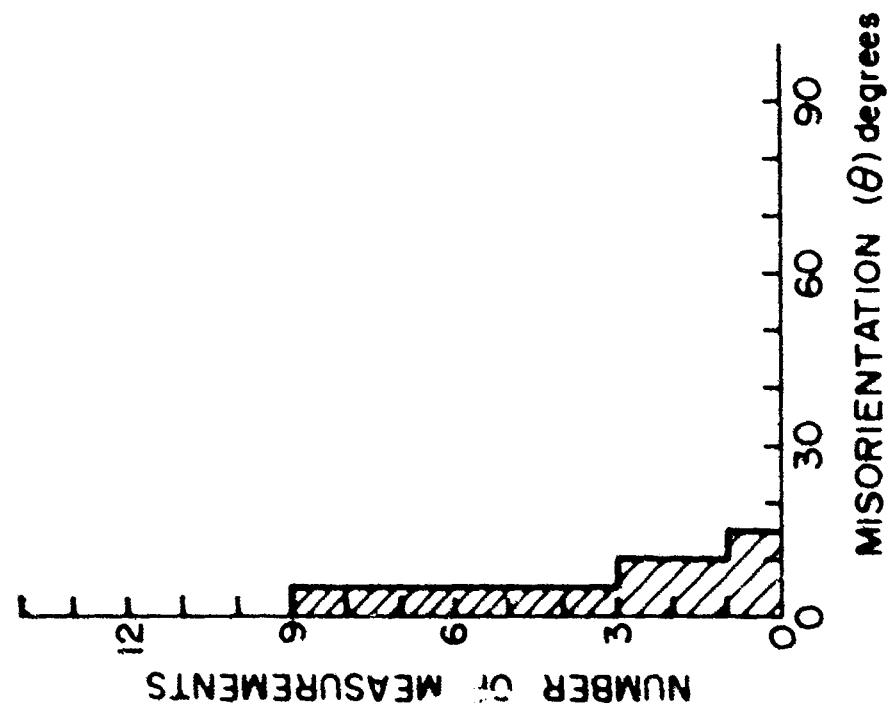
Fig. 1. Angular coincidence distribution of grains on opposing sides of a grain boundary in type 304 stainless steel as measured in the electron microscope. (a) low-angle grain boundaries. (b) High-angle grain boundaries. The angular measurements were made for [110].

the grain orientations in the twinned matrix and the opposing grain will be recorded and the misorientation of [110] determined for each junction system. In this way, we hope to relate the average grain boundary free energy to the angular misorientation of the competing grains assuming a constant twin boundary free energy, δ_{tb}, of 18 ergs/cm^2 as determined previously[2].

References

1. L. E. Murr, Phys. Stat. Sol. 19, 7 (1967).

2. L. E. Murr, Acta. Met., 16, 1127 (1968).

1.5.4 Vapor Deposition of Metals

We have continued the fabrication of ultra-high vacuum systems for evaporation of uncontaminated thin foils for studies relating to thin film energetics. We are also fabricating an evaporation unit to be incorporated into a standard evaporation chamber to accommodate some pilot studies on the vapor deposition of gadolinium, with the view towards studying dynamic recrystallization and grain growth kinetics in the pure foil or its oxide following the previous work of Murr[1].

Initial designs have also been drawn for the fabrication of a special vacuum unit having the capability of aiding in the investigation of the influence of electric and magnetic fields on the nucleation and

growth of vapor deposited thin films.

References

1.   L. E. Murr, Phys. Stat. Sol., <u>24</u>, 135 (1967).

2. APPLIED ELECTROMAGNETICS AND PLASMAS

2.1 PLASMAS

2.1.1 Reflection and Transmission of Waves from Magnetized Nonuniform Plasma Slabs

GK 1115, National Science Foundation

AF-AFOSR-496-67, Joint Services Electronics Program

H. H. Kuehl, B. B. O'Brien

The study of the plasma slab formed by using a pulsed high-frequency transmitter as the energy source has been continued[1]. The Buchsbaum-Hasegawa resonances[2] have been observed in several noble gas afterglow plasmas. Probe measurements are presently being carried out to determine the density profile and temperature during the afterglow.

References

1. Consolidated Semiannual Progress Report No. 7, USC.

2. S. J. Buchsbaum and A. Hasegawa, Phys. Rev. **143**, 303 (1966).

2.1.2 Photolithography Laboratory for the Fabrication of Microwave Devices

AF-AFOSR-496-67, Joint Services Electronics Program

W. V. T. Rusch, E. D. Garlinger

Complete facilities for the fabrication of microwave devices using photolithographic planar photoresist techniques have been established and are currently in operation. These facilities include:

1. A complete furnace system for the deposition of SiO_2 on semiconductor substrates.

2. A spinner for the application of photoresist to substrates.

3. Masks, mask alignment and exposure system.

4. All requisite chemical facilities for the photoresist processes and other subsequent procedures.

5. Electrolytic baths and a vacuum strip-heater for the preparation of back contacts.

6. Electrolytic baths and facility to fabricate Schottky-barrier interfaces on planar structures.

7. Electronics to test the DC characteristics of the devices.

8. Mechanical equipment to mount the finished devices in appropriate waveguide configurations.

Activities to the present time have been primarily concerned with the fabrication of one to two micron diameter Schottky-barrier diodes for 90-GHz mixer applications.

Additional projects have involved electrolytic procedures for the plating of gold and tin.

2.2 MILLIMETER WAVE RADIOMETRY

2.2.1 Millimeter-Wave Radiometry for Radio Astronomy

NASA7-100, National Aeronautics and Space Administration

952 210, Jet Propulsion Laboratory

W. V. T. Rusch, A. Cooper, S. Slobin

The total integrated opacity of the atmosphere can be determined by measuring the radiation from an extra-terrestrial microwave source over a range of zenith angles. The sun is a strong source of millimeter-wave radiation that can be used for this purpose. In the interest of acquiring large amounts of atmospheric data, a semi-automated sun tracking system (STS) is being constructed. The data obtained in this manner can be correlated with ground-level atmospheric parameter data. Correlations of these two sets of data should provide information useful in many types of communication systems such as, for example, satellite repeater stations. Furthermore, the present nodding subdish system[1], because of its beam switching capabilities, should be particularly well suited for such a sun-tracking system.

The STS will consist basically of the existing 90-GHz radio telescope with appropriate modifications. The antenna will be tilted into its equatorial position. Accurate automatic tracking of the sun will be provided by a closed-loop control ystem such as the one proposed below.

The error sensing element will be a refracting telescope consisting of a two-inch achromatic objective having a 24-inch focal length

-107-

and a Barlow lens having a magnification of 4X. The effective focal length of this optical system will then be 120 inches. The diameter of the sun's image produced by this telescope will be one inch; movement of the sun through one minute of arc will move the image by 0.35 inches. Four photoconductive cells will be placed in the focal plane of this optical system, as indicated in Figure 1. When the sun is centered evenly on the four cells, the resistances of all cells will be equal, and no error signal is produced. If the sur's image should shift, the cells would be illuminated unequally, thereby producing an error signal. Suitable optical filters will be provided to obtain optimum response from the photoconductive cells.

Figure 2 shows the electrical equipment necessary to convert error signals from the photoconductive cells into control pulses. These control pulses will then be fed into SLO-SYN stepping motors located on the right ascension and declination areas of the telescope. These motors will redirect the telescope toward the sun. The photoconductive cells controlling the right ascension axis will also control the speed of a sidereal tracking motor. This system can be converted into an open-loop tracking system with appropriate modifications.

The electrical equipment shown in Figure 2 has been constructed and installed in the telescope drive system. The teslescope and its associated equipment for the photocells has been constructed. This telescope is currently being installed on the 90-GHz radiometer.

TELESCOPE (1/4 scale)

R. A. Axis

Dec. Axis

Photoconductive cells are positioned by set screws working against spring loads.

Photo Cell Assembly (full scale)

Figure 1

Figure 2

Equipment above the dashed line is to be added. Equipment below the dashed line is already in the system.
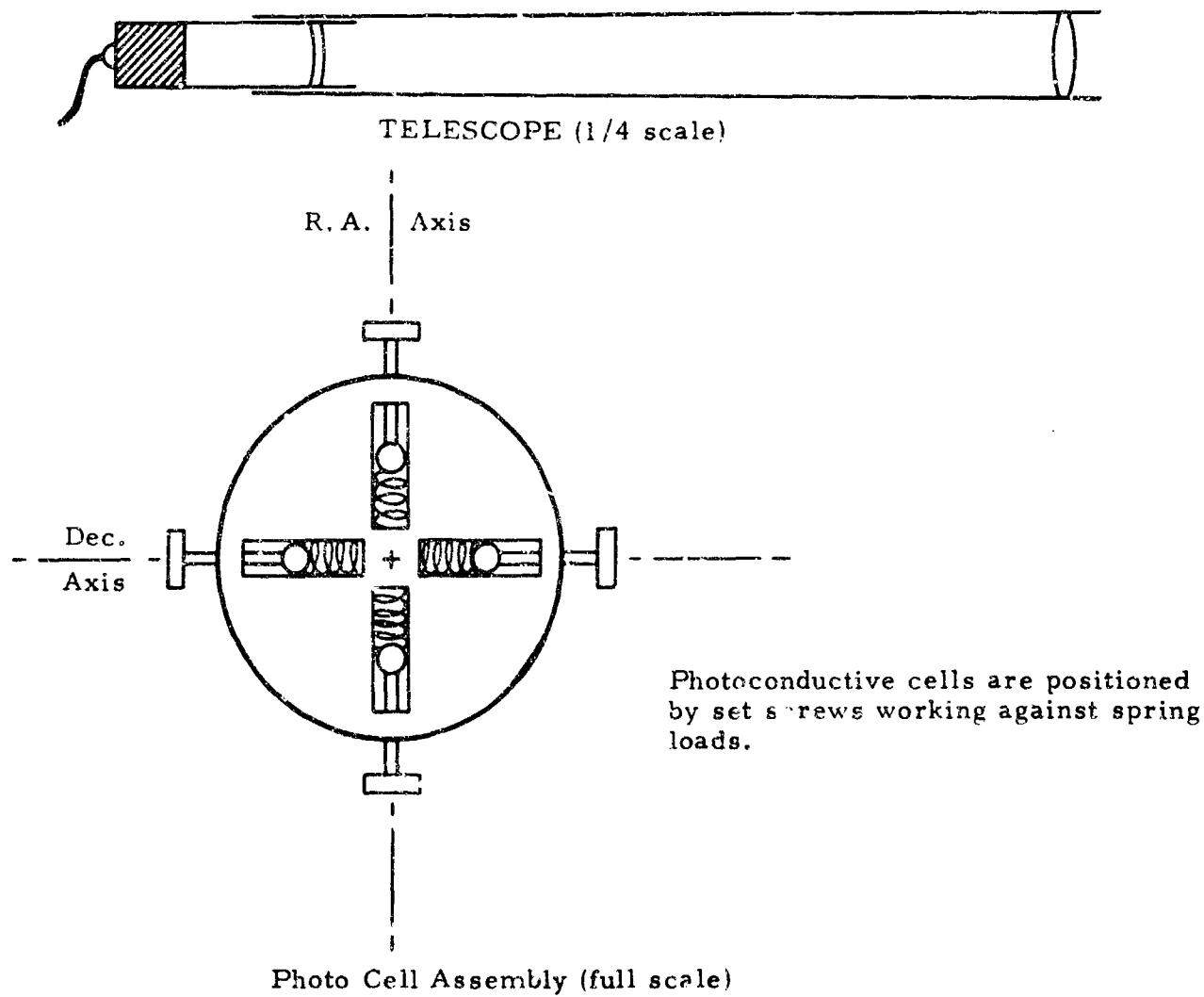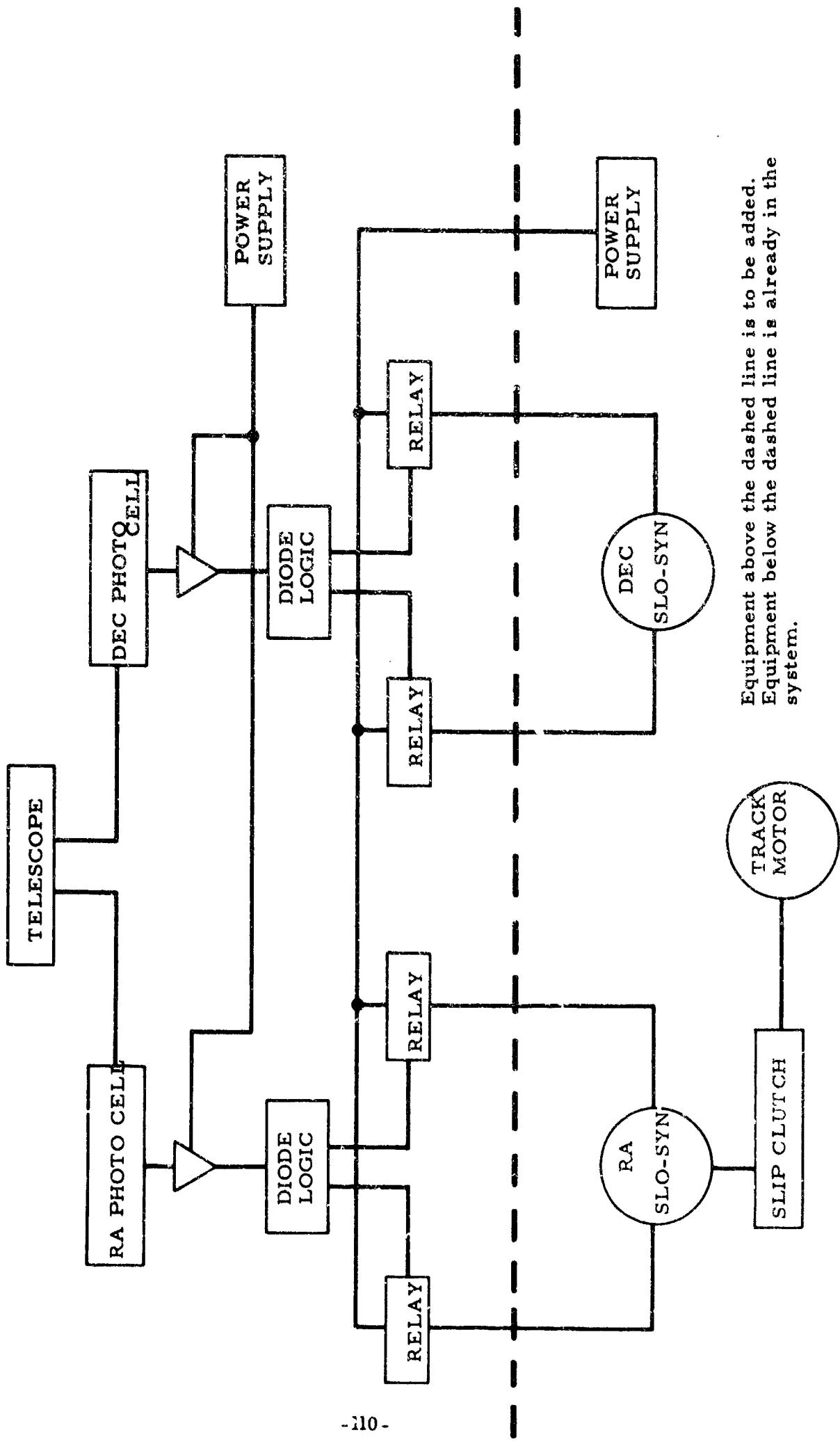
Reference

1. Consolidated Semiannual Progress Report No. 7, The Electronic
    Sciences Laboratory, School of Engineering, University of Southern
    California.

2.2.2 Phase-Center Relationships in an Asymmetric

Cassegrainian Feed-System

NASA7-100, National Aeronautics and Space Administration

952 210, Jet Propulsion Laboratory

W. V. T. Rusch, S. Slobin

Introduction

In an attempt to develop a beam-switching, synchronous

detection radio telescope for use in radio astronomy, the problem of

electromagnetic wave scattering from a tilted hyperboloidal subreflector

in a Cassegrainian antenna system was encountered. Beam switching is

accomplished by periodically nodding the subreflector from one asymme-

tric position to another at the synchronous detection rate. It is necessary

to know the position of the phase center of the scattered field in order to

accurately predict the displacement and position of the resultant primary

antenna beam.

The methods of phase center determination developed in this

report utilize techniques of geometrical optics and diffraction theory, in

several different forms. Which method is used depends to a large extent

on the accuracy of the result desired and the availability of high-speed

computing facilities. However, each method presented here gives a

-iii-

determination of phase center position with considerable accuracy.

All phase center determinations are for the specific geometry of the nodding subdish system. Various hyperboloid D/λ ratios are considered also.

Geometrical Concepts

Figure 1 indicates the geometry of the tilted hyperboloid system. In contrast to the symmetric geometry, where the axes of both the hyperboloid ($\overline{F'F''}$) and the paraboloid ($\overline{)F}$) are colinear, the source of spherical electromagnetic waves (Q) no longer lies on the hyperboloid axis of symmetry ($\overline{F'F''}$). Three reflected rays R_1, R_2, and R_3 are shown. With these reflected rays are associated virtual rays V_1, V_2, and V_3. In the tilted configuration there is no specific geometrically exact point of intersection of all the virtual rays. There is, rather, an envelope of points or caustic formed by the intersections of all neighboring virtual rays. The geometrical foci of the tilted hyperboloid are the points F' (virtual) and F'' (real). The prime focus of the paraboloid is at point F. Neither F' nor F may be regarded as the phase center of the scattered field in the tilted configuration.

Methods of Phase Center Determination

A. Determination of the Caustic Curve. It can be shown by a simple geometrical analysis that the caustic curve represents the locus of localized phase centers of sets of adjacent rays scattered from the hyperboloid. Consequently, it is informative to investigate the

Fig. 1

-113-
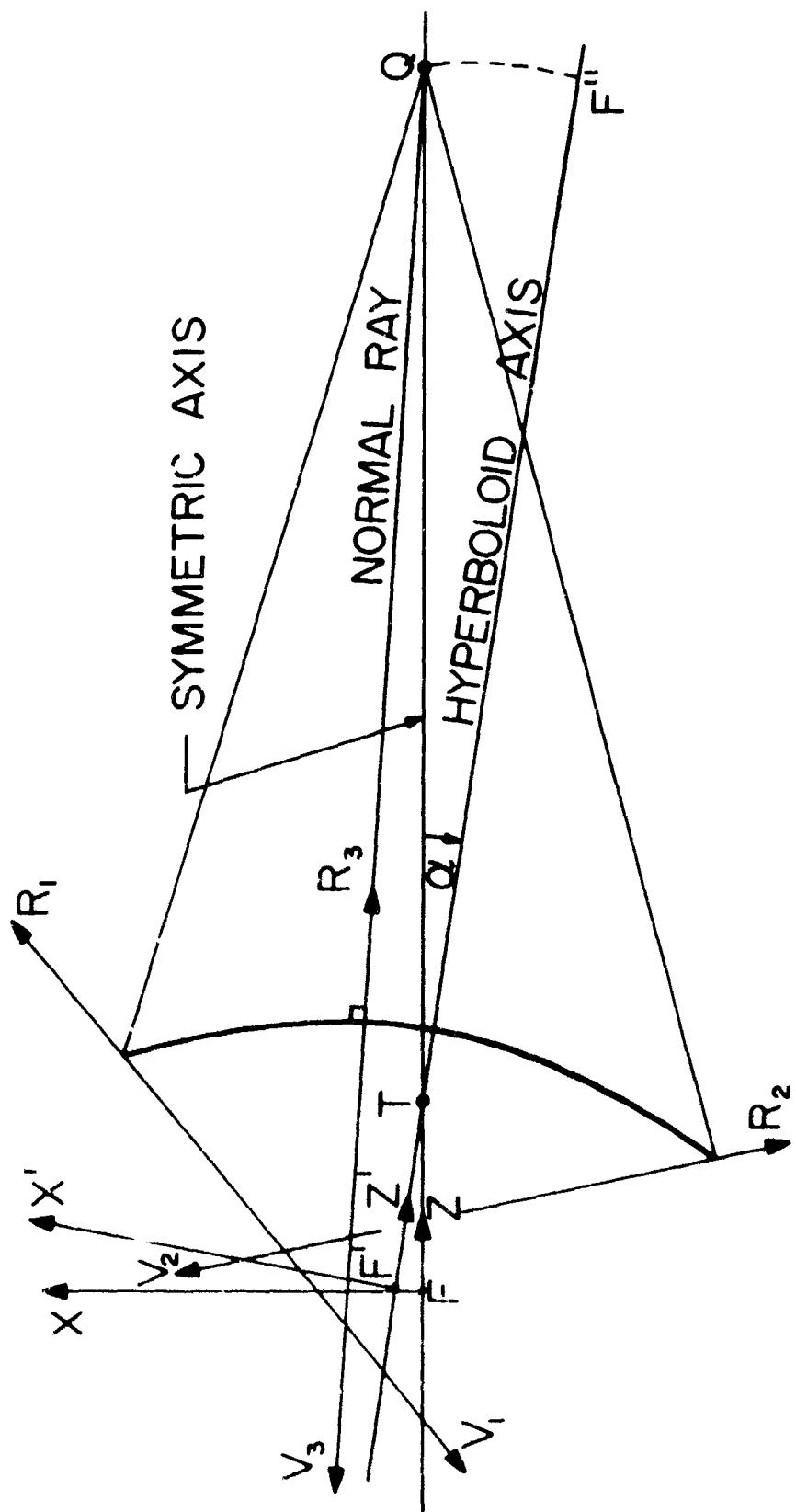
position of the caustic. The equations of the caustic curve are obtained

from the principles of differential geometry. It is found that the caustic

curve has two branches, each of which corresponds to the loci of the

two principal centers of curvature for each point of the reflected wave-

front. Of special interest is the point of intersection of the two branches

of the caustic curve, because of its nearness to the subsequently deter-

mined phase centers of the total scattered field. The position of the

caustic intersection point is listed in Table I and shown in Figure 2.

B. Phase Center Determination by Geometrical Optics. By

carrying out a ray tracing procedure in the case of the asymmetric geome-

try, a path length "phase" of the reflected field may be calculated on a

circle centered at the origin of the tilted (X'-Z') coordinate system. For

an asymmetric geometry, the phase on this circle will not be constant.

A best-fit phase center point may be postulated to exist; and this point is

found by a least-squares curve fitting technique in which the rms differ-

ence between the phase on circles centered at point F' and the phase on

circles centered at the postulated best-fit phase center is minimized. A

weighting technique is used to account for the non-uniform illumination

from the source Q. The position of this phase center point and all other

phase center points is shown in Figure 2.

C. Phase Center Determination by Physical Optics. A more

accurate representation of the scattered field for moderately sized hyper-

boloids can be obtained using the principles of physical optics. Using

results of a diffraction theory analysis of scattering from a tilted

No.	Analysis	Radius (a), wavelengths	Radius (a), millimeters	Angle (ψ)
1	Geometrical Optics Best-Fit Weighted, 117 pts.	---	5.714 mm	87.15°
2	Diffraction Theory Best-Fit Weighted, 121 pts., D/λ = 59.54, λ = 3.33 mm	1.707λ	5.684 mm	88.11°
3	Diffraction Theory Best-Fit Weighted, 121 pts., D/λ = 24, λ = 8.26 mm	0.689λ	5.691 mm	89.37°
4	Diffraction Theory Best-Fit Weighted, 121 pts., D/λ = 10 λ = 19.83 mm	0.289λ	5.731 mm	94.04°
5	Intersection of Caustic Curve	---	5.321 mm	88.76°
6	Application of Demagnification Formula D/λ = 59.54, λ = 3.33 mm	1.595λ	5.318 mm	87.82°

Table I

hyperboloid, the phase of the scattered field may be specified on circles
centered at point F, the origin of the untilted (X-Z) coordinate system.
A least-squares curve fitting technique, identical to that described in
Section D, is utilized to determine a best-fit phase center for the physical
optics case. Hyperboloid D/λ ratios of 59, 54, 24, and 10 are considered.
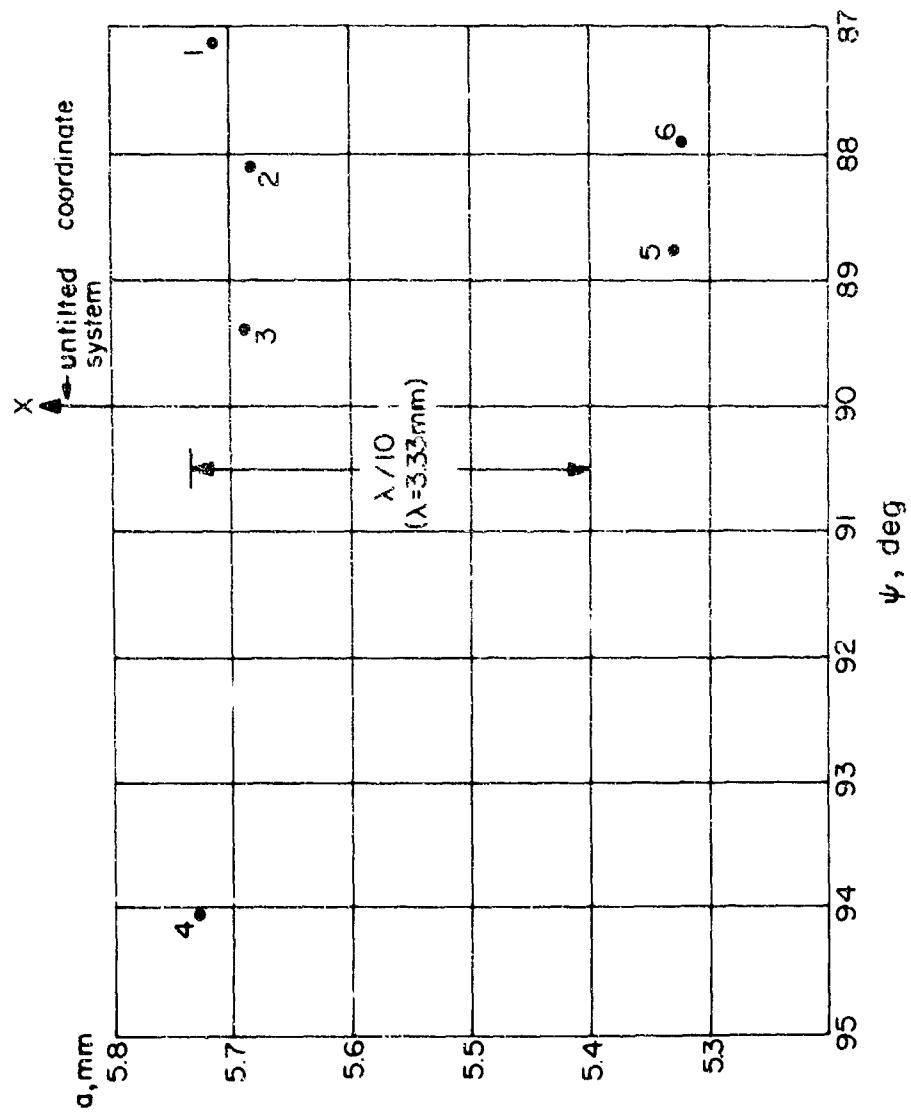
Fig. 2

and phase center positions for the three cases are found to lie within approximately 0.7 mm of each other. A fifteen-fold decrease in rms phase variation around the best-fit phase centers has been determined, compared to the phase variations around the paraboloid prime focus (F).

D. Phase Center Determination from Demagnification

Formulas. The hyperboloidal subreflector in a Cassegrainian antenna system acts like a demagnifying optical system. Following optical rules regarding image movement as a function of source movement, an optically equivalent system may be set up for the tilted hyperboloid geometry. The simple rules yield a remarkably accurate determination of phase center position. It is to be expected, however, that for more extreme tilt angles than that in the nodding subdish system (2.06 deg) the demagnification formulas will produce less accurate results than those obtained by previously discussed methods.

Summary of Results and Conclusions

The coordinates of all phase centers determined by the methods of the previous section are shown in Figure 2 and tabulated in Table 1. Not shown in the figure is the actual physical position of the hyperboloid geometric focus (F') in its tilted position. The position of F' is almost 3mm below the points shown in Figure 2.

In general, the phase center determination by the methods of physical optics yields the most accurate results; however, for D/λ ratios of 10 or larger and moderate tilt angles, the results of all techniques agree to within 0.1 to 0.2 wavelengths.

-117-

The geometrical focus F' of the tilted hyperboloid may not be regarded as the phase center of the scattered field.

The computed phase center displacement may be used in conjunction with standard beam-deviation-factor formulas to estimate the displacement of the primary antenna beam with considerable accuracy.

2.2.3 Pioneer VI Solar Faraday Rotation Experiment

J. E. Ohlson, W. V. T. Rusch, C. T. Stelzried

Introduction

In November 1966, the Pioneer VI Spacecraft will undergo solar occultation as it passes approximately one earth orbital radius behind the sun. During the immersion and emersion phases of the occultation the spacecraft radio signals to earth will pass through the solar corona. This offers a unique opportunity to measure the Faraday Rotation undergone by a linearly polarized electromagnetic wave upon passing through the solar corona. The data obtained will give information on the free electron density and magnetic field in the corona. This experiment is being performed jointly with personnel of the Communications Elements Research Section of the Jet Propulsion Laboratory, G. S. Levy, B. Seidel and T. Sato, in support of a NASA contract 150-22-13-05033.

Theory

The rotation of the plane of polarization of a linearly

-118-

polarized electromagnetic wave upon passing along a path in a magneto-
ionic medium is

$$\Omega = \frac{\text{const.}}{f^2} \int_{\text{path}} N(s) \, \overline{B}(s) \cdot \overline{ds}$$

where f is cyclic frequency, N(s) is free electron density and $\overline{B}$(s) is the
vector magnetic field. By obtaining continuous data on Ω for several
hours each day during the occultation phases, a large body of data will
be available for fitting to various models of the corona.

Measurement Techniques

Several physical constraints make the measurement of Ω very
difficult:

(1) The 270,000,000 kilometer spacecraft-earth distance
produces an extremely weak signal at earth (-161 dBm).

(2) As the spacecraft nears the sun (in angle), intense solar
radio noise enters the antenna pattern sidelobes and it appears that
tracking the spacecraft closer than about 1° to the sun will not be
possible.

(3) Coronal plasma turbulence produces spectral spreading
of the signal, which makes signal tracking difficult. This effect also
worsens as the sun is neared.

(4) The earth's ionosphere contributes a varying rotation of
$1-5^{\circ}$ to the signal. This effect must be determined to allow corrections
of the data.

-119-

(5) An apparent rotation of the spacecraft is caused by the earth's rotation and also by the motion of the tracking antenna, since it has an Az-El instead of polar mounting.

The 210 foot diameter NASA/JPL antenna at Goldstone with maser receivers is the most sensitive facility in the world for S-band spacecraft signals. Extensive modification of the r.f. hardware and receiver configuration has produced an antenna with a mechanically driven cross-polarized feed system. Using monopulse-radar circuitry, one feed produces an error signal which serves the primary feed to the received polarization. The primary feed thus receives maximum signal for a phase-locked-loop for frequency tracking and determination of a detection reference phase for the error channel. The mechanical position of the feeds is the estimate of received signal polarization. This is digitally recorded and later transformed (taking into account the effects of (5) above) by a computer to give polarization rotation. Measurement accuracy is not limited by mechanical errors, but by signal to noise ratio.

A prediction of Ω indicates that it will reach a maximum of about 10° before real-time tracking of the signal, as described above, will not be feasible due to small SNR. At that point, open-loop recording at i.f. will be made with the polarizer feeds in a fixed position and the receiver using a fixed local oscillator. Computer spectral analysis processing will allow following the signal down to a smaller SNR than the real-time system will permit. The reason for not using open-loop recording and processing for all data is that phase and amplitude

instabilities of the masers and receiver, while negligible for most applications, produce first-order errors in angle measurements in post-experiment processing. These effects are negligible in the real-time system.

Specific Accomplishments

(1) Design of antenna feeds and receiver configuration.

(2) Nearly completed implementation of (1).

(3) Analysis of system measurement capability. A good approximation to the error in measurement of polarization angles has been shown to be

$$\sigma_\theta = C \sqrt{\frac{T_{op}}{\tau}} \qquad C \approx 1$$

where σ_θ is r.m.s. error in degrees, T_{op} is system operating temperature in ^oK, and τ is the system response time in seconds.

(4) A computer program has been implemented to determine refractive effects of the corona.

(5) A set of computer programs to allow transformation of polarization data between terrestrial and celestial coordinates has been written.

(6) A receiver with a separate antenna has been installed to measure the rotation produced by the earth's ionosphere in order to remove this effect from the data. This is being done by tracking a stationary satellite.

(7) Preliminary data indicate a system accuracy in agreement with (3).

Future Plans

(1) The final experiment configuration will shortly be completed.

(2) Data will be taken through the occultation period.

(3) The second phase of the experiment will begin as the data are evaluated, coronal models are determined and solutions of coronal parameters are found. This will involve extensive use of data from other experimenters who have measured coronal parameters in other ways.

3. INFORMATION SCIENCES

3.1 CONTROL SYSTEMS

3.1.1 Optimal Control Problems

AF-AFOSR-1029-67A, Air Force Office of Scientific

Research

L. W. Neustadt

Necessary conditions for optimal control problems with
restricted phase coordinates and delay-differential equation constraints
were obtained and were published in the Ph. D. dissertation of Dr. S. C.
Huang. These conditions extend the well-known Pontryagin maximum
principle. This work was extended by Dr. Huang to obtain necessary
conditions for optimal control problems where there are constraints in
the form of integral equations. Investigations have begun on optimal
control problems with functional differential equation constraints. The
results that will be obtained will hopefully include those of Huang as
special cases.

Three articles, describing the results of previous research
which consider conventional optimal control problems from a new view-
point and which also give a general abstract theory of extremality, have
been completed by L. W. Neustadt.

3.1.2 Optimum Inputs for Parameter Estimation

N. E. Nahi, D. E. Wallis, Jr.

The quality of estimates of parameters of nonlinear dynamic
systems is effected by the inputs to the system. It is then desirable to
choose the input, from an admissible class, in order to enhance the
quality of the optimum estimator.

A method for finding optimal deterministic inputs for estima-
tion of system para. eters from noisy output data is given. Analytical
difficulties connected with the Bayesian approach to this joint optimal
control and optimal estimation problem are overcome by postulating that
an "efficient" estimator of the parameter exists. For such estimators,
the Cramer-Rao lower bound (CRLB) is equal to the optimal (minimum)
estimation variance, and its formulation is shown to be a functional only
of the system input. Therefore, if an input minimizes the CRLB, it is
(together with the postulated efficient estimator) the optimal input for
joint minimum-variance system parameter estimation. Minimization of
the CRLB is made possible by a sensitivity-theoretic extension of a
result of Slepian to the case where a signal is generated as the output of
a differential equation containing the parameter. This extension leads
to a deterministic integral-quadratic-cost optimal control problem which
may be solved by established techniques. In a certain sense, the method
presented enables determination of an input which optimizes the 'potential"

for subsequent minimum-variance parameter estimation. The required efficient estimator is not derived.

3.1.3 Wide Angle Optical Tracking

NGR-05-018-044, National Aeronautics and Space Administration

N. E. Nahi

The application of linear (Kalman-Bucy) filtering to estimation of target trajectory is well known. Typically the problem is formulated as follows. The unknown trajectory is presented as the output of a dynamical system. The possible variations of this trajectory due to unpredictable variations of acceleration and other effects are characterized by random inputs to this dynamical system. Some function of the trajectory is observed by means of an instrument, such as Radar. This observation is always corrupted by noise. An estimator (filter) is then designed to operate on the noisy observation and yield a best estimate of the target trajectory (a present or future value), recursively.

What is assumed in such an estimator as described above is that any observation belongs to the trajectory (which we are estimating) with certainty. In other words, any time an observation is received, if we exclude the contribution of the observation noise, we assume that we have received a known function of the trajectory.

Let us consider the problem of tracking a target in a wide-

angle field of view. Now any observation is either a function of the

trajectory (of course corrupted by observation noise) or it may not

belong to that trajectory at all. Examples of these appear in tracking

a target existing on an optical or IR picture. The observation may then

consist of detecting, as time proceeds, bright points on the picture.

However, at any time, false bright points (false alarms) may appear

which are not connected with the trajectory being tracked. Consequently,

a probability is associated with each observation indicating the probability

that the observation belongs to the trajectory. A recursive filter is then

derived on the basis of utilizing this information.

Reference

1. N. E. Nahi, Estimation Theory and Applications, John Wiley & Sons, 1968.

3.1.4 Optimum Design of Vehicles with Constrained Observation

NGR 05-018-044, National Aeronautics and Space

Administration

F04(695)-67-C-109, Space Systems Division, Air Force

Systems Command

N. E. Nahi, T. Cooper

The feedback operation of many systems is based on the

information obtained by various on-board sensors. Often these sensors

have discrete outputs, such as the output of a track-scan radar system.

Due to various effects of random noise there is a non-zero probability

that a specific observation in the future may not be received. Clearly, the optimum design of the vehicle should utilize this critical information. In other cases, the designer may have influence over the observation scheme used. For example, he may increase the observation sampling rate. However, this, in general, results in more complex devices (such as those yielding higher scan rate) and higher data processing capability (due to the larger volume of data to be processed). It is then logical to associate a "cost" to each observation and to incorporate this cost into the criterion of system design.

The problem of design of linear feedback systems with quadratic cost function, and when both the system and the observations include additive random noise, has been satisfactorily solved over the last decade. It has been shown that the optimum design involves a cascade of a Kalman filter and an optimum gain matrix. Procedures for derivation of the gain matrix have been derived leading to feasible computer algorithms. The problems posed in introduction can be considered as extension and modification of these results.

Various approaches to solution of the mentioned problem are considered. Basically the procedure of dynamic programming is utilized. At present, this attempt has yielded partial success toward solving the first problem, namely, design of optimum linear discrete systems with given probabilities for making future observations. The second problem is transformed into a linear system with a new cost, by means of associating a cost to making observations. It is expected that, in conjunction

with the derivation of the optimum feedback control system, we arrive
at optimum observation schemes, such as how often it is necessary to
make an observation.

3.1.5 Design of Random Circuits

AF-AFOSR-1029-67, Air Force Office of Scientific
Research

D. F. Elliott and D. D. Sworder

Where applicable, stochastic approximation provides a tool
which permits the engineer to include component uncertainties in his
design work. The question of convergence of this algorithm in circuit
applications was explored in [1] using Dvoretzky's fundamental theorem.
Recently the problem posed in [1] has been investigated and conditions
sufficient to guarantee convergence have been given a sensitivity inter-
pretation.

Suppose an engineer wishes to synthesize a circuit to perform
a specified task and suppose that the performance measure is denoted by
h. The performance of the circuit depends upon its component elements,
some of which are imperfectly known. Let the vector of system param-
eters to be selected by the circuit designer be denoted by $\underline{b}$. For example,
if the behavior of a circuit is very sensitive to a pair of "10-percent"
resistors, $\underline{b}$ might be a two component vector with the first component equal
to the nominal value of the first resistor. The performance measure can
be written as $h(\underline{b})$.

The classical methods of circuit design simply neglect component tolerances and the designer selects as best that parameter vector which minimizes $h(\underline{b})$. In truth, however, choice of $\underline{b}$ only fixes the probability distribution function of the random variable $h(\underline{b})$ since the parameters actually realized in the circuit will deviate from their nominal values. A more appropriate performance measure might be the expected value of $h(\underline{b})$;

$$H(\underline{b}) = E\{h(\underline{b})\} \ .$$

To be more precise, suppose that there are q system design parameters (resistor values, capacitor values, amplifier gains, etc.). Any specific circuit configuration is described by a q-dimensional vector $\underline{b}$ with components b_i; $i=1,\ldots,q$. Suppose that there are constraints on the allowable parameter values:

$$b_i \ \epsilon \ [\alpha_i, \beta_i]; \quad i=1,\ldots,q \ ,$$

where $\|\underline{\beta} - \underline{\alpha}\| < \infty$. Denote the q-fold Cartesian product of intervals $[\alpha_i, \beta_i]$ by $C(\underline{\alpha}, \underline{\beta})$. The engineer then seeks that $\underline{\theta} \ \epsilon \ C(\underline{\alpha}, \underline{\beta})$ such that

$$H(\underline{\theta}) = \inf_{\underline{b} \ \epsilon \ C(\underline{\alpha}, \underline{\beta})}$$

In [2] it is shown that under suitable restrictions, a modified Kiefer-Wolfowitz procedure will generate a sequence of parameter settings which converge to $\underline{\theta}$ with probability one. The most interesting restriction is one which constrains the relative magnitude of the eigenvalues

of the Hessian matrix of the regression function at θ. The implication of this result is that convergence may not occur if the system performance is overly sensitive to a circuit parameter.

References

1. K. B. Gray, "The Application of Stochastic Approximation to the Optimization of Random Circuits", Proceedings of Symposia in Applied Mathematics, Vol. 26, pp. 178-192, 1964.

2. D. F. Elliott and D. D. Sworder, "On the Design of Random Circuits", IEEE Trans. on Circuit Theory, (to appear).

3.1.6 Control of Stochastic Systems

AF-AFOSR-1029-67, Air Force Office of Scientific

Research

D. D. Sworder

Recently it has been shown that the maximum principle may be employed to design controllers for stochastic systems[1]. Indeed, it was demonstrated that the differential equations for the adjoint variables are identical to those of Pontryagin when the random disturbance is additive white noise. This success with the problem posed in the indicated reference might lead one to hope that perhaps the maximum principle formalism can be extended to a wide class of stochastic systems.

Actually, this extension may not be made without introducing additional complexity. While a technique similar to the maximum principle may be employed to find the best control policy for an important class of systems with multiplicative disturbances, fundamental changes must be

-130-

made in the equations for the adjoint variable^2. Instead of leading to a set of stochastic ordinary differential equations as in Kushner's work, the formalism leads to a set of stochastic partial differential equations.

The motivation for this work stems from a need to design controllers for systems whose components are subject to failure. The natural model for plants of this type must include multiplicative disturbances of the jump type. If random variations occur in the system, a feedback controller is necessary to insure adequate performance under all operating conditions. The question then arises as to how best to process the information available to the controller.

In [3] and [4] several interesting cases in which the design equations could be solved explicitly were studied. For analytical convenience, attention was restricted to linear plants although the controller and hence the total system was nonlinear. It should be explicitly noted that the class of problems was not restricted to Markov decision problems.

References

1. H. J. Kushner, "On the Stochastic Maximum Principle: Fixed Time of Control", J. of Math. Analysis and Applications, Vol. 11, pp. 78-92, June 1965.

2. D. D. Sworder, "On the Stochastic Maximum Principle", J. of Math. Analysis and Applications (to appear).

3. D. D. Sworder, "Feedback Control of a Class of Linear Stochastic Systems", 1968 Joint Automatic Control Conference, pp. 34-44, 1968.

4. D. D. Sworder, "On the Control of Stochastic Systems; II", Int. J. of Control, (to appear).

5.1.7 Fuel Optimum Spacecraft Attitude Control

H. J. Payne, R. B. McGhee, W. H. Spuck

Since the mission life of long duration space flights is often

limited by fuel supply, it becomes important to utilize fuel, a for

attitude control, in optimal or near optimal fashion. It has been the

objective of this program to determine for simple models of attitude

control systems (1) optimal control laws and the related fuel   expenditure

rate, and (2) the relative efficiency of practical controllers, i. e. , con-

trollers which are specified in such a way that implementation is relatively

easy.

As previously reported, the first portion of the effort was

completed for a system described by

$$\ddot{x} = u + n(t)$$

in which x represents angular position, u the control force and n(t) the

perturbing forces. These results have been reported internally[1] and

submitted for publication[2].

Work has been initiated which is intended to provide the

basis for the study of practical controllers. This effort includes the

refinement of numerical methods so that results may be obtained more

efficiently. It was sufficient in the study of optimal control laws to use

simpler number numerical methods, i. e. , explicit schemes, since a

limited number of cases had to be computed. But if several practical

controllers are to be examined, more efficient numerical schemes become

necessary. Among the schemes being considered is the implicit Crank-

Nicolson procedure.

References

1. R. B. McGhee, H. J. Payne and W. H. Spuck, "A Numerical Method
    in Fuel Optimum Stochastic Attitude Control", Department of
    Electrical Engineering Report No. USCEE 284, University of
    Southern California.

2. R. B. McGhee, H. J. Payne and W. H. Spuck, "Fuel Optimum
    Stochastic Attitude Control", submitted for publication to PG-AC.

3.1.8 High Density Freeway Traffic Control

AF-AFOSR-496-67, Joint Services Electronics Program

H. J. Payne

Bottlenecks on the freeway of recurrent (arising because of

geometry, e.g., points of on-ramp merging and freeway intersections)

and nonrecurrent (e.g., due to accidents) nature add considerably to the

transit times for freeway users. It has been generally agreed that the

most efficient means of influencing traffic flow is to control on-ramp

flow. The intelligent design of on-ramp control schemes will require

an understanding of high density freeway traffic in the form of reasonably

accurate mathematical models.

Due to the large number of vehicles involved, it is appropriate

to introduce and develop equations involving variables which represent

gross properties of the traffic flow. Appropriate variables are ρ, density (number of cars per unit length of road); q, flow rate (number of cars passing a fixed observer per unit time); and u, mean speed (average speed of vehicles in a fixed length of road). The conservation of cars equation

$$\rho_t + q_x = 0$$

and the relation

$$q = \rho u$$

must be supplemented by an equation describing the dynamic behavior of traffic.

The model

$$q = Q(\rho) - \nu \rho_x$$

has been found to be inadequate in the sense that perturbations in traffic always dissipate, precluding, for example, a description of the development of "stop and go" traffic.

The model presently being studied is described by

$$u_t + uu_x = -\alpha (q - Q(\rho) + \beta u \rho_x) / \nu$$

Stationary solutions, in which all variables are functions of x-Ut for some fixed U have been investigated and used to describe some bottleneck situations. One interesting feature of these solutions is that traffic breaks down to near crawl conditions if the rate of traffic flow into a bottleneck exceeds a critical value. Stability analysis, using a linearized

-134-

perturbation equation with uniform flow the standard, shows that uniform

flow becomes unstable above a certain critical density.

Since the model depends on parameters α and β and the Road

Diagram function $Q(\rho)$, empirical data is necessary to complete the

mathematical description.

3.1.9 Asymptotic Control Theory and Two-Point Boundary-
Value Problems

GP8960, National Science Foundation

R. Bellman

Work has continued on the development of a stability theory

for two-point boundary-value problems paralleling the classical stability

theory of Poincare and Lyapunov. The following three papers are devoted

to this:

1.   R. Bellman, "On Analogues of Poincare-Lyapunov Theory for Multi-
     point Boundary-Value Problems--I," J. Math. Anal. Appl. Vol. 14,
     1966, pp. 522-526.

2.   R. Bellman, "On Analogues of Poincare-Lyapunov Theory for Multi-
     point Boundary-Value Problems--Correction," J. Math. Anal. Appl.,
     to appear.

3.   R. Bellman, "A Note on Asymptotic Control Theory," J. Math. Anal.
     Appl., to appear.

Secondly, an analogue of classical iteration

theory for two-point boundary-value problems was developed. See

R. Bellman, "Two-Point Boundary-Value Problems and Iteration,"
Aequationes Mathematicae, to appear.

3.1.10 Dynamic Programming and Partial Differential Equations

GP-8960, National Science Foundation

AT(11-1)-113, Atomic Energy Commission

R. Bellman, E. Angel

Work has continued in the application of dynamic programming
to the analytic and computational solution of nonlinear partial differential
equations of elliptic type. New methods, based on dynamic programming,
have been introduced which are far simpler than any existing methods
and thus easier to teach and carry out, and which seem to be more effec-
tive in a number of cases. This work is contained in Angel's thesis,
Dynamic Programming and Partial Differential Equations, and in the
following references.

References

1.   E. Angel, "Discrete Invariant Imbeeding and Elliptic Boundary-Value
     Problems Over Irregular Regions", J. Math. Anal. Appl., Vol. 23,
     1968, pp. 471-484.

2.   E. Angel, "A Building Block Technique for Elliptic Boundary-Value
     Problems Over Irregular Regions," J. Math. Anal. Appl., to appear.

3.   E. Angel, "Noniterative Solutions of Nonlinear Elliptic Equations,"
     J. Assoc. Computing Machinery, to appear.

3.2 COMMUNICATION AND RADAR SYSTEMS

3.2.1 Image Processing and Coding

NGR 05-018-044, National Aeronautics and Space

Administration

JPL 952312, Jet Propulsion Laboratory

W. K. Pratt and H. C. Andrews

The introduction of the fast Fourier transform algorithm has
led to the development of the Fourier transform image coding technique
whereby the two dimensional Fourier transform of an image is transmitted
over a channel rather than the image itself. This development has further
led to a related image coding technique in which an image is transformed
by a Hadamard matrix operator. The Hadamard matrix is a square array
of plus and minus ones whose rows and columns are orthogonal to one
another. A high speed computational algorithm, similar to the fast
Fourier transform algorithm, which performs the Hadamard transforma-
tion, has been developed. Since only real number additions and subtrac-
tions are required with the Hadamard transform, an order of magnitude
speed advantage is possible compared to the complex number Fourier
transform. Transmitting the Hadamard transform of an image rather
than the spatial representation of the image provides a potential toleration
to channel errors and the possibility of reduced bandwidth transmission.

Let the array $f(x, y)$ represent the intensity samples of an
original image over an array of N^2 points. Then the two dimensional

Hadamard transform, $F(u, v)$, of $f(x, y)$ is given by the matrix product

$$[F(u, v)] = [H(u, v)][H(u, v)]$$

where $[H(u, v)]$ is a symmetric Hadamard matrix of order N. Pre- and post-multiplication of $[F(u, v)]$ by the Hadamard matrix gives

$$[H(u, v)][F(u, v)][H(u, v)] =$$

$$[H(u, v)][H(u, v)][f(x, y)][H(u, v)][H(u, v)]$$

But, for a symmetric Hadamard matrix, $HH = NI$ where I is the identity matrix. Hence,

$$[f(x, y)] = \frac{1}{N^2}[H(u, v)][F(u, v)][H(u, v)]$$

and, aside from the constant scaling factor, N^2, the arrays $f(x, y)$ and $F(u, v)$ are two dimensional transform pairs.

Experiments have been performed to determine the nature of the two dimensional Hadamard transform of an image, and to assess the effects of a double Hadamard transformation. Figure 1a contains a cathode ray tube display of the logarithm of the magnitude of the ordered Hadamard transform of a Surveyor spacecraft scene. In this photograph the origin (zero frequency) appears in the lower left corner. As the frequency increases the magnitude of the samples tend to decrease. This is an indication that there are relatively few high amplitude brightness transitions between elements in the original scenes. Figure 1b shows

-138-
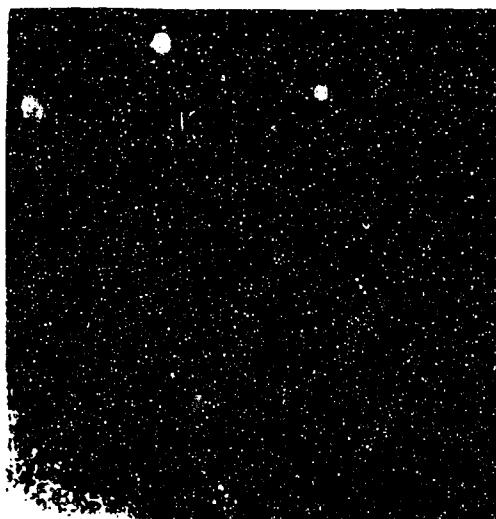
(a) Logarithm of the Magnitude of the
Hadamard Transform

(b) Double Hadamard Transform

Figure 1. Hadamard Transforms of an Image.

the double Hadamard transform of the scene. There is no noticeable

image degradation between the originals and the double Hadamard trans-

forms.

3.2.2 Optical Coherence

AF-AFOSR-188-67, Air Force Office of Scientific Research

R. S. Macmillan

The fundamental objective of the research is to develop a

technique for maximizing the information transfer through an optical

system by adjusting the variable parameters of the system optimally.

In general, these parameters include the amplitude and phase shadings

of the system apertures. It has been shown that maximization of the

first-order and higher-order transcoherence functions accomplishes this

objective.

The experimental investigation of both amplitude and intensity

transcoherence theory[1] is continuing. The experimental results indicate

that a U-shaped amplitude shading function, for intensity, is optimum for

maximum information transfer. These results are in good agreement

with theoretical results which show that such shading maximizes the

transcoherence function and consequently the information transfer.

Experimental studies and theoretical analyses are continuing into

variously shaped one- and two-dimensional apertures. The experimental

results not only verify the theory, but suggest that a generalized adapta-

tion of the basic theory can be employed as an optimal lens design technique

as well as an optimization procedure for optical information-carrying

systems.

Reference

1. Macmillan, R. S., and G. O. Young, "Optimization of Information-Processing Optical Systems by Transcorrelation-Function Maximization", the Journal of the Optical Society of America, volume 58, number 3, page 346, March, 1968.

3.2.3 Synchronization Coding

DA-ARO-D 31-124-G929, U.S. Army Research Office

R. A. Scholtz and R. M. Storwick

In a coded communication system, synchronization is of

utmost importance, and the ability to attain and maintain sync is a

significant design factor. For the discrete noiseless channel, the usual

approach to this problem is to encode the message so that, whatever its

initial point of observation, the receiver will attain sync after observing,

at most,some bounded number of consecutive code symbols.

Relaxation of the bounded sync delay property results in

codes known as statistically synchronizable (ss) codes. Under these

circumstances, it is possible to use many more of the available

sequences as codewords, permitting the use of shorter codewords for

a given dictionary size. One approach to ss code design is to eliminate

one n-tuple as a possible codeword and to encode messages with the

remaining n-tuples so that the forbidden n-tuple can occur randomly in

every out-of-sync position in a codeword sequence. Hence the sync

acquisition delay is a random variable with sync occuring when the forbidden n-tuple has been observed in all but one possible sync position (the correct one). When messages are produced independently, an expression for the average sync acquisition delay is easily computed. A simple synchronizer for this scheme exists.

Another method of designing ss codes is to permit a fixed synchronizing sequence to appear in only one position relative to correct sync. Although this restricts the maximal dictionary size more, synchronization is immediately attained upon observing the synchronizing sequence. When the messages are produced by a memoryless source, the average sync acquisition delay may be minimized through an encoding procedure which is also developed. For a given synchronizing sequence, the maximal dictionary size has been found, and the average sync acquisition delay minimized as a function of synchronizing sequence structure and position. These two minimization techniques, when used together, provide a complete minimization of average sync acquisition delay.

The methodology of these two synchronization techniques is easily extended to more complex systems and sources.

3.2.4 Frequency Tracking

DA-ARO-D31-124-G929, U.S. Army Research Office

R. A. Scholtz, W. Cascell

The problem under consideration is the estimation of a time varying center frequency of a random process. The analytic representation of the process is $x(t) = N_c(t, \cos\left(\int^t \omega(\alpha)\,d\alpha\right) + N_s(t) \sin\left(\int^t \omega(\alpha)\,d\alpha\right)$ where $N_c(t)$, $N_s(t)$ and $\omega(t)$ are Gaussian processes. An integral equation has been derived for the maximum a posteriori estimate of the time varying center frequency $\omega(t)$. This equation can be interpreted in terms of a feed-back loop with non-realizable filters. A linear model of a similar realizable loop has been derived and analyzed. The realizable loop has been simulated on a digital computer and its performance obtained in terms of the normalized error variance. The linear model appears useful in determining optimum loop parameters and in predicting trends in the mean squared error.

3.2.5 Arithmetic Norms and Arithmetic Error-Detecting and -Correcting Codes

DA-ARO-D31-124-G929, Department of Army, Army Research Office

A.C.L. Chiang and I. S. Reed

Any integer N can be expressed as a polynomial in radix-r:

$$N = \sum_{i=0}^{n} a_i r^i, \quad 0 \le |a_i| < r.$$

The smallest number of non-zero coefficients a_i such that this formula holds is called the r-ary norm of the integer N and is denoted by $\|N\|_r$. In particular, if $r = 2$, $\|N\|_2$ is called the binary norm or norm of the integer N. Properties of the binary norm of integers have been extensively investigated[1]. A programmable algorithm for the computation of the binary norm of an arbitrary integer is developed and a table of norms of the natural numbers is generated.

Properties of the binary norm of integers have been applied to the development of arithmetic error-detecting and correcting codes[2]. In order to enumerate the total number of possible error patterns of an e-error arithmetic error-correcting code, one needs to derive the number of integers with norm less than $(e+1)$. This motivates the generation of a certain abelian group which we call a norm group. The number of equivalence class of a norm group is derived and the distribution of integers of a given norm in a norm group is computed. From this the number of possible error patterns of an arithmetic error-correcting code can be found.

Let X be a set of consecutive integers $\{0, 1, 2, \ldots, N-1\}$ and Y be an m-bit register which stores positive integers 0 through $2^m - 1$. An arithmetic error-correcting code is defined to be a code whose coding function $\emptyset$ maps each x in X into y in Y such that $\emptyset(x_1 + x_2) = \emptyset(x_1) + \emptyset(x_2)$

holds for all x_1, x_2 and $x_1 + x_2$ in X. This definition can be extended to any r-dimensional vector space $Y = \{Y_1, Y_2, \ldots \ldots, Y_r\}$. In such a case Y can be considered to be a register which is a concatenation of all disjoint subregister Y_i's. Now let the coding function $\emptyset(x) = (\emptyset_1(x), \emptyset_2(x), \ldots \ldots, \emptyset_r(x))$ be a mapping from X into Y where $\emptyset_i: X \to Y_i$ such that $\emptyset_i(x_1 + x_2) = \emptyset_i(x_1) + \emptyset_i(x_2)$ holds for all x_1, x_2 and $x_1 + x_2$ in X. We are particularly interested in a set of residue class codes for which $\emptyset_i(x) = b_i x$ modulo a_i, where b_i and a_i are relatively prime. Emphasis is given to two subclasses of such codes: the arithmetic error-correcting AN code for which $\emptyset(x) = ax$ and the arithmetic error-correcting BN modulo A code for which $\emptyset(x) = (x, bx$ mod a).

We have found bounds on the arithmetic error-correcting codes. It is shown that the upper bound on the single error correcting AN code can be achieved if and only if the constant a is a prime and 2 or -2 is a primitive root modulo a. A programmable algorithm for computing the best bounds on the higher order error-correcting AN codes is developed.

An arithmetic error-correcting BN modulo A code is constructed in such a way that there is no interaction between its information symbol and check symbol. A necessary and sufficient condition for the construction of a single error correcting BN modulo A code is developed. Some new results on optimal single error and multiple error correcting BN modulo A codes have been found.

References

1. A. C. L. Chiang and I. S. Reed, "Some Properties of Arithmetic Norms", USCEE Report 190, March 1967.

2. A. C. L. Chiang and I. S. Reed, "Some Aspects of the Norm Representation for Arithmetic Error-Checking and -Correcting Codes", USCEE Report 276, May 1968.

3.2.6 Phase Locked Loops in Cascade

DA-ARO-D-31-124-G929, U.S. Army Research Office

J. J. Stein and C. I. Weber

Approximations to the joint density of the phase errors of two second order phase locked loops in cascade have been obtained. These approximate solutions to the corresponding Fokker-Planck equations have been shown to agree very favorably with empirical data at low as well as intermediate signal-to-noise ratios.

In addition, the approximate solutions have been shown to compare favorably with a variety of computer simulations of two second order phase-locked loops in cascade.

One technique, which has been developed exclusively for this application, appears to be sufficiently general to be classified as a general method for simulating stochastic nonlinear differential equations on the digital computer. The details of this technique are presently being prepared in report form.

References

1. W. C. Lindsey and C. L. Weber, "On the Theory of Automatic Phase Control in Stochastic Optimization and Control, John Wiley, New York, 1968.

2. W. C. Lindsey and C. L. Weber, "Nonlinear Analysis of Phase Locked Loops in Cascade," JPL Space Programs Summary 37-50, Vol. III, 1968.

3. J. J. Stein and C. L. Weber, "Cascaded Phase Locked Loops," National Electronics Conference, Chicago, 1968.

3.2.7 Signal Design for Coherent Systems

AF-AFOSR-1555-68, Air Force Office of Scientific Research

S. Moskowitz, D. Sworder, C. Weber

The signal design problem of M-ary coherent communication systems is not in general amenable to direct analytical solution. Because of the form of the problem, gradient ascent techniques suggest themselves. The gradient of the detection probability with respect to the signal vectors $\{\bar{S}_j\}$ can be approximated using Monte Carlo techniques by considering the probabilities of detection of a set of M perturbed signal sets $\{\bar{S}'_{j,k}\}_{k=1}^{m}$ where

$$\bar{S}'_{j,k} \quad \begin{cases} \bar{S}_j & \text{if } j \neq k \\ \bar{S}_j + \bar{\tau} & \text{if } j = k \end{cases}$$

The vector $\bar{\tau}$ is such that $\bar{S}_j + \bar{\tau}$ satisfies the given energy restrictions imposed on the signal set. The gradient vector is then approximated by

$$P_D(\lambda, \{S_j\}) = \frac{1}{\|\delta\|} \begin{bmatrix} P_D(\lambda, \{\overline{S}_{j.}\}) - P_D(\lambda, \{\overline{S}_j\}) \\ \vdots \\ P_D(\lambda, \{\overline{S}_{j,m}\}) - P_D(\lambda, \{\overline{S}_j\}) \end{bmatrix}$$

Initially, a study was made of sequentially moving each signal in the signal set as a function of the appropriate component of the gradient vector. That is, if $\{\overline{S}_j\}_o$ is the original signal set, then

$$\{\overline{S}_j\}_{n+1} = \{\overline{S}_j\}_n + K\left[P_D(\lambda, \{\overline{S}_{j,k}\}_n) - P_D(\lambda, \{\overline{S}_j\}_n)\right], \quad n \geq 1$$

where $k = n \bmod M$. An important outcome of the study was that sequential movement of the signals can lead to false optimum points although convergence to a true optimal point could be attained when $\{\overline{S}_j\}_o$ was properly chosen.

As a result of the above, the technique was modified to calculate the total gradient vector and then to move the total signal set in the direction of the ascending path. The Mth signal vector is initially held fixed and when necessary is moved in the radial direction so that the energy constraints of the signal set is satisfied. Employment of this technique has produced good results. That is, for equal energy signals restricted to two dimensions all results have been verified including those for unequal a priori signals. For this latter case, results exist only for signal sets composed of three signals. Hence, through use of the proposed scheme an unlimited number of new results can be attained. Furthermore, for equi-likely, unity equal energy signal sets confined to

three dimensions, all previous existing results, i.e., for 6 signals, 5

signals, and 4 signals, have been verified with good accuracy. Additionally,

the gradient approach has shown that,for 7 signals in 3-space,a locally

optimum signal set is one composed of 5 equally spaced signals on the

equator and 2 signals at the north and south poles. Analytically, first

order conditions for this signal set have been verified at all SNR. Com-

puter results also indicate that another locally optimal set has one signal

placed at the north pole, three signals equally spaced above the equator

and at a distance of $1/3$ from the origin, and three equally spaced signals

below the equator shifted 60 degrees from those above the equator and $2/3$

of the distance to the south pole. As noted, $\sum_{i=1}^{7} S_i = 0$ in both of the above

cases.

The technique also applies with a slight modification to signal

sets constrained in average energy by $\sum_{i=1}^{M} p_i \| S_i \|^2$. And, through the use

of generalized spherical coordinates the method can be extended to

accommodate signal sets confined to any finite dimensional space.

References

1. C. L. Weber, "Elements of Detection and Signal Design", McGraw-
    Hill, New York, 1968.

2. S. Moskowitz, D. Sworder, C. Weber, "A Gradient Approach to
    Signal Design for M-ary Communication Systems", First International
    Conference on System Sciences, Honolulu, Hawaii, January 1968.

3.2.8 Optimal Physically Realizable Analog Demodulation

JPL 952108, Jet Propulsion Laboratory

C. L. Weber

Nonlinear recursive filtering techniques are being applied to the problem of obtaining optimal analog demodulation under a variety of modulation methods, signal assumptions, and channel conditions. The emphasis is being placed on obtaining physically realizable receivers, both from the nonanticipative point of view and the system complexity point of view. Optimal analog demodulating receivers are being obtained for phase, frequency, and amplitude modulating transmitters. Systems are being considered in which the received signal contains unknown parameters such as amplitude (as in slow fading), frequency offset (Doppler effect), and unknown phase reference.

The results clearly indicate that the true optimal demodulator is, in most cases, prohibitive from the system complexity and implementation standpoints. However, whenever the signal-to-noise ratio is above some nominal threshold, significant approximations can be made which result in the deletion of a substantial portion of the system. That is, the deleted portion has only second order effects. The end structures are therefore approximately optimal, physically realizable, and not excessively complex.

Preliminary results are presently being prepared.

References

1. N. Nahi, "Estimation Theory", Wiley, New York, 1969

2. R. W. Bass, V. D. Norum, L. Schwartz, "Optimal Multichannel
    Nonlinear Filtering," Journal of Math. Analysis and Applications,
    Vol. 16, No. 1, October 1966.

3.2.9 Generalized Tracking Theory

AF-AFOSR-496-67, Joint Services Electronics Program

W. C. Lindsey

Using the theory of Markov processes, the response probability

density function $p(\underline{y}, t)$ of a generalized tracking system is shown to be the

solution to a (N+1)-dimensional Fokker-Planck equation. The vector

$\underline{y} = (\Phi, y_1 \ldots, y_N)$ is Markov in the state variables and Φ is the system

phase error.

It is further shown that the response distributions $[p(\Phi, t),$

$p(y_k, t); k = 1, 2, \ldots, N]$ of the state variables satisfy a set of second-

order partial differential equations. In the steady state, this set of equa-

tions becomes ordinary, first-order differential equations for which the

exact solutions which specify the marginal probability densities $[p(\Phi),$

$p(y_k); k = 1, 2, \ldots, N]$, are determined by two sets of conditional expec-

tations. In particular, the marginal density $p(\Phi)$ of the phase error is

embedded in a knowledge of the conditional expectations $\{ E(y_k | \Phi),$

$k = 1, 2, \ldots, N \}$ while the marginal density $p(y_k)$ of the state variable

y_k is embedded in a knowledge of the conditional expectation $E(g(\phi) | y_k)$;

$k = 1, 2, \ldots, N$. Here $g(\phi)$ belongs to that class of nonlinearities for

which $g(\phi)$ is an odd function. The conditional expectations are approximated by two methods and, for the case of greatest interest, i.e., $g(\phi) = \sin \varphi$, the conditional expectation $E(y_1 | \varphi)$ is measured via computer simulation methods. Agreement of the simulation results with those obtained from theoretical considerations are within less than one percent of each other.

Synthesis procedures for effecting stochastic optimization of a generalized tracker are presented. For zero detuning, it is shown that the tracker which minimizes the mean-squared value of the phase-error is obtained when $N = 0$ and $g(\phi)$ is proportional to sgn (ϕ). In the case of nonzero detuning, it is shown that the loop which minimizes the mean-squared phase-error is second-order, i.e., $N = 1$, and the optimum nonlinearity for this loop is also proportional to sgn(ϕ). For large loop signal-to-noise ratios and equal mean-squared loop phase-errors, the second-order PLL system requires a loop signal-to-noise ratio, ρ, of approximately $\rho/2$ times larger than that required in the optimum second-order tracker. At low loop signal-to-noise ratios it is shown that all trackers perform approximately the same. For second-order trackers some results are presented to the case where $g(\phi)$ must be physically realizable.

The field of probability currents is derived and it is shown that this field is rotational when there is zero detuning in the loop. From these currents the average number of phase-jumps (cycles-slipped) per unit of time is derived. With zero detuning this average is zero.

-152-

Reference

1. Lindsey, W. C., "Nonlinear Analysis and Synthesis of Generalized Tracking Systems", Pending publication Sept., 1968.

3.2.10 Phase Tracking in Shot Noise Environments

F 04701-68-C-0234, Space Systems Division, Air Force

Systems Command

M. Haney, R. M. Gagliardi

Timing for synchronization and/or ranging in an optical communication system can be accomplished by intensity modulating with the timing signal and phase locking at the receiver after optical demodulation. When direct photodetection is used for demodulation, however, the demodulated intensity appears as a shot noise current signal with the desired timing signal immersed within.

The shot noise current can be represented by

$$i(t) = \sum_{m=1}^{N(t)} h(t-t_m)$$

where $h(t-t_m)$ is the current waveform due to a single electron emitted in the photodetector at time t_m. $N(t)$ is a time varying Poisson distributed random variable such that the probability of k electrons being emitted in the time interval $\lceil o, t \rceil$ is

$$P(N(t) = k) = \frac{\left[\int_o^t \eta n(\tau) d\tau \right]^k e^{-\left[\int_o^t \eta n(\tau) d\tau \right]}}{k!}$$

-153-

where η is the photodetector emission probability and $n(\tau)$ is the "timing signal + background noise" photon particle rate incident on the photo-detector.

Let the current, $i(t)$, be the input to a phase locked loop and let the photon particle rate, $n(t)$, be

$$n(t) = A \left(1 + \sin(\omega_o t + \theta_1(t)) \right) + M$$

where A is the amplitude of a sinusoidal timing signal with phase $\theta_1(t)$, and M is the level of the background noise. Also, let the local oscillator generate a signal represented by $\cos(\omega_o t + \theta_2(t))$. The phase error, $\phi(t)$, is then

$$\phi(t) = \theta_1(t) - \theta_2(t)$$

The nonlinear stochastic integro-differential equation describing the behavior of the loop becomes

$$\frac{d\phi(t)}{dt} = \frac{d\theta_1(t)}{dt} - K \int_o^t f(t-\tau) \sum_{m=1}^{N(\tau)} h(\tau - \tau_m) \cos\left(\omega_o t + \theta_2(t) d\tau \right)$$

where K is the loop gain constant and $f(t-\tau)$ is the impulse response of the filter within the loop.

A study is presently being conducted to determine the statistical behavior of the phase error and the overall loop performance. An analysis involving the Chapman-Kolmogorov method and its equation in series form became mathematically unsound because the higher order moments of the

incremental phase error divided by the time increment Δt do not go to zero as they do in the conventional Gaussian noise phase locked loop. In the Gaussian case the loop statistics are governed by the Fokker-Planck equation involving only the first and second moments. Other methods of loop analysis are presently being investigated.

3.2.11 Hybrid Processing of Complex Radar Signals

GK-3303, National Science Foundation

J. E. Ohlson

Because of peak-power limitations in radar systems, the pulse energy (which determines the system detection threshold) can be increased only by using long pulse lengths. Range resolution can still be the same as that of a very short pulse if the time-bandwidth product is sufficiently large. One way of producing a large time-bandwidth product is to linearly increase the carrier frequency during the pulse length. This type of signal, known as a "linear-FM" or "chirp" waveform, has been used for several years[1]. Generation of the transmitted signal and processing of the returned signal are quite difficult procedures since stability in both time and frequency is particularly critical. Virtually all chirp procedures utilize analog techniques and are subject to the vagaries of these methods.

In this research, effort is being made to utilize digital methods to contribute stability and precision to chirp techniques. For small frequency sweeps ($\sim$ 100 kHz) direct digital synthesis is possible[2],

but for large sweeps (>100 MHz) direct synthesis cannot be performed because of state-of-the-art limitations on computer storage and operational speed. Effort is thus being devoted to developing digitally assisted signal generation and processing. The problem areas are (1) repeatable signal distortion (e.g., nonlinearity of sweep), and (2) fluctuations of system gain and phase characteristics. Work to date has produced the following preliminary results:

(1) A "sampling" technique can be employed to adaptively linearize the frequency sweep. This will remove repeatable distortion (i.e., constant from pulse to pulse).

(2) System fluctuations of a slow nature (e.g., temperature effects) can also be compensated by (1). Fast system changes appear as a noise, which because of the large bandwidths involved can only be compensated by good design practice.

(3) A problem which has application to optical (intensity) data storage has been examined. It was shown that a set of bounded, orthonormal, non-negative definite basis functions cannot exist for $L_2[a,b]$. The result is that an arbitrary function in $L_2[a,b]$ (in particular, the non-negative subset of $L_2[a,b]$) cannot be represented as a sum of positively weighted non-negative orthonormal basis functions. A method for constructing a bounded, linearly independent set of non-negative basis functions from a trigonometric fourier series is found, which then allows the desired representation to be found under somewhat weaker conditions.

(4) When the output of a causal filter is to be sampled for

-156-

digital processing, the Nyquist sampling rate of twice the bandwidth is undefined since the signal spectrum is not bandlimited. A higher sampling rate always produces greater fidelity, but at greater expense. Take the case of a constant-valued signal immersed in white noise which is then filtered by a single pole filter, sampled, and the samples summed to estimate the signal level. The variance of this estimate is found as a function of sampling rate and is compared to that of the estimate obtained by a finite-time-average of the signal and noise over the same time interval. The exact solution has also been found for a second order filter. For a particular filter, the sampling rate necessary for a desired efficiency is thus found.

References

1. Cook, C. E. and M. Bernfeld, Radar Signals, Academic Press, New York, 1967.

2. Barry, G. H. and R. B. Fenwick, "HF Measurements Using Extended Chirp-Radar Techniques", TR-103, Nonr-225(64), SU-SEL-65-058, Stanford Electronics Laboratories, Stanford, California, June, 1965.

3.2.12   USC Speech Processing Program

AF-AFOSR-68-1555, Air Force Office of Scientific Research

DA ARO-D-31-124-G930, Department of the Army, Army

Research Office

S. W. Golomb, D. Sherman, C. Fuzak, H. Trachtenberg

3.2.12.1 A Model for Voicing Duration

D. Sherman

I. The Model

In constructing a model for voicing duration based upon
phoneme durations, two extremes are possible. The first extreme involves
simplifying as much as possible the phoneme duration distribution. Essen-
tially, this means assuming that all voiced phonemes, in all positions in
the speech stream (i.e., all phonemic environments), are drawn from a
common population in terms of duration. Statistical tests (see part III)
indicate that so simple an assumption is unjustified.

The other extreme in modeling involves examining the duration
of each phoneme class individually, as a function of phonemic environment.
This, of course, is an extremely tedious approach, perhaps interesting in
itself, but does not necessarily yield the most useful voicing duration
model. The fine detail involved in a model constructed in this manner
would be lost in practical tests and applications.

As a compromise between these extremes. a voiced segment

was considered to be composed of four types of phonemes--those which

initiated voicing, those which terminated voicing, those which neither

initiated nor terminated voicing, and those which did both. These classes

were called Initial, Terminal, Medial, and Isolated, respectively. It was

felt that these classes represented the basics of phonemic environment,

while ignoring differences due to the phonemes themselves. If later tests

indicated need for further refinement, the phonemic differences might be

considered within the classes.

Given these ground rules, the model for voicing duration

follows immediately.

Let: P_i = Probability of i phonemes in a voiced segment.

$p_I(t)$ = Duration density for an Initial voiced phoneme.

$p_M(t)$ = Duration density for a Medial voiced phoneme.

$p_T(t)$ = Duration density for a Terminal voiced phoneme.

$p_S(t)$ = Duration density for an Isolated voiced phoneme.

$p_D(t)$ = Duration density for a voiced segment.

Then the duration density for a voiced segment is given by

$$P_D = P_1 p_S + P_2 (p_I * p_T) + P_3 (p_I * p_M * p_T) + \cdots$$

$$+ P_n \underbrace{(p_I * p_M * \cdots * p_M * p_T)}_{n-2 \text{ fold}} + \cdots ,$$

where the densities, p, are understood to be functions of t. In order to

make use of this expression, each of the terms on the right must be

determined up to a set of parameters. These parameters would then be

-159-

estimated from the voicing duration data, and fit tests performed. If a good fit results, it is then expected that the parameters should prove useful in determining such factors as language, speaker, sex, or speech rate.

Note that in deriving this model it was assumed that the duration of consecutive phonemes were independent; that is, the duration is a function only of the class to which the phoneme belongs.

II. The Data

A two minute continuous speech sample was obtained, and attempts were made to phonemically segment it on the basis of the amplitude waveform. These attempts proved unsuccessful, so spectrograms of the sample were obtained utilizing the Kay Electric type B/65 sonagrams produced by the USC Asian Studies Department. The resulting phoneme duration data is shown in Table I.   The entries in the table are measurement units, equal to 3 1/8 milliseconds. Casual inspection indicates that the Isolated phonemes appear to come from a different population than the other three categories. The remaining three categories were tested for a possible common population.

The tests performed were of the fit type. In all cases, a significance level of 10% ($\alpha = .10$) was selected. This allowed a probability of .1 of a Type I error (rejection of the hypothesis when it is actually true). This fairly large value for α was used in an attempt to assure that the resulting model would be as accurate as possible based

Initial		"vowels"		Medial stops & fricatives		Terminal "vowels"		stops & fricatives	Isolated
7	25	8	20	33	7	11	28	9	15
9	25	10	20	34	7	15	28	9	17
9	25	11	21	34	7	16	29	10	21
9	25	11	21	35	7	18	29	10	25
9	25	11	21	38	7	18	29	12	25
9	26	11	21	38	8	19	32	12	26
10	28	11	21	39	8	19	33	13	26
11	28	11	21	39	8	19	33	19	28
12	29	11	22	41	9	20	34		29
12	29	12	22	43	9	20	35		29
12	30	12	23	45	9	21	35		30
12	30	13	23	46	9	21	35		31
13	31	13	23	50	9	22	36		33
13	32	13	24	53	10	22	36		33
13	33	14	24	65	10	22	36		35
14	33	14	24	75	10	22	37		40
14	35	14	25		10	22	37		40
15	35	14	25		11	22	38		45
16	36	14	25		11	23	38		49
16	36	14	25		11	23	39		53
17	37	14	26		12	23	41		58
18	39	15	26		13	23	41		60
18	40	15	26		15	23	42		61
18	40	16	26		15	24	43		72
19	42	16	26		16	24	45		73
19	43	16	27		16	24	46		77
20	43	17	27		17	24	48		81
20	44	17	28		17	24	50		
20	44	17	29		26	25	51		
21	46	17	29			25	55		
21	51	17	29			25	59		
21	51	17	29			25	63		
22	52	17	29			25	64		
22	53	18	30			25			
23	56	18	30			25			
23	61	19	30			25			
23	61	19	31			25			
24	61	19	33			26			
24	66	20	33			27			
24	67	20	33			27			
	75								

Table I

Phoneme Durations   1 = 3.125 msec

upon the available data. Hereafter, rather than simply reporting

acceptance or failure at the 10% level, the minimum significance level

for acceptance is reported, which will give an estimate of "quality" of

acceptance or rejection.

A three sample Kruskal-Wallis H test on the Initial-Medial-

Terminal data yielded a value of H = 14.32. For this value, the hypothesis

that the three samples are drawn from a common population is rejected

for any significance level larger than .001, and we may safely conclude

that more than one population is involved. This test was performed on

the data after excluding voiced stops and fricatives in the Medial and

Terminal positions. (Stops and fricatives were not treated separately

in the Initial case due to their low frequency of occurrence.)

Pairwise (Mann-Whitney) tests on the same data gave the

following results:

Initial-Medial X = 1.70, corresponding to α = .09

Initial-Terminal X = 1.47, corresponding to α = .14

Medial-Terminal X = 4.02, corresponding to α = .001.

Since, at most, one hypothesis may be accepted, we would accept the one

which would be accepted for the largest value of α. At this point we might

reasonably accept the hypothesis that the Initial and Terminal samples

are drawn from populations with the same distribution functions. This

decision is postponed, however, in favor of further tests.

Earlier investigations indicated that vowel durations might

be well represented by a log-normal density; that is,

$$p(t) = \frac{1}{\sqrt{2\pi}\,\sigma t} \exp\left[-\frac{1}{2}\left(\frac{\ln t - \mu}{\sigma}\right)\right].$$

It was decided to investigate this possibility, so chi-squared goodness of fit tests were performed using maximum-likelihood estimates of μ and σ. Again, a 10% ($\alpha = .10$) significance level was established. The results are presented in Table II. Since the fit was extremely poor in the case of the Terminal data, fit tests were also performed against a normal density function. As a result of the tests we can conclude that each of the following phoneme categories may be represented by log-normal duration density functions: Initial; Medial "vowels"; Medial Stops & Fricatives; Isolated. In addition, we may conclude that the best fit in the Terminal case occurs for total Terminal data vs. a log-normal density. Thus the best available reasonable assumption is that the Terminal data is drawn from a population with a log-normal density. The fit in the Terminal case was expected to be the least accurate, due to the voiced-unvoiced decision process used on the spectrograms. (The decision was based upon the low frequency power, a value judgement based on the degree of blackness of the spectrogram. The power onset time is much less than the decay time, and timing errors tend to accumulate in the terminal position.) Due to the tentative nature of the acceptance of log-normal density for the Terminal phonemes, we will reject the hypothesis that the Initial and Terminal data come from populations with the same densities.

Chi-Squared Goodness of Fit Tests

Phonemes	x^2	Number of Regions	Significance Level
Fit to Log-Normal Density			
Initial (total)	4.07	15	.98
Medial "vowels"	14.79	20	.20
Medial stops & frictatives	4.29	6	.25
Terminal "vowels"	25.24	14	.007
Terminal (total)	23.79	16	.04
Isolated	3.20	5	.20
Fit to Normal Density			
Terminal "vowels"	33.38	14	.005
Terminal (total)	25.26	16	.02

Table II

Note: "vowels" are vowels, $/r/$, $/l/$, glides, nasals, and diphthongs.

Table III illustrates the measured frequency of occurrence for various numbers of phonemes per voiced segment. Due to the long "tail", the fit to Posson is quite poor, failing the $\alpha = .1$ test. The log-normal is suggested by the fact that the number of letters per word and the number of phonemes per word both appear to be log-normal for English. Maximum likelihood estimates give $\mu = .881$, $\sigma^2 = .422$, and a value of x^2 (for a chi-squared fit test) of .8698 for 6 regions. This passes the test for $\alpha = .10$, giving in fact a significance level of roughly 80%. Thus, in the model for p_D, we will use a log-normal expression to

give the P_i's.

The decision to treat the medial phonemes in two separate categories means that p_M in the expression for p_D will have the form

$$P_M = P_V P_{MV} + P_S P_{MS} \cdot$$

The ratio of occurrence of the "vowel" group (v) to the stop-fricative group (s) is theoretically about 3.13. The measured frequencies (103/20 from Table IIA) yield about 3.56. Accepting the theoretical values as approximately correct, we have $P_V = .76$ and $P_S = .24$. These values will be used in the model.

# of Phonemes in Voiced Segment	# of Occurences
1	25
2	34
3	18
4	13
5	6
6	3
7	0
8	3
9	2
10	1
11	1
12	1

Table III

-165-

III.   Continuation

The next step in constructing the model is a determination of the exact form of the P_i's.   Once this is accomplished, maximum likelihood estimators must be found for the twelve parameters in the model. (These parameters are μ and σ for p_I, p_{MV}, p_{MS}, p_T, p_S and for the expression for the P_i's.

The model must then be tested against duration data, and if fit tests prove successful, then experiments must be designed to test the parameters for dependencies on factors such as speaker, language, sex, and speech rate.

3.3 SWITCHING, AUTOMATA THEORY, AND COMPUTERS

3.3.1 Minimum Length Race-Free Coding for Asynchronous
Sequential Machines

AF-AFOSR-1018-67A, Air Force Office of Scientific
Research

R. B. McGhee and R. M. Kashef

The preliminary work reported in previous progress reports
have been generalized for augmented parity check (APC) codes[1] and
extended for flow table columns whose states can be partitioned into
maximum distance pairs and published in the form of R. M. Kashef's[*]
Ph. D. Dissertation[2]. An abstract of the dissertation follows:

One of the basic problems in the design of asynchronous
sequential machines is the determination of an assignment of binary codes
to the states of a machine in a way which avoids critical race conditions.
Solutions to this problem can be found either by means of a coding algor-
ithm or by the use of general codes capable of encoding any machine.
This dissertation is concerned with the latter approach and is aimed at
the specific problem of obtaining a race-free encoding with a minimum
number of bits.

Up to the present time, the shortest length general race-free
code known has been the intermeshed row set code devised by D. A.

---

[*]Middle initial of R. M. Kashef has recently been changed to S from M.

Huffman[3]. This code encodes a table of 2^{S_o} rows with $2S_o-1$ bits. In this dissertation, a new family of codes, called augmented parity check codes (APC codes), is introduced. An APC code, S, is a set of 2^{S_o} n-bit code words such that any element, s, of S contains an even (or odd) number of ones in S_o specified bit positions, and all but one of the remaining bits of s are equal to a constant value. If each element of an APC code is assigned to one of the states of a 2^{S_o}-row state table, then the remaining $2^n-2^{S_o}$ binary n-tuples are available for connecting the state codes as required by the state table. The main problem to be solved is thus the determination of a minimum value for n as a function of S_o.

A lower bound on n can be obtained by considering a column of a 2^{S_o}-row state table which can be partitione! into 2^{S_o-1} pairs of states such that number of bits in which the corresponding code words differ is the maximum possible for any two code words of S. In this dissertation, it is shown that it is impossible to code such a column so that every pair of states of the column to be connected is joined by disjoint race-free chains of n-tuples with less than $S_o + < Log_2 \left(< \dfrac{S_o+1}{2} > + 1 \right) >$ bits, where $< x >$ denotes the next integer greater than or equal to x and $S_o \geq 4$. In addition to this result, it is also shown that no more $2 < \dfrac{S_o}{2} > + < Log_2 \left(2 < \dfrac{S_o}{2} > \right) >$ bits are ever required to encode such a maximum distance partition. For large values of S_o, both of the above numbers are substantially less than $2S_o - 1$.

By the use of the concept of equivalence classes of mappings

of a finite set S into a finite set $R = \{0, 1\}$, under a permutation group
G on S, it was possible to reduce the number equivalence classes of
stable state configurations for $S_o = 3$, $n = 4$, to 13 by letting S be a 4-
bit APC code and G be the group of distance preserving transformations
on S^4. Furthermore, it was possible to code a canonical member of
each equivalence class directly, hence implying that any 4-bit APC code
can be used to obtain a race-free encoding of all 8 state flow tables. The
above concept was used for state tables with $S_o = 4$ and $n = 6$ and the number
of equivalence classes of stable state configurations reduced to 271. By
the use of a computer program based on backtrack programming[5], every
possible type of columns of 16-row state tables were coded with the
exception that for about one percent of the columns with 5, 6, and 7 stable
states the coding was not attempted. There is no evidence to indicate that
the uncoded columns could not be coded by a further expenditure of com-
puter time. An isomorphism between the group of distance preserving
transformations on the set of APC codes and the group of the symmetries
of the S_o-cube was established for S_o-odd, and it was therefore concluded
that it is not practical to carry out the proof for $S_o \geq 5$, using the method
for $S_o = 4$. The result for $S_o = 4$ encourages the conjecture that the bounds
obtained for maximum distance partitions are valid for any type of flow
table columns. Further research is required to determine whether or not
this is actually the case.

Presently, a modified computer program has been written
in order that the remaining one percent of 16-row tables with 5, 6 and 7

-169-

stable states can be coded. It is anticipated that the program run time

will exceed 100 hours on the IBM 360, Model 44, and methods are being

investigated to reduce this time. Furthermore, since this research

indicates that the number of bits required to code the states of an asyn-

chronous sequential machine using APC codes is the same as the number

of bits for a synchronous sequential machine with the same number of

states, plus the bits required for the clock, then the race-free coding

problem of an asynchronous sequential machine would be completely solved,

if it would be possible to prove that the columns which can be partitioned

into maximum distance pairs are the only columns which require the use

of all 2^{n-S_o} unused code words among the set of all possible 2^n n-bit code

words for a 2^{S_o}-row state table, using APC codes. Hence, further research

is under way to investigate the methods by which the above can be proven.

References

1.   Consolidated Semiannual Progress Report No. 5 (1 October 1966
     through 31 March 1967), Electronic Sciences Laboratory, University
     of Southern California, Los Angeles, California, pp. 187-188.

2.   Kashef, R. M., "Augmented Parity Check Codes for Encoding of
     Asynchronous Sequential Machines", Ph.D. Dissertation, University
     of Southern California, August 1968.

3.   Huffman, D. A., "A Study of Memory Requirements of Sequential
     Switching Circuits", MIT Tech. Report 293, April, 1955.

4.   de Bruijn, N. G., "Generalization of Polya's Fundamental Theorem
     in Enumerative Combinatorial Analysis", Neder. Akad, Wetensch.
     Proc. Ser. A62 = Inday. Math. 21, pp. 59-69.

5.   Golomb, S. W. and Baumert, L., "Backtrack Programming", ACM
     Journal, October, 1965.

3.3.2 Interactive Hybrid Computer Systems

GK 2716, National Science Foundation

M. J. Merritt, G. A. Bekey

1. Background

When an analog computer and a digital computer are tied
together by suitable linkage devices, the result is called a hybrid com-
puter. The diverse nature of the two basic computing devices makes it
difficult for a single individual to master all aspects of both analog and
digital computation. Recent developments in computer generated graphic
displays have made possible the development of software systems to supply
the needed expertise. In addition, the graphic display devices allow the
user to communicate with the hybrid computer in a single, task oriented
language. The resultant improvement in the man-hybrid computer inter-
face is necessitated by the increasing scope of hybrid computation.

2. Research Objectives

The research objectives of this study all involve the improve-
ment in man-hybrid computer communication. Graphic sketches, line
drawings, and schematic diagrams are the natural forms of expression
used by engineers and scientists. Studies are underway to determine
the most effective graphic language format for hybrid computation.
Existing, nongraphic, simulation languages provide a base for these
studies.

Additional work is in progress to develop graphically oriented

application and support programs to enhance existing hybrid computer software systems. Man may be put back into the parameter adjustment, optimization loop by providing him with suitable graphic displays and on-line controls. A large class of search procedures, trial and error procedures, and iterative computational procedures may be adopted to allow on-line supervision and control by a human operator observing graphic presentations.

3.3.3 Realization of Fault Detection Sequences in Linear Cascades of Identical Machines

AF-AFOSR-196-67, Joint Services Electronics Program

M. A. Breuer

Our research deals with the problem of constructing fault detection tests for sequential machines. This is currently one of the most significant problems related to the successful acceptance of the new LSI technology. We consider a specific machine model, namely a linear cascade of identical sequential machines, as illustrated below.
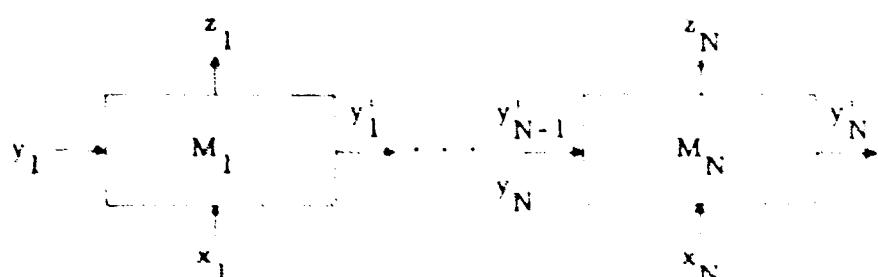
M_i is called a cascade machine and $M = M_1 \cdot M_2 \cdots M_N$. Examples of linear cascade machines are shift registers and parallel

adders.   Our main interest is to find test sequences for these machines which are much shorter than those produced by the classical techniques of Hennie[1] and Kohavi and Lavallee[2].

The following properties were investigated, and results obtained:

a) When are two linear cascades of N identical machines equivalent?

b) What is the reduced structure of a linear cascade of N identical machines?

c) What information lossless properties of cascade machines are sufficient in order to insure testability of the linear cascade?

d) The concept of a complete sequence generation is introduced, and its influence on testability examined.

(Briefly, M is a complete sequence generator if,starting in the initial state, there exists input sequences which will produce any desired sequence on the y_i' output.)

e) If M_i is information lossless of finite order and is also a complete sequence generation, then we show how to test the linear cascade of N identical machines with a sequence of N uniform experiments.

f) Ultra efficient testing procedures are studied, which allow for many of the M_i's to be tested simultaneously.

g) Sufficient conditions are derived on M in order to insure that either every second machine or every third machine can be tested simultaneously.

As one practical example of this work, we have constructed

a sequence of length 16 which will test an N bit parallel binary adder.

This sequence is independent of N. This work will be presented at the

1968 IEEE Conference on Switching and Automata Theory.

Work on generating a test sequence of the general model of

a sequential machine is continuing.

References

1. F. C. Hennie, "Fault Detecting Experiments for Sequential Circuits",
    Proc. 5th Annual Symposium on Switching Circuit Theory and Logical
    Design, pp. 95-110   764.

2. Z. Kohavi and P. Lavalle, "Design of Sequential Machines with Fault-
    Detecting Capabilities", IEEE Trans. on Electronic Computers,
    Vol. EC-16, pp. 473-485, 1967.

3.3.4 Abstract Pattern Recognition

NGR-05-018-044, National Aeronautics and Space

Administration

W. S. Meisel, W. Yuan

In abstract pattern recognition one is presented with samples

(in a finite-dimensional vector space) of various pattern classes. The

problem is to classify other points in the space on the basis of this limited

information. One might describe the motivation for such studies as a

desire to identify the contents of a "black box" which does not contain

memory. Obvious applications lie in engineering, economics, and

biomathematics.

The problem has two aspects: feature selection and pattern classification.

Three basic approaches have been applied to the latter:

a) <u>Nonlinear parameterization</u> - The discriminant function is assumed to take a certain form specified completely by a finite set of parameters; the parameters appear nonlinearly. A common example is the assumption that the distribution is Gaussian.

b) <u>Linear parameterization</u> - The discriminant is assumed to be of the form

$$p(x) = \sum_{i=1}^{R} C_i \emptyset_i(x) \ ,$$

where the $\emptyset_i$ are given functions, and the C_i paremters to be determined. This expression may represent, for example, a general multivariate polynomial.

c) <u>Composition</u> - The discriminant is assumed to take the form

$$\rho_i(x) = \frac{1}{|S_i|} \sum_{y \varepsilon S_i} \lambda(x,y) \ ,$$

where S_i is the set of samples of class i. This latter equation may be viewed as the superposition of contributions from each of the sample points of class i.

Our work has concentrated on methods of type (b) and (c). The choice of linear parameters by least-square or least-mean-square

-175-

approximation to the unknown probability function has resulted in some practical algorithm[1]. A study of potential functions has led to an algorithm with distinct advantages over similar algorithms[2].

We have generated artificial data to test and compare techniques for abstract pattern recognition[3,4].

References

1. "Mean-squares Methods in Abstract Pattern Recognition", Information Science, Vol. I, to be published.

2. "Potential Functions in Abstract Pattern Recognition", to be published.

3. W. S. Meisel, "On the Generation of Artificial Data for Pattern Recognition", to be published.

4. W. S. Meisel and W. Yuan, "Tables of Artificial Data for Pattern Recognition", USCEE Report 302, August 1968.

3.3.5 Automata and Formal Language Theory

AF-AFOSR-496-67, Joint Services Electronics Program

R. Card, W. Chandler, S. Ginsburg

Background

During the past five years, a multitude of different types of acceptors and the languages they recognize have been introduced. Recently, it was observed[1] that most of these devices and languages would be subsumed and unified within the notions of an "abstract family of acceptors", abbreviated AFA, and "abstract family of languages", abbreviated AFL. This has resulted in a flood of new questions and results, hitherto unsuspected. Whereas before the advent of AFA, this

was a surfeit of devices; after AFA there was a sudden scarcity. This

situation arose because there were not enough different types of extant

devices to answer the new questions. A typical new question which is

receiving attention is: Find types of AFA whose associated family of

languages is not closed under substitution.

Progress

Roger Card is studying the properties of "associative memory

acceptor" languages. In particular, he is examining their elementary

closure properties and relations to well-known families of languages.

William Chandler is studying languages accepted by one-way

deterministic acceptors. He has obtained a characterization of these

languages in terms of closure operations and is now examining their

elementary properties.

A paper, "Substitution in Families of Languages", was written

and submitted for publication. In it, the role of substitution to AFL is

studied. For example, it is shown that if L_1 and L_2 are AFL, then so is

the set of all languages obtained by substituting languages of L_1 into those

of L_2.

For a number of years, linguists have been searching for

faithful models of classes of natural languages. Among the models pro-

posed, the one receiving the most attention these days is that of a

"transformational grammar". As yet, no mathematically sound model of

these grammars has been formulated which has received the blessings of

-177-

a large number of linguists. In a report, "A Mathematical Model of

Transformational Grammars", submitted for publication, an attempt is

made to provide such a mathematical model.

Two papers, items (3) and (4), were published.

References

1. S. Ginsburg and E. H. Spanier, "Substitution in Families of Languages", submitted to the Journal of Computer and System Sciences.

2. S. Ginsburg and Barbara Partee, "A Mathematical Model of Transformational Grammars", submitted to Information and Control.

3. S. Ginsburg and M. A. Harrison, "On the Elimination of Endmarkers", Information and Control, Vol. 12, pp. 103-115, 1968.

4. S. Ginsburg and M. A. Har ison, "One-Way Nondeterministic Real-Time List-Storage Languages", Journal of the Association for Computing Machinery, Vol. 15, pp. 428-446, 1968.

4. BIOMEDICAL ENGINEERING AND MATHEMATICS

4.1 CARDIOVASCULAR AND RESPIRATORY SYSTEMS

4.1.1 Regulations of Pulmonary Ventilation

He-11915-01, National Institutes of Health

NGR-05-018-044, National Aeronautics and Space
Administration

S. Yamashiro, M. B. Wolf and F. S. Grodins

The goal of the current laboratory investigation is to determine
the role of the central chemosensitive area in the respiratory response to
acute metaboloic disturbances of acid-base balance. We plan to do this
by simultaneously monitoring respiration and the acid-base state of
arterial blood, brain venous blood, and CSF (cerebrospinal fluid) following
acute metabolic disturbances. Some preliminary results have been
obtained from experiments in which respiration, arterial blood, and CSF
were monitored following infusion of bicarbonate into anesthetized dogs.

Acute metabolic alkalosis has been induced in 20 anesthetized
mongrel dogs by injecting (.3M-1M) $NaHCO_3$ intravenously via a femoral
vein. Doses of 10 mEq/Kg were used and were infused at a rate of 20
ml/min. Respiration was monitored by a spriometer filled with 100%

oxygen and connected to the animal via a tracheal cannula. Arterial

blood samples were drawn from a femoral artery before infusion and

periodically following infusion. Blood pH and Pco_2 were directly

measured with appropriate electrodes (Corning Model 16 Blood Analyzer).

In 5 dogs, CSF was sampled via a spinal needle placed into the cisterna

magna, and its pH and Pco_2 were determined in the same way as in blood.

In general, our results agreed with the findings of Robin et al[1]. There was

a consistent rise in ventilation following infusion of bicarbonate in all

experiments not involving a gross technical error. In 3 of 5 dogs in

which CSF was sampled, the average pH change in CSF immediately

following bicarbonate infusion was -.008 of a pH unit. Results from the

other two dogs were discarded because of gross technical errors. In all

three dogs a net alkaline shift of CSF pH was seen one hour after infusion.

Robin et al.[1] report a depression of ventilation following bicarbonate

infusion at exactly the same time. These results fully support the impor-

tance assigned to CSF pH by Pappenheimer[2] in the control of ventilation

during chronic metabolic disturbances. The present results suggest that

CSF pH is also important in acute disturbances.

References

1. Robin, E. D., Whaley, R. D., Crump, C. H., Bickelmann, A. G.,
    and Travis, D. M., "Acid-Base Relations Between Spinal Fluid and
    Arterial Blood with Special Reference to Control of Ventilation", J.
    Appl. Physiol. 13 (37, 1958, pp. 385-392).

2. Pappanheimer, J. R., "The Ionic Composition of Cerebral Extra-
    cellular Fluid and Its Relation to Control of Breathing", The Harvey
    Lectures, 61, 1967, pp. 71-94.

4.1.2 Blood Pressure and Heart Rate Regulation in the Fetus

GMO1724-02, National Institutes of Health

W. Morrison and G. A. Bekey

This project has been concerned with both experimental and computer studies of the fetal cardiovascular system. During the report period, the emphasis of the project was on computer studies.

The fetal cardiovascular system was simulated both with and without blood pressure control (the so-called "baroceptor reflex"). Model sensitivity studies were carried out to determine the influence of various parameters on the agreement between model behavior and experimental behavior. Some improvement in the fit of model responses to experimental data was obtained when certain nonlinearities were added to the model, namely:

(a) the resistance of certain vessels to blood flow was assumed to be a nonlinear function of vessel diameter.

(b) the elastance of the ascending aorta and pulmonary artery were made piecewise constant functions of the vessel diameter.

The final portion of the computer study was concerned with mathematical models of the baroreceptor reflex. Optimum parameter values in the controller equations were obtained by relaxation methods. The detailed results will be published in W. Morrison's Ph.D. dissertation.

4.2 FLUID-ELECTROLYTE AND RENAL SYSTEMS

4.2.1 Simulation of the Combined Artificial Kidney-Patient System

GMO1724-02, National Institutes of Health

M. B. Wolf

This research proje t is directed towards the the retical prediction of optimum parame ers for hemodialysis in individual "ure nic" patients.

A mathematical model has been developed[1] to simulate the combined artificial kidney-patient chemical dynamics, and has been tested against actual patient data for two of the prime chemical sub-stances of interest. Predictions of the dynamics of exchange of these substances as a function of patient and treatment parameters were made, and these should provide the clinician with a rational basis for choosing the duration of the dialysis treatment.

Further efforts are underway to theoretically investigate the dynamics of other substances such as potas ium and water and to predict optimum treatment time with respect to them.

Reference

1. Wolf, M. B., Watson, P. D., and Barbour, B. H., "A Theoretical Evaluation of the Patient-Artificial Kidney System Using a Kiil Western Dialyzer, (to be published in M- hematical Biosciences).

4.3 NEURAL SYSTEMS

4.3.1 Studies of Neuronal Interaction

NB 08207-01, National Institutes of Health

G. P. Moore

The Neurophysiology Research Laboratory of the Biomedical Engineering program is pursuing a program of investigation into the signal processing behavior of small neuron networks. In the past we have succeeded in developing, in conjunction with others, the mathematical techniques for describing neuron pulse signals and the computer programs for data processing and simulation[1-3]. These fundamental studies have enabled us to characterize nerve cell activity and to detect and characterize interactions between cells.

In the past period, therefore, we have concentrated on (1) applying the basic theory to real neuron on-line experiments; (2) adapting large-scale simulation programs (developed elsewhere) to the IBM 360/44 computer in the School of Engineering.

An extensive literature survey in the use of models in the study of the generation and processing of signals by nerve cells was completed with the publication of USCEE Report 290, entitled "Models of the Generation and Processing of Signals by Nerve Cells: A Categorically Indexed Abridged Bibliography".

I. General Background

        In the past twelve months a laboratory capability has been

developed which is suitable for neurological investigation upon both verte-

brate and invertebrate specimens. To accomplish this has required the

acquisition and integration of equipment as well as the utilization of

available equipment. The instrumentation includes microelectrodes,

amplifiers and multi-channel tape recording system, CRT display devices,

and more significantly, a PDP-8 digital computer with appropriate peri-

pheral devices to permit both on- and off-line evaluation of experimental

data. A library of programs for the computer is being developed on a

continuing basis. An extensive capability already exists, and with the

recent addition of a large capacity disc storage, these programs can be

kept readily available for call-up on an on-line basis. Hence, for example,

various statistical calculations can be performed on experimental data

while they are being gathered, the results displayed for evaluation during

the experiment, and then discarded or saved on disc for future utilization

as appropriate.

II. Neural - Net Modeling Program

    Objectives

        The objective of this study is to formulate, for simulation on

a general purpose digital computer, a nerve-net model. This model is

to be used both as an analytical tool in research concerning the functional

relationships of neurons, and as a pedagogical tool for use by students

studying functional relationships in nerve cells.

The three principal areas covered in the study are:

1) The development of a nerve-net model consisting of an explicit statement of the network configuration, and of the nerve cell dynamics.

2) Formulation of data processing package, for use with both the spike-train data generated by the simulation, and experimentally derived data.

3) Development of a digital computer program which permits the model to be used as a general simulation tool on the USC 360/44 IBM Computer.

Results and Conclusions

An explicit statement of the nerve model is formulated, including a detailed description of the network configuration and of the nerve cell dynamics. This formulation is presented in a form suitable for use in further work in the areas of model and parameter identification.

Summary of the Model

The neural net is described by

$$\underline{S} = [c]\underline{\Gamma} + [\Gamma]\underline{\Gamma}$$

where: $\underline{S}$ is an $\underline{n}$ vector called the "stimulation vector"

$[c]$ is an $(n \times n)$ matrix called the "configuration matrix"

$[\Gamma]$ is an $(n \times n)$ diagonal matrix called the "extremal configuration matrix"

τ is an $\underline{m}$ vector describing the input to the network from sources exterior to the network and is called the "extremal cell firing vector".

Γ is an $\underline{n}$ vector describing the set of firing times for each cell in the network and is called the "internal cell firing vector".

The dynamics of the $\underline{n}$ cells are represented by a set of $2\underline{n}$ first order differential equations

$$\dot{\underline{x}} = [A]\underline{x} + [B]\underline{S} + [D]$$

where: $\underline{x} = \dfrac{x_1}{\substack{\cdots \\ x_2}}$ is a $2\underline{n}$ state vector. x_1 representing the membrane threshold potential, and x_2 representing the trans-membrane potential.

The cell firing vector $\underline{T}$ is generated by solving $\dot{\underline{x}}$ for the following condition:

$$\Gamma_j = \{ t/ | x_{1j} - x_{2j} = 0 \} \, v_j, \, 2, \ldots n .$$

The nerve model is shown in block diagram form:

Network Configuration   Cell Dynamics

Nerve Net Model
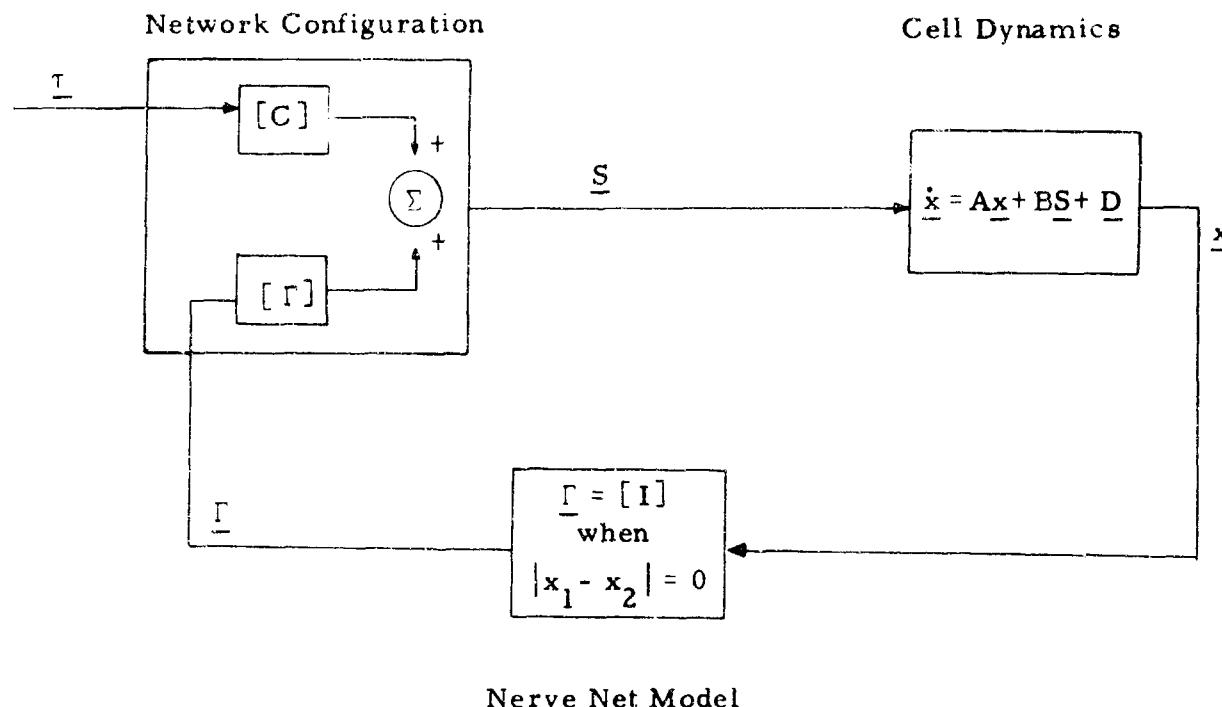
References
_____

1.   Moore, G. P., D. H. Perkel, and J. P. Segundo, "Statistical
     Analysis and Functional Interpretation of Neuronal Spike Data", Ann.
     Rev. of Physiol. 28: 493-522, 1966.

2.   Perkel, L. H., G. L. Gerstein, and G. P. Moore, "Neuronal Spike
     Trains and Stochastic Point Processes, I: Single Spike Trains",
     Biorh... ̃ 7 391-418, 1967

3.   Perkel, D. H., G. L. Gerstein, and G. P. Moore, "Neuronal Spike
     Trains and Stochastic Point Processes, II: Simultaneous Spike
     Trains", Biophys. J., 7: 419-440, 1967.

4.4 NEUROMUSCULAR SYSTEMS

4.4.1 Mathematical Models of Force Generation in Skeletal

Muscle

NB-06196-02, National Institutes of Health

NGR-05-018-022, National Aeronautics and Space

Administration

J. C. Coggshall and G. A. Bekey

This research project is concerned with the synthesis of
mathematical models of the force generation properties of skeletal
muscle. Experimental data have been obtained by recording the electro-
myographic activity and force produced by elbow flexor and extensor
muscles (specifically the biceps, triceps, and brachioradialis muscles)
of normal human subjects.

Any particular muscle may be viewed as composed of a set
of motor units. The motor unit (a single motoneuron fiber and the muscle
fibers it innervates) is the basic functional unit of muscle. The starting
point for this study was the formulation of a mathematical model for the
electrical and force generating activity of a single motor unit on the basis
of available physiological data. The motor unit model was used to postu-
late a model for the aggregate features of a group of motor units: namely,
the myoelectric activity and force produced by a whole muscle. In addi-
tion, transfer relationships between the EMG and force produced by a
muscle were determined using on line parameter tracking with an analog

computer.

The validity of both the postulated whole n. scle model and the EMG to force transfer characteristics was tested by cor paring these models with each other and with published data on whole muscles. The resulting comparisons are shown in the amplitude vs frequency plots of Figure 1. Curve A is a plot of the amplitude ratio obtained from human tricepts muscle models during the study[1]. Curve B shows the results of an aggregate model obtained by summing the properties of single motor units of the cat soleus muscle[2]. Curve C illustrates the changes of amplitude obtained by Partridge when whole cat soleus muscle was stimulated by sinusoidally varying nerve impulse frequencies[3]. In spite of the variety of sources, there is general agreement among these curves over a wide range of frequencies.

References

1. Coggshall, J. C., "Mathematical Models of Muscle", USCEE Report 303, August 1968.

2. Levanandan, M. S., et al., "Single Motor Units of Mammalian Muscle", J. of Neurophysiology, vol. 178, pp. 359-367, 1965.

3. Partridge, L. D., "Modifications of Neural Output Signals by Muscles: A Frequency Response Study", J. of Appl. Physiology, vol. 20, pp. 150-156, 1965.
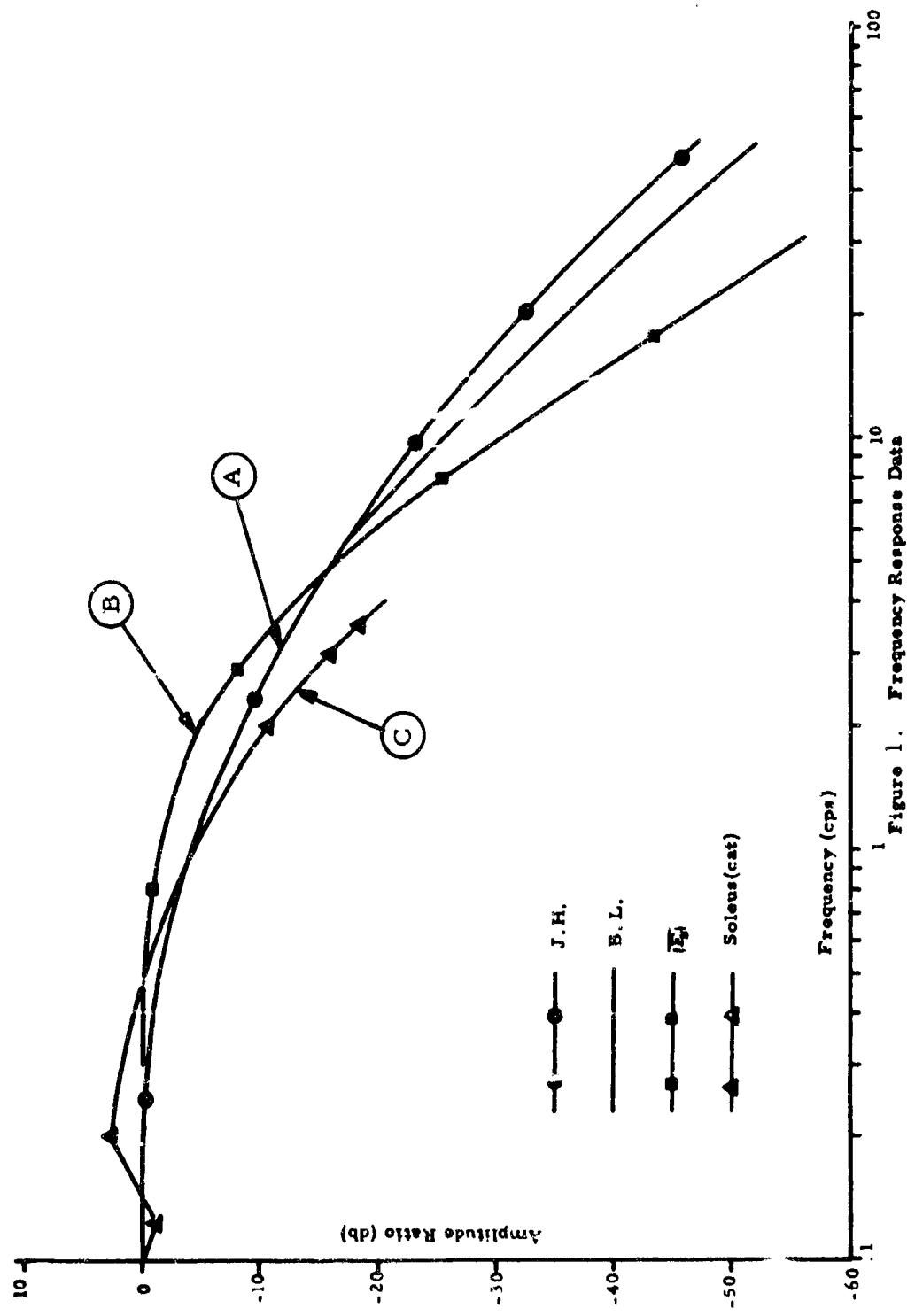
Figure 1. Frequency Response Data

4.5 BIOMATHEMATICS

4.5.1 Application of Control Theory to Administration of
Digitalis and Antibiotics

GM-16197-01, Department of Health, Education and Welfare

J. Buell, R. Kalaba, and R. Bellman

Buell and Kalaba, working closely with Jelliffe of the LACGH, have developed mathematical models for the administration of such drugs as digitalis and antibiotics using control theory and dynamic programming techniques. These preliminary models have proved surprisingly effective. Programs based on them have been written, and now are actually being used in the hospital. This work opens the door to the development of more complex and significant models in the entire area of drug administration and pharmacokinetics. We have high hopes that this work will significantly improve patient treatment. Furthermore, a number of new and interesting types of control processes arise from this study.

An investigation has been made by Kaplan of certain matrix theoretic problems connected with linear compartmental models of drug distribution in the body. For several categories of n-compartment models, theorems have been developed showing the character of the eigenvalues and eigenvectors, and providing upper and lower bounds on the eigenvalues. Further theorems have been developed showing what properties of the system are deducible in principle from the customary type of radioisotope experiment. Algorithms for making these deductions

have been provided and incorporated into a computer program.

Numerical examples have been worked out for the cases of digoxin and

albumin.

Reference   .

1.   J. Buell and R. Kalaba, "Modern Control Theory and Optimal Drug
      Regimens, I: The Plateau Effect", to appear.

4.5.2   Identification of Systems

GM-16197-01, Department of Health, Education and Welfare

J. Buell, R. Kalaba and R. Bellman

Over the last year, Buell and Kalaba, working with a well-
known physical-chemical process, the Michaelis-Menten model, have
applied the theory of quasilinearization to the identification of rate
constants in this process. The successful applications of methods of
this type will have a tremendous influence upon experimental techniques
in chemistry, biochem... : ·· --' 5. ..neering. Buell and Kalaba have
prepared a quasilinearization program which will make these methods
readily accessible. A great deal of further work in this area is being
done with the aim of introducing modern sophisticated techniques into
experimental work.

Reference

1.   J. Buell and R. Kalaba, "Quasilinearization and the Filtering of
      Nonlinear Models of Drug Metabolism to Experimental Kinetic Data",
      USCEE Report 312.

APPENDIX A

PUBLISHED PAPERS

Bekey, G. A.

Hybrid Computation, with W. J. Karplus; John Wiley and Sons, N. Y., 1968.

"Optimization of Discrete Systems with Combined Modulation", with
L. R. Nardizzi, IEEE Transactions on Automatic Control, AC-13: 286-289,
June 1968.

"The Changing Role of Analog and Hybrid Computer Systems", with W. J.
Karplus, Proc. Congress of Intern. Fed. for Information Processing (IFIP)
Edwinburgh, Scotland,

"Fetal and Neonatal Circulation", with N. A. Assali and W. Morrison,
Chapter 2 of Biology of Gestation, Vol. 2, ed. by N. S. Assali, pp. 51-142,
Academic Press, 1968.

Bellnan, R. E.

"Closure and Preservation of Moment Properties", with J. M. Richardson,
USCEE Report 266, March 1968.

"The Spectral Brightness of an Inhomogeneous Spherical Planetary
Atmosphere", with H. Kagiwada, R. Kalaba, and S. Ueno, USCEE Report 286,
June 1968.

"Diffuse Reflection of Solar Rays by a Spherical Shell Atmosphere", with
H. Kagiwada, R. Kalaba, and S. Ueno. to appear.

"Stratification and the Control of Large Systems with Applications to Chess
and Checkers", USCEE Report 269, April 1968.

"On Analogues of Poincare-Lyapunov Theory for Multipoint Boundary-value
Problems--Correction", USCEE Report 295, July 1968.

"An Algorithm for the Tourist Problem", USCEE Report 307, October 1968.

Breuer, M. A.

"Some Properties of (0, 1) Circulant Matrices", Proc. of the Hawaii
International Conference on System Sciences, pp. 793-794, January, 1968

"Heuristic Switching Expression Simplification", Proc. ACM National
Conference, 1968, pp. 241-250.

"Fault Detection in Linear Cascades of Identical Sequential Machines", Proc. IEEE Conference on Switching and Automata Theory, 1968, (to be published).

"Hardware Fault Detection", F.J.C.C., 1968 (to be published).

"Combinatorial Equivalences of (0, 1) Circulant Matrices", Journal of Computer and System Sciences (to be published).

"Generation of Optimal Code for Expressions via Factorization", Comm. ACM (to be published).

Brook, R.J.

"The Impurity Drag Effect and Grain Growth Kinetics", Scripta Met. (2) 375 (1968).

Crowell, C.R.

"Richardson Constant and Tunneling Effective Mass for Thermionic and Thermionic-Field Emission in Schottky Barrier Diodes", Solid St. Electron (in press).

"Normalized Thermionic Field (T-F) Emission in Metal-Semiconductor (Schottky) Barriers", with V.L. Rideout, Solid St. Electron (in press).

"Metal-Semiconductor Interfaces", Surface Science (in press), invited paper presented at American Chemical Society Symposium on Semiconductor Surface Phenomena, San Francisco, April 1968.

"Surface State and Interface Effects on the Capacitance - Voltage Relationship in Schottky Barriers", with G.I. Roberts, submitted to Jour. Appl. Phys.

"Thermionic-Field Resistance Maxima in Metal-Semiconductor (Schottky) Barriers", with V.L. Rideout, submitted to Appl. Phys. Letters.

DeShazer, L.G.

"Spectral Control of Laser Oscillators by Secondary Light Sources", with E.A. Maunders, paper 1683, International Quantum Electronics Conference, Miami, Florida, May 13-17, 1968.

"Energy Levels and Spectral Broadening of Rare Earth Ions in Laser Glass", with D.K. Rice and M.M. Mann, paper FC 11, Meeting of the Optical Society of America, Pittsburgh, Pennsylvania, October 9-11, 1968.

"Spectral Broadening of Europium Ions in Glass", with D.K. Rice, to be published.

"Atomic Multipole Radiation in Anisotropic Media", with M.M. Mann, to be published.

Ginsburg, S.

"Substitution in Families of Languages", with E.H. Spanier, submitted to the Journal of Computer and System Sciences.

"A Mathematical Model of Transformational Grammars", with B. Partee, submitted to Information and Control.

"On the Elimination of End Markers", with M.A. Harrison, Information and Control, Vol. 12, pp. 103-115, 1968.

"One-Way Nondeterministic Real-Time List-Storage Languages", with M.A. Harrison, Journal of the Association for Computing Machinery, Vol. 15, pp. 428-446, 1968.

Lindsey, W.C.

"Nonlinear Analysis and Synthesis of Generalized Tracking Systems", September 1968, pending publication.

Macmillan, R.S.

"Optimization of Information-Processing Optical Systems by Transcorrelation-Function Maximization", with G.O. Young, Journal of the Optical Society of America, Vol. 58, no. 3, page 346, March 1968.

Meisel, W S.

"Hazards in Non-Critical Races", with D.C. Collir , Proc. IEEE, August 1968.

"Variable-threshold Threshold Elements", IEEE Trans. on Computers, July 1968.

"Nets of Variable-threshold Threshold Elements", IEEE Trans. on Computers, July 1968.

"Periodic Sequential Machines", with R. A. King, USCEE Report 128, June 1968.

"Tables of Artificial Data for Pattern Recognition", with W. Yuan, USCEE Report 302, August 1968.

Moore, G. P.

"A Neuromuscular Actuation System Model", with D. T. McRuer and R. E. Magdaleno, presented IFAC Symposium on Technical and Biological Problems of Control, Yerevan, Armenia. September 1968.

"Applications of the Theory of Stochastic Point Processes in the Detection and Analysis of Neuronal Interactions", with D. H. Perkel and J. P. Segundo, IFAC Symposium on Technical and Biological Problems of Control, Yerevan, Armenia, September 1968.

"Input-Output Relations in Computer-Simulated Nerve Cells: Influence of the Statistical Properties, Strength, Number and Inter-dependence of Excitatory Pre-Synaptic Terminals", with J. P. Segundo, D. H. Perkel, H. Wyman, and H. Hegstad, Kybernetic, 4: 157-171, 1968.

Murr, L. E.

"Thermal Recovery of Explosive Shock-Loaded Stainless Steel, with M. F. Rose, Phil. Mag., 18, 281, 1968.

Lattice Defects in Stainless Steel Shock-Loaded to Pressures Above 1 Megabar", with M. F. Rose, Proc. Electron Microscopy Soc. America, 26th Annual Meeting, p. 254 (1968).

"Applications of Transmission Electron Microscopy in the Characterization of Metal Machinability", with A. B. Draper, Proc. Electron Microscopy Soc. America, 26th Annual Meeting, p. 442 (1968).

"Electron Microscopy Investigation of the Relationship of Deposition Parameters to Structural Characteristics in Metal and Alloy Films Vapor Deposited in High and Ultra-High Vacuum", Proc. 2nd Colloquium on Thin Films (Budapest), Ed. E. Hahn, August 1968.

"Investigation of Relative Interfacial Free Energies in 304 Stainless Steel by Electron Transmission and Diffraction Microscopy, Acta. Met. 16, 1127 (1968).

Reed, I. S.

"Some Aspects of the Norm Representation for Arithmetic Error-Checking and Correcting Codes", with A. C. L. Chiang, USCEE Report 276, May 1968.

Sworder, D. D.

"Feedback Control of a Class of Linear Stochastic Systems", 1968 Joint Automatic Control Conference, pp. 34-44, 1968.

"Minimax Controllers for Systems with Unknown Parameters", 1968 Joint Automatic Control Conference, pp. 751-752, 1968 (invited).

"On the Control of Stochastic Systems; II", Int. J. of Control (to appear).

"On the Stochastic Maximum Principle", J. of Math. Analysis (to appear).

Wagner, W. G.

"Self-trapped Optical Beams in Liquids", with J. D. Reichert, IEEE Journal of Quantum Electronics, Vol. QE-4, No. 4, pp. 221-225, April 1968.

"High Rate Optical Amplification", with H. A. Haus and K. T. Gustafson, IEEE Journal of Quantum Electronics, Vol. QE-4, No. 5, pp. 267-273, May 1968.

Weber, C. L.

"A Gradient Approach to Signal Design for M-ary Communication Systems", with D. D. Sworder and S. Moskowitz, First International Conference on System Sciences, Honolulu, Hawaii, January 1968.

"Cascaded Phase Locked Loops", with J. J. Stein, National Electronics Conference, Chicago, 1968.

Elements of Detection and Signal Design, McGraw-Hill, N. Y., 1968.

On the Theory of Automatic Phase Control in Stochastic Optimization and Control, John Wiley and Sons, N. Y., 1968.

Wolf, M. B.

"A Theoretical Evaluation of the Patient-Artificial Kidney System Using a Kiil Western Dialyzer", with P. D. Watson and B. H. Barbour, to be published in Mathematical Biosciences.

Nahi, N. E.

"Absolute Stability of Dynamic Systems Containing Nonlinear Functions of Several State Variables", with S. Partovi, IFAC Symposium on Multivariable Control Systems, Dusseldorf, Germany, October 1968.

"On the Absolute Stability of a Dynamic System with a Nonlinear Element Function of Two State Variables", with S. Partovi, IEEE Transactions on Automatic Control, October 1968.

Estimation Theory and Applications, John Wiley and Sons, N. Y., 1968.

Payne, H. J.

"An Approximation Method for Nearly Linear, First-Order Stochastic Differential Equations", Int. J. Control, vol. 7, no. 5, 1968.

"Fuel Optimum Stochastic Attitude Control", with R. B. McGhee and W. H. Spuck, Submitted for publication to PG-AC.

Payne, R. T.

"The Excitonic Insulator in GaAs Junctions", Physical Review Letters 21, 284 (1968).

"Quantitative Observations of Physics", with John McKim, and Charles Dietz, Physics Department, University of Southern California, Los Angeles, 1968.

Porto, S. P. S.

"Light Scattering with Laser Sources", Spex Industries Speaker 13, No. 2, 1968, to be reproduced in "Bathsheba de Rothchilds Lectures in Applied Physics", Jersalem, Israel 1968.

Proc. of International Conference in Light Scattering in Solids, G. B. Wright, ed., 1968.

"Auger-like Resonant Interference in Raman Scattering from and Two-phonon States in $BaTiO_3$", with D. L. Rousseau, Phys. Rev. Lett. 20, 1354, 1968.

"Rayleigh Scattering of Linearly Polarized Light From Optically Active Quartz", with C. A. Arguello and D. L. Rousseau, Appl. Opt., Oct. 1, 1968.